Fabrication and Characterization of Gallium Nitride Based Diodes

by

Yaqi Wang

A dissertation submitted to the Graduate Faculty of
Auburn University
in partial fulfillment of the
requirements for the Degree of
Doctor of Philosophy

Auburn, Alabama
August 6, 2011

Key words: GaN, Schottky diode, Raman spectroscopy

Approved by

Minseo Park, Chair, Associate Professor of Physics
John R. Williams, Professor of Physics,
Michael J. Bozack, Professor of Physics,
Jianjun Dong, Associate Professor of Physics,

Abstract

This dissertation describes research to the fabrication and characterization of Gallium nitride (GaN) based diodes. GaN is considered to be probably one of the most significant semiconductor material ever discovered dissertation describes research to the fabrication and characterization of Gallium nitride (GaN). Because of its direct wide bandgap and outstanding electric properties, GaN is widely used in solid state lighting applications and considered as an alternative to Silicon in power electronics devices.

High performance GaN based Schottky diodes were fabricated using n- bulk GaN substrates synthesized by Hydride Vapor Phase Epitaxy (HVPE) process. Full back ohmic contact was deposited on the N face and circular Schottky contacts on the Ga face. The Schottky diodes showed excellent forward and reverse bias characteristics, which resulted in a high figure of merit (FOM). We have also fabricated GaN Schottky diodes on n- epilayer/ n+ bulk GaN structure, where the epilayers were deposited using Metal-Organic Chemical Vapor Deposition (MOCVD) on HVPE grown substrate. The devices showed very high breakdown voltages. Electrical measurements such as current-voltage (I-V) and capacitance-voltage (C-V) were used to extract ideality factors, series resistance and other important parameters from the diodes. Raman spectroscopy was also carried out to determine the average junction temperature of the commercial ultraviolet (UV) light emitting diodes (LEDs).

Acknowledgments

The author would like to express his sincere appreciation to Dr. Minseo Park for his invaluable guidance, support and encouragement during the study at Auburn University. The author is also thankful to all the committee members, Dr. John Williams, Dr. Michael J. Bozack and Dr. Dong for their time and assistance.

The author would like to thank Dr. Claude Ahyi and Ms. Tamara Isaacs-Smith for their help with the semiconductor device fabrication and measurement. He would like to thank Mr. Max Cichon for his training on the vacuum systems, Dr. An-jen Cheng for his help on the Raman and Photoluminescence (PL) measurements, and Dr. Guofu Niu for his guidance on the Sentaurus simulations.

The author would also like to thank Kyma Technologies, Inc., Dr. Andrew A. Allerman from Sandia National Laboratories, and Dr. Mark Johnson from the North Carolina State University for providing high quality GaN substrates.

In addition, the author would like to thank Dr. Hui Xu, Dr. Siddharth Alur, Mr. Yogesh Sharma, Mr. Resham Thapa and Ms. Fei Tong for discussion of the problems encountered in the research.

Finally the author would like to thank his parents, Shaojun Wang, Shaoping Fang and his wife Jun Liu for their continuous love and support.

Table of Contents

List of Tables

List of Figures

List of Abbreviations

AFM	Atomic force microscopy
BFOM	Baliga figure-of-merit
CCD	Charged coupled device
CFOM	Combined figure-of-merit
C-V	Capacitance Voltage
DOE	Department of Energy
DC	Direct current
DI	Deionized
EL	Electroluminescence
EV	Electric vehicle
FOM	Figure-of-Merit
FWHM	Full-width at half-maximum
HEV	Hybrid electric vehicle
HFET	Heterostructure field effect transistor
HVPE	Hydride Vapor Phase Epitaxy
IGBT	Insulated-gate bipolar transistors
IR	Infra-red
I-V	Current Voltage
JFOM	Johnson figure-of-merit
LED	Light Emitting Diode
LEEBI	Low-energy electron-beam irradiation

LLO	Laser lift-off
MBE	Molecular beam epitaxy
MOCVD	Metal-Organic Chemical Vapor Deposition
MOSFET	Metal oxide semiconductor field-effect transistor
MQW	Multiple-quantum-well
MYPP	Multi-Year Program Plan
PHEV	Plug-in hybrid electric vehicle
PL	Photoluminescence
R&D	Research and development
RF	Radio frequency
RHEED	Reflection high energy electron diffraction
RIE	Reactive ion etching
RPM	Revolutions per minute
RTA	Rapid thermal annealing
SCR	Space charged region
TCE	Trichloroethylene
UV	Ultra-violet
WBG	Wide bandgap

Chapter One

Introduction

GaN is a typical III-V compound wide band gap (WBG) semiconductor material and has many superior physical properties. The first successful synthesis of GaN was achieved by *Johnson et al.* [1] back to the 1930's by direct reaction between liquid gallium and ammonia (NH_3). The material appeared as dark grey powder and was chemically stable in air, acids and bases at room temperature. In 1969, *Maruska* and *Tietjen* [2] first reported the growth of single-crystalline GaN film on sapphire substrate using HVPE. The authors attributed the high background electron concentration of GaN to nitrogen vacancies. In 1971, *Pankove et al.* [3] reported the first device application of GaN, LED with an insulating-to-n-type structure, where insulating layer was formed by Zinc doping. The diode was able to emit green light and the power efficiency was 0.1%. Unfortunately, because of the difficulty encountered in p-type doping, research on GaN virtually ceased. The breakthrough was finally made in 1989 when *Amano et al.* [4] achieved distinct p-type conduction with Mg-doped GaN. Drastically lowering of the resistivity and remarkable enhancement of PL efficiency were observed after the low-energy electron-beam irradiation (LEEBI) treatment. The successful p-type doping resulted in a great improvement of device performance. In 1995, *Nakamura et al.* [5] made the first InGaN LEDs with high output power, quantum efficiency and luminous intensity, which tremendously boosted the research activities on GaN.

There are two common crystal structures of GaN: the hexagonal close packed (HCP) wurtzite and face-centered cubic (FCC) zinc blende. The most common crystalline form of GaN under ambient condition is wurtzite. The lattice constants of the wurtzite structure are a = 3.1892 ± 0.0009 Å and c = 5.1850 ± 0.0005 Å. Epitaxial-grown GaN film on certain foreign substrates is found in zinc blende form. The lattice constant of the zinc blende form varies from a = 4.49 Å to a = 4.55 Å [6]. The two structures are shown in Figure 1.1.

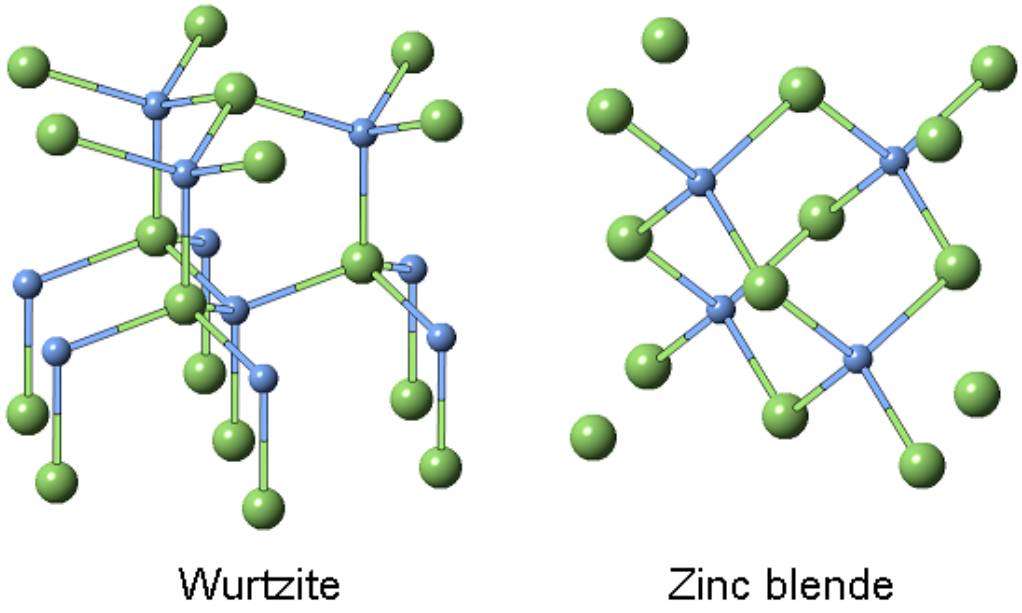

Figure 1.1 Wurtzite and Zinc blende structures of GaN

GaN is a thermally and chemically stable compound. The decomposition temperature of the GaN under atmosphere pressure is approximately 850 °C [7], which can offer a wider range of processing temperature of GaN based devices. GaN does not dissolve in water, acid, bases at room temperature and can only be etched slowly in strong base such as KOH and NaOH at elevated temperature. Because of the difficultly of wet etching, dry etching thus becomes the major etching technique in GaN device fabrication.

Table 1.1 shows the electrical properties of GaN and other common semiconductor materials. The band gap of GaN is 3.4 eV. The wide band gap gives GaN large maximum junction temperature of operation. The high thermal conductivity facilitates the heat transfer of the devices. Those two factors enable GaN based devices work at harsh temperature environment and also reduces the cost on heat extraction part of the system. GaN can be alloyed with other III-N materials to form large range of direct band gap, which also makes GaN a perfect material for optoelectronics. GaN is suitable for high voltage applications because the breakdown field of GaN is much higher than conventional semiconductor materials such as Si and GaAs, and even other wide band gap materials such as SiC. GaN's high electron mobility and electron velocity characteristics also make GaN a perfect material for high frequency applications.

Properties	Si	GaAs	4H-SiC	GaN
Band gap (eV)	1.12, I [8]	1.42, D [8]	3.25, I [8]	3.40, D [9]
Breakdown field (MV/cm)	0.3 [8]	0.4 [8]	3.0 [10]	4.0 [9]
Electron mobility at RT ($cm^2V^{-1}s^{-1}$)	1500 [10]	8500 [10]	1000 [11]	1250 [10]
Dielectric Constant	11.8 [9]	12.8 [9]	9.7 [9]	9.0 [9]
Saturated electron velocity (10^7 cm/s)	1 [10]	2 [10]	2 [10]	2.5 [12]
Thermal conductivity ($Wcm^{-1}K^{-1}$)	1.5 [9]	0.5 [9]	4.9 [9]	2.3 [13]

Table 1.1 Comparison of electrical properties of common semiconductor materials

Figure-of-merits (FOMs) of Si, GaAs, 4H-SiC and GaN are shown in Figure 1.2 to compare their inherent capabilities and maximum device performance. The Johnson's figure-of merit, defined by $E_c^2 V_s^2/4\pi^2$, describes the power-frequency product of low-voltage transistor; the Baliga's figure-of-merit, defined by $\varepsilon\mu E_c^3$, describes the ability to minimize conduction loss in low-frequency transistor; the combined figure-of-merit, defined by $\lambda\varepsilon\mu V_s E_c^2$, describes the overall performance of high power, high frequency and high temperature applications. The FOM comparison shows the advantage of the GaN clearly.

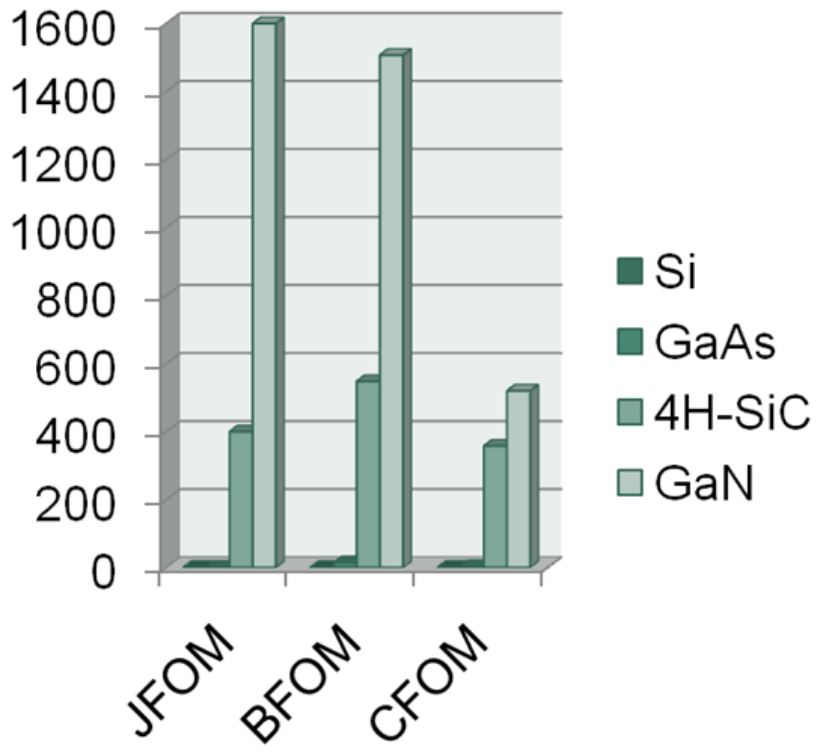

Figure 1.2 JFOM, BFOM and CFOM of Si, GaAs, 4H-SiC and GaN normalized to Si

There are three main methods widely used in GaN growth: HVPE, MOCVD, and Molecular Beam Epitaxy (MBE). HVPE can produce thick and crack-free bulk GaN substrates,

while MOCVD and MBE are generally used in depositing high quality thin films for devices such as LEDs, laser diodes (LDs) and high electron mobility transistors (HEMTs).

HVPE is one of the earliest methods developed in GaN growth and is the most successful technique that provides thick layers with high growth rate. In HVPE growth process, gallium chloride (GaCl) is first formed by passing hot hydrogen chloride (HCl) gas over liquid gallium. Two hydride precursors GaCl and NH_3 are then carried to the deposition chamber, usually a high-quality quartz furnace, by hydrogen gas, nitrogen gas or argon. P-type doping can be achieved by passing magnesium vapor during the process and n-type by silane gas. The chemical reaction is shown below:

$$\mathrm{HCl(g) + Ga(l) \Rightarrow GaCl(g)}$$

$$\mathrm{GaCl(g) + NH_3(g) \Rightarrow GaN + HCl + H_2}$$

Schematic view of HVPE system for GaN growth is shown in Figure 1.3

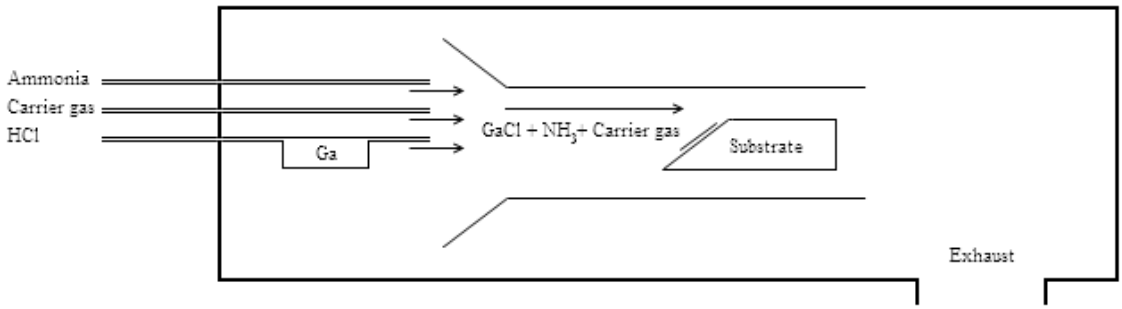

Figure 1.3 Schematic view of HVPE system for GaN growth

MOCVD has been widely used in the LED industry to grow high quality film of GaN and its ternary alloys. Deposition of GaN by MOCVD involves two processes: the transportation of the metalorganic precursor gases and nitrogen source to the reaction chamber and reaction on the surface of a heated substrate. TriMethylGallium (TMG) and high purity NH_3 are the most

common Ga and N sources. TMG is first vaporized by flowing hydrogen into bubbler, and mixed with NH_3 in the main flow. The two reactant gases are then introduced parallel to a rotating heated substrate, where the precursors decompose and GaN is formed and deposited. The auxiliary sub flow gas is introduced perpendicular to the substrate, which can help to keep a reactant gas rich zone near the substrate. Popular N-type and p-type dopants used in MOCVD are silane and Bis cyclopentadienyl magnesium (Cp_2Mg). The chemical reaction is shown below:

$$Ga(CH_3)_3(g) + NH_3(g) \Rightarrow GaN + 3CH_4$$

Schematic view of MOCVD system for GaN growth is shown in Figure 1.4

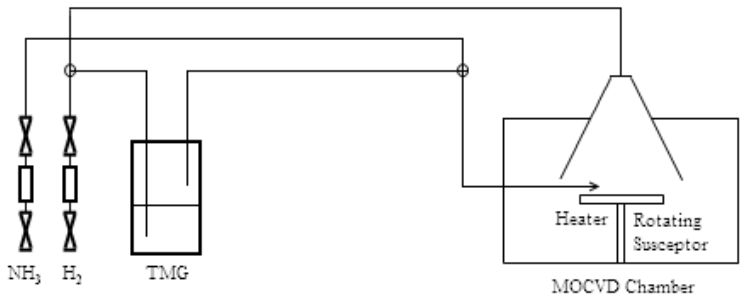

Figure 1.4 Schematic view of MOCVD system for GaN growth

MBE has great advantages over other GaN growth techniques because its film purity and in-situ monitoring capability. All the growth processes are operated in ultra-high vacuum environment. As a result, GaN films grown by MBE have better purity. Reflection high energy electron diffraction (RHEED) system is usually incorporated into the MBE system to provide information about growth rate and crystal quality during the growth. Ga vapor beam from an effusion cell and nitrogen beam from radio frequency (RF) plasma source are directed into the MBE chamber. Under specific circumstance, adsorption of the atoms on substrate surface, diffusion of the atoms along the surface, incorporation of the Ga and N atoms to form GaN take

place sequentially, and thin film of GaN can be formed on the surface of the heated substrate. Schematic view of MOCVD system for GaN growth is shown in Figure 1.5

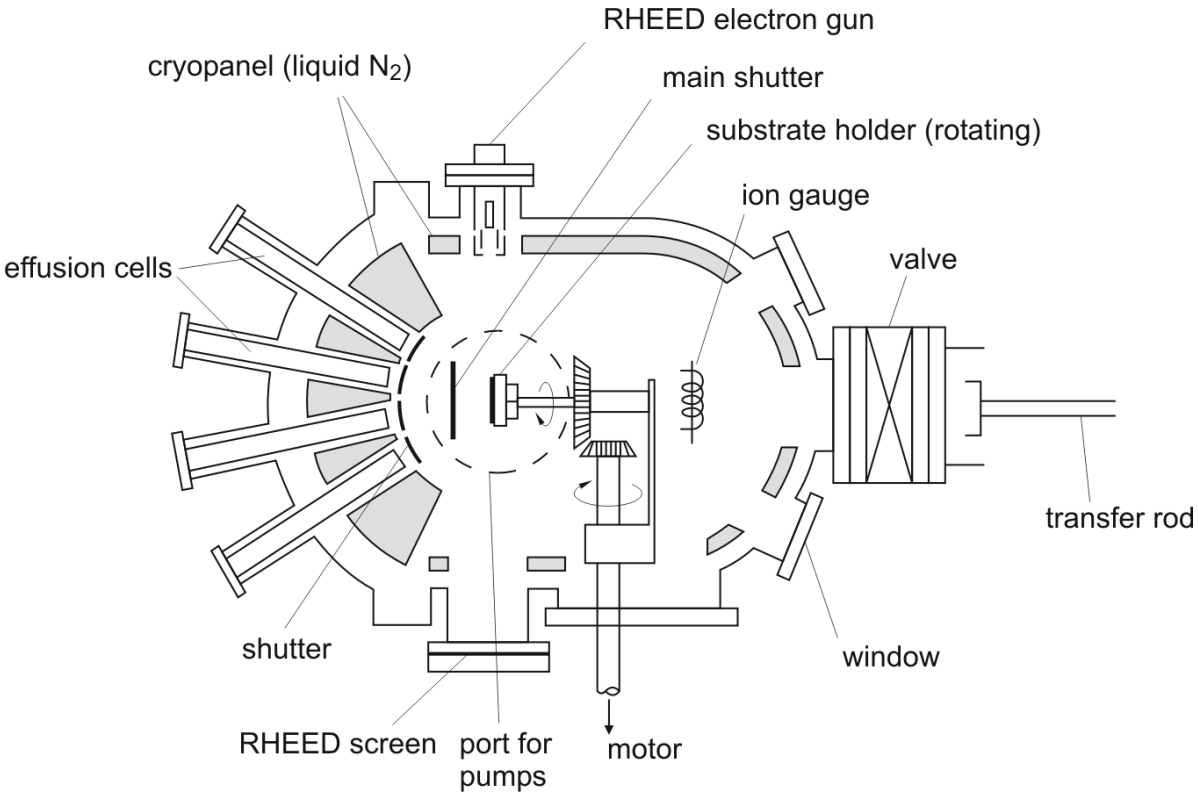

Figure 1.5 Schematic view of MBE system for GaN growth, adapted from [14]

For the past ten years, the improving substrate quality, improvement of process techniques, device design and reduction in cost have enabled GaN based devices to compete in two major industries: solid state lighting and power electronics. According to the 2010 Solid State Lighting Research and Development (R&D) Multi-Year Program Plan (MYPP) by the U.S. Department of Energy (DOE) [15], the market share of LEDs in global lighting market is still small but growing rapidly. GaN and its related ternary alloys based LEDs, which can cover a wide spectral range from green to ultraviolet, are expected to make significant contribution to the

growth. The 2010-2014 Smart Grid R&D MYPP by the U.S. DOE [16] stated that small-scale power converters, which can increase the operational flexibility, will be the key components in the power delivery system. The power inverters can be applied to hybrid electric vehicle (HEV) and plug-in hybrid electric vehicle (PHEV) [17] in order to achieve high motor power. RF power amplifiers are the most critical parts in wireless transmitters [18]. In those above-mentioned applications, WBG semiconductor materials such as GaN are favored because of their better performance at high temperature and high frequency. It can be foreseen that GaN based devices will gradually change the way people live just as their silicon counterparts.

A background study and literature review of the fabrication and characteristics of the GaN based diodes are presented in Chapter 2. This chapter focuses on the past work on improving the GaN Schottky diode performance and to explore the current transportation mechanism across the interface. The electrical, optical and temperature characterization methods are also introduced in this chapter.

In Chapter 3, fabrication processes of the Schottky diode and measurement methods were presented. The fabrication processes include wafer dicing, cleaning, photolithography, sputtering, rapid thermal annealing, and reactive ion etching. Characterization techniques, such as I-V, C-V, Raman spectroscopy and photoluminescence is also introduced.

Ultra-low leakage vertical Schottky diodes on bulk GaN substrate was demonstrated in Chapter. 4. Low leakage current and high breakdown voltage properties are very important at reverse bias regime of the Schottky diode. An array of ultra-low leakage current as well as high breakdown voltage Schottky diodes was fabricated without degradation of forward device performance. Device simulation using Synopsis' Sentaurus was carried out to explore the current transportation mechanism.

In Chapter 5, High breakdown voltage Schottky diode was fabricated on MOCVD grown n- epilayer/ HVPE grown n+ bulk substrate. The relationship between on-state resistance and breakdown voltage were studied systematically. The devices showed a highest breakdown voltage of 980V.

Chapter 6 discuss about *in-situ* junction temperature determination of UV LEDs under operation by micro-Raman spectroscopy. The method offers a good accuracy as well as temperature mapping capability. A downshift and broadening of the Raman peak as temperature increased was observed. Based on the shift, the relationship between the shift and the temperature was derived and used to determine the temperature of operating LEDs. We have demonstrated that micro-Raman spectroscopy is a viable technique for UV LED junction temperature determination.

References

[1] W.C. Johnson, J.B. Parson and M.C. Crew, “Nitrogen Compounds of Gallium III.Gallic Nitride”, J. Phys. Chem. **36**, 2561 (1932).

[2] H. P. Maruska and J. J. Tietjen, “The preparation and properties of vapor-deposited single-crystalline GaN”, Appl. Phys. Lett. **15**, 327 (1969).

[3] J. I. Pankove, E. A. Miller, and J. E. Berkeyheiser, “GaN Electroluminescent Diodes”, RCA Rev. **32**, 383 (1971).

[4] H. Amano, M. Kito, K. Hiramatsu, I. Akasaki, “P-Type Conduction in Mg-Doped GaN Treated with Low-Energy Electron Beam Irradiation (LEEBI)”, Jpn. J. Appl. Phys., **28**, L2112 (1989).

[5] S. Nakamura, M. Senoh, N. Iwasa, S. Nagahama, “High-Brightness InGaN Blue, Green, and Yellow Light-Emitting Diodes with Quantum Well Structure”, Jpn. J. Appl. Phys., **34**, L797 (1995).

[6] H. Morkoç, *Nitride Semiconductors and Devices* (Springer, Berlin, 1999)

[7] H.Morkoç, *Handbook of Nitride Semiconductors and Devices* (Wiley, New York, 2008), Vol. 1

[8] J. L. Hudgins, G. S. Simin, E. Santi and M. A. Khan, “An assessment of wide bandgap semiconductor for power electronics”, IEEE Transactions on Power Electronics 18, 907 (2003).

[9] S. J. Pearton, F. Ren, A. P. Zhang, K. P. Lee, “Fabrication and performance of GaN electronic devices”, Mat. Sci. Eng. **R 30**, 55 (2000).

[10] M. N. Yoder, “Wide bandgap semiconductor materials and devices”, IEEE Trans. Electron. Dev. **43**, 1633 (1996).

[11] J. B. Casady and R. W. Johnson," Status of silicon carbide (SiC) as a wide-bandgap semiconductor for high-temperature applications: A review" , Solid-State Electron. **39**, 1409 (1996).

[12] U. Bhapkar, M. Shur, " Monte Carlo calculation of velocity-field characteristics of wurtzite GaN", J. Appl. Phys. **82**, 1649 (1997).

[13] C. Mion, J. F. Muth, E. A. Preble, D. Hanser, "Temperature and Dislocation Density Effects on the Thermal Conductivity of Bulk Gallium Nitride", Mater. Res. Soc. Symp. Proc, Vol 892, 0892-FF29-05.1-05.6. (2006).

[14] H. Ibach and H. Lueth, *Solid State Physics* (Springer, Berlin, 2003)

[15] http://apps1.eere.energy.gov/buildings/publications/pdfs/ssl/ssl_mypp2010_web.pdf

"Solid-State Lighting Research and Development: Multi-Year Program Plan"

[16] http://www.oe.energy.gov/DocumentsandMedia/SG_MYPP.pdf

"Smart Grid Research & Development Multi-Year Program Plan"

[17] T. Kachi, "GaN Power Devices for Automotive Applications", IEEE CSIC Symp. Tech. Dig., pp.14-17, (2007)

[18] T. Kikkawa, T. Maniwa, H. Hayashi, M. Kanamura, S. Yokokawa, M. Nishi, N. Adachi, M. Yokoyama, Y. Tateno, and K. Joshin, "An Over 200-W Output Power GaN HEMT Push-Pull Amplifier with High Reliability", IEEE MTT-S Int. Microwave Symp. Dig. 3, 1347 (2004).

Chapter Two

Background and Literature Review

1.1 GaN based Schottky diode

Schottky barrier is formed at the metal semiconductor interface when they are in contact. The Schottky barrier height is the difference of the work function of the metal and the electron affinity of the semiconductor. Metals with high work function can usually form a high Schottky barrier height on semiconductor. The band structure of Schottky barrier formation is shown in figure 2.1.

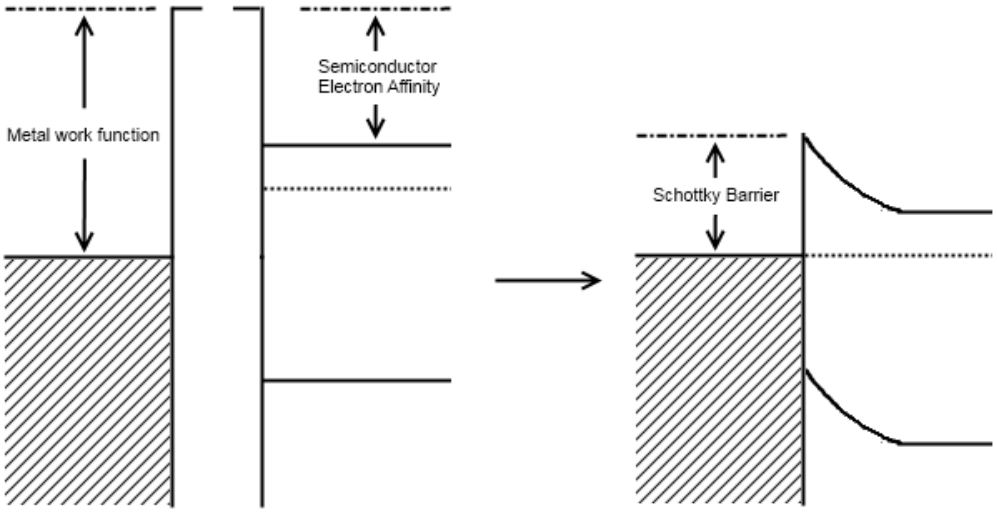

Fig 2.1 Band structure of Schottky barrier formation

Schottky diode is a majority carrier device, only one type of carrier is dominant in the current transportation. In the case of GaN, Schottky diode is usually fabricated on n substrate; and the dominant carrier is electron. In order to have good reverse blocking capability, Schottky diode is usually fabricated lightly doped substrate. The carrier transportation mechanism is usually thermionic emission or Thermal field emission depending on the doping concentration.

An ideal Schottky diode should have characteristics such as: high breakdown voltage, low leakage current, low forward voltage drop, low on-state resistance and fast recovery. The keys lead to ideal Schottky diodes are: semiconductor material intrinsic properties, high quality intrinsic layer as drift region with desired thickness, low resistivity highly doped substrate, proper device structure and design, good edge termination, rectifying Schottky contact and low contact resistance ohmic contact [1].

The most significant is the semiconductor material's intrinsic properties. Current Si based Schottky diodes suffer from high leakage current and low blocking capability due to the narrow bandgap and low Schottky barrier height. Si based p-i-n diodes offer better reverse characteristics at the expense of much slower switching which is due to the longer minority carrier lifetime [2]. The increasing demands meeting those criteria leads to the development of new materials, better device design and processing techniques. WBG semiconductor materials such as SiC and GaN are considered as excellent materials for rectifiers because of their chemical stability, thermal stability and superior electrical properties [3]. The longer history of research gives SiC better material quality and device technology and thus better device performance. However, GaN has better physical properties and has been developed fast in both material and device fields. The device performance of GaN based Schottky diodes begin to catch up and will finally exceed their SiC counterparts.

The high quality intrinsic layer should have a minimized dislocation density and a low unintentional background doping concentration. Traditional MOCVD heteroepitaxy grown GaN epilayer on sapphire or SiC has typical dislocation densities of 10^{8}-10^{10} cm^{-2} and impurity densities of 10^{16}-10^{20} cm^{-3} [4]. Dislocations in GaN, especially screw dislocation, have significant impact on the leakage current [5,6]. The high dislocation densities are due to the lattice and thermal expansion coefficient mismatch between GaN and the foreign substrate. GaN and sapphire have a 14% lattice mismatch [7] and a 27% thermal expansion coefficient mismatch [8,9]. The lattice mismatch between GaN and 6H-SiC is only 3.4%, but the thermal expansion coefficient mismatch is as high as 54% [10]. To overcome the mismatch difficulties mentioned above, a technique named lateral epitaxial over growth (LEO) was introduced [11]. However, this technique can provide improvement of crystal quality in a small window area. High background n doping concentration can decrease the barrier thickness and, as a result, increase the tunneling current. Defects and impurities such as nitrogen vacancies [12], oxygen, silicon [13], hydrogen [14] and carbon [15] may contribute to the n-type conductivity. Carbon is a common impurity in GaN which can be introduced from the organic precursors used in the MOCVD growth. Unintentional carbon doping is undesired because of its amphoteric behavior of acceptors as well as donors [16]. Bulk GaN substrate synthesized by HVPE can overcome the drawbacks of heteroepitaxial growth listed above. The dislocation density of the HVPE grown bulk GaN substrate decreased to 5×10^{5} cm^{-2} [17]. Typical order of magnitude of carbon concentration of MOCVD grown GaN is over 10^{17} cm^{-3} [18,19], while the carbon concentration is about 10^{16} cm^{-3} or lower in HVPE grown GaN [20,21]. Highly doped substrate can be also achieved by introducing gas which contains Si, such as silane. The silicon atom concentration can reach the magnitude of 10^{19} cm^{-3} [22].

GaN grown by HVPE can offer not only high quality substrate with low dislocation and impurity density but also a large crack-free growth thickness and a very high growth rate. The typical thickness of MOCVD and MBE grown GaN epilayer is about 2-3 μm. Cracking is very likely to occur after the critical thickness is reached, which is presumably due to the tensile growth stress [23]. The deposition rates of GaN by MOCVD and MBE are also very low. The GaN epilayer is usually grown at a rate of ≤ 0.4 μm/h in MBE [24] and ~5 μm/h in MOCVD [25]. HVPE grown GaN can easily reach a thickness of ≥ 1 mm with a growth rate of ≥ 1 μm/min [26]. The quality of the HVPE grown GaN substrate keeps improving. Fujito *et al.* recently reported very thick c-plane GaN grown by HVPE with a diameter of 52 mm and a thickness of 5.8 mm [27]. The dislocation density of the substrate is of the order of magnitude of 10^6 cm^{-2}, and the impurities (O, C, Cl, H, Fe, Ni and Cr) were close to or below the detection limits by SIMS measurements.

GaN growth by HVPE is mostly carried out on sapphire substrate. A buffer layer is usually deposited to overcome the difficulties of the large lattice match. ZnO [28], Ga + HCl treatment [29], AlN [30] and MOCVD grown GaN [31] are the most common buffer layer materials. The strain variation with sample thickness in GaN is studied by Reynolds et al. [32]. By using optical measurement, a full relaxation of the surface strain for a layer thickness near 75 μm was estimated, which enables further strain free epitaxial growth. Fang et al. used TEM, C-V, DLTS to study deep centers and dislocation densities [33]. As the layer thickness increase, both concentration of deep centers and dislocation density decreased. Paskova et al. also observed a reduction of impurity concentrations of HVPE grown GaN along the direction growth by SIMS measurement [34]. Therefore, the HVPE grown GaN with large thickness can offer strain-free, low dislocation density and impurities which is preferable in GaN based device fabrication.

The separation of GaN from the sapphire substrate involves a laser lift-off (LLO) process. In the LLO process, a high-power laser (third harmonic of a Q-switched YAG:Nd laser) is focused on the interface of the GaN/sapphire interface. The absorption of the heat leads to a decomposition of irradiated GaN layer into metallic Ga and gaseous N_2 [35]. After LLO process, a chemical mechanical polish treatment is carried out to remove the defective interfacial GaN layer (~10 μm).

It is of great importance not only to improve the material quality but also to improve the device structures and designs. There are three typical device structures: lateral, semi-vertical mesa and vertical, in GaN based Schottky diode. The early advances of GaN based Schottky diodes usually have the previous two structures because of the lack of native bulk GaN substrate. First concept of high barrier Schottky diode was presented by Wang *et al.* [36]. The prototype devices were fabricated on MOCVD grown GaN/sapphire substrate. Schottky and ohmic circular patterns were deposited on the un-doped GaN film by electron-beam evaporation. The devices had a lateral structure and exhibited Schottky characteristics. Performance of the devices was limited by the poor lateral conductivity. Bandić *et al.* applied mesa etching techniques and fabricated high breakdown voltage semi-vertical Schottky diodes on HVPE grown GaN/sapphire [37]. Schottky contacts were deposited on the mesa; while ohmic contacts were deposited on the bottom which is highly doped. The lateral conductivity was improved because the layer under the ohmic contact was highly doped. However, current transportation was still limited by the thickness of the epilayer. Zhou *et al.* fabricated vertical Schottky diodes on HVPE grown bulk substrate with ultrafast reverse recovery characteristics [38]. Un-doped GaN bulk substrate offered reverse blocking capability but sacrificed the forward on-state resistivity. Lu *et al.* improved the structure by depositing a MOCVD homoepitaxial layer onto a highly doped HVPE

GaN substrate [39]. Highly doped substrate offered low resistance while leakage current is suppressed by the intrinsic epilayer. However, the thickness of the epilayer was limited by the MOCVD growth. Xu *et al.* presented low leakage Schottky diode fabricated on all HVPE grown homoepitaxial epilayer on bulk substrate [40]. The single batch HVPE process can provide a smooth transition between the intrinsic layer and highly doped substrate. There is no limit of the thickness of the intrinsic layer either. The devices structures are shown in Figure 2.2 (a) - (e) sequentially.

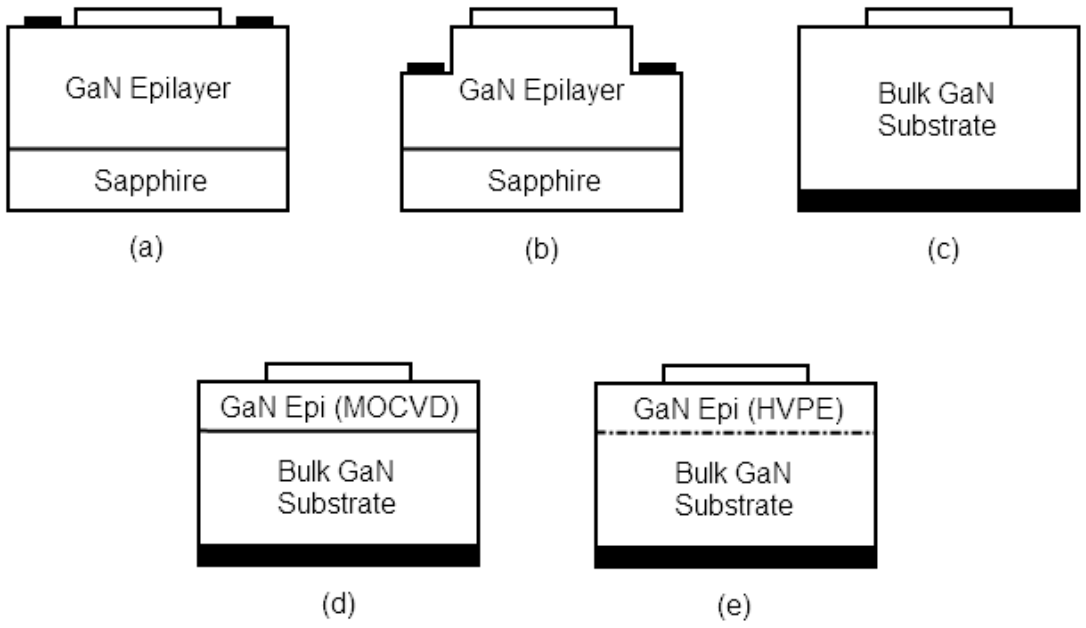

Figure 2.2 Schematics of GaN based Schottky diode device structures:

(a) Lateral structure (b) Semi-vertical structure by mesa-etching

(c) Vertical structure on HVPE bulk substrate

(d) Vertical structure of homoepitaxial MOCVD GaN epilayer on HVPE bulk substrate

(e) Vertical structure of single batch HVPE GaN epilayer on bulk substrate

The purpose of the edge termination is to smooth the distribution of the electric field around the contact periphery. Four methods, mesa, guard rings, field plates and high resistivity region by ion implantation can be used to reduce the chance of premature breakdown [41]. Zhu *el al.* reported high voltage mesa-structure GaN Schottky diode [42]. The mesa structure etched in two methods, photoelectrochemical etching and reactive ion etching. The devices showed good breakdown voltages. Dielectric field plate techniques can be utilized to reduce the electric field around the edge of the contact. Kang *et al.* reported temperature dependent characteristics of Schottky diodes fabricated on freestanding GaN [43]. The breakdown voltages of the devices ranged from 200 V to 250 V. Float metal rings (FMR), which can decrease the maximum electric field by expanding the depletion layer, is also effective in improving the devices performance under reverse bias. Lee *et al.* fabricated 750 V Schottky barrier diodes with multiple FMRs. The devices also showed good recovery characteristics at room and elevated temperatures [44]. The effectiveness of the p^+ guard rings has been proved by Zhang *et al.* as they successfully used this technique to improve the breakdown voltage of the GaN diodes from 2.3 kV to 3.1 kV [45]. Implanting high dose ion such as boron and argon at the contact periphery can create a thin layer with high resistivity which can cause the spread of the potential and reduction of the edge electric field. Baliga *el al.* showed this concept in SiC and fabricated diodes with 1000 V breakdown voltage [46]. Schematics of the edge termination techniques are shown in Figure 2.3 (a) - (e).

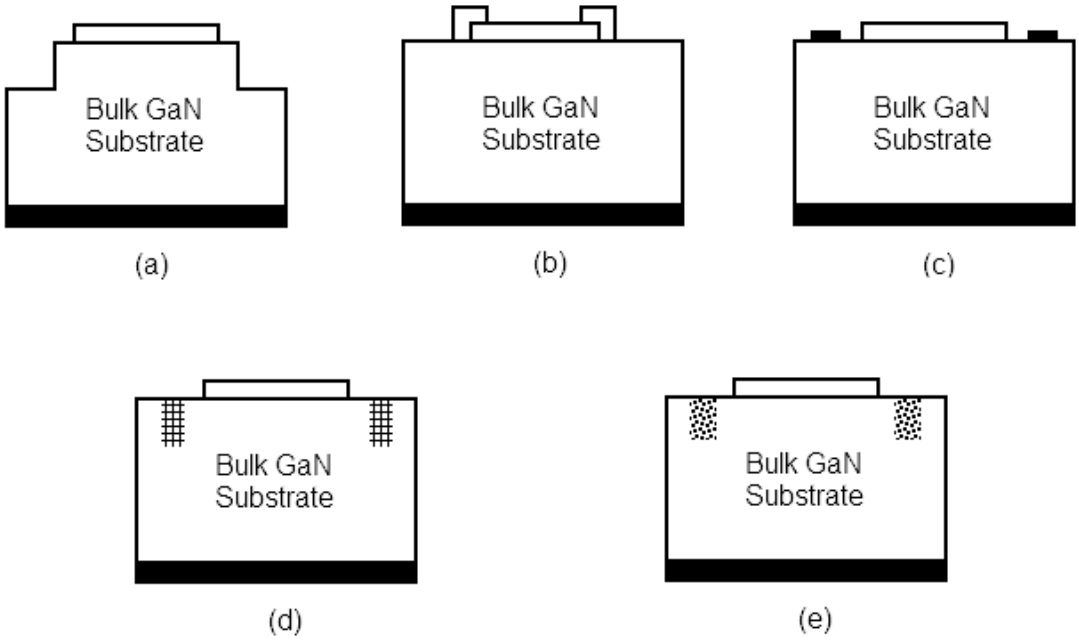

Figure 2.3 Schematics of edge termination techniques for GaN based Schottky diode

(a) Mesa (b) Dielectric field plate (c) Floating metal ring

(d) P^+ guard ring (e) High resistivity region by ion implantation

Metal contact to GaN also has a very important role in GaN Schottky diode. Good Schottky contact should exhibit a high barrier height and an ideality factor which is close to 1. Good ohmic contact should have a small contact resistance. Although Pt, Ni and Pd are proved to be good Schottky metals for n-type GaN because of their large work function, the Schottky contact on GaN is still far from ideal. First of all, the Richardson's constant varies from theoretical value significantly and the reported value covers a large range. Second, the barrier height measured by C-V is higher than that measured from I-V. Third, the ideality factors of the Schottky diodes are observed to be much larger than 1. Last but not least, C-V measurement shows a frequency dependent capacitance and flat band voltage [47]. Experimental results

confirmed that deposition of Schottky metal onto Ga face is preferred over N face for higher barrier height [48]. However, the Schottky metal/GaN interface is not yet fully understood. The typical ohmic contact metal for n-type GaN is Ti for its low work function as well as the TiN formation process. Low Schottky barrier height of Ti/GaN interface can behave like ohmic. When annealed at high temperature, N atoms from GaN can diffuse to the Ti metal layer to form TiN. N vacancies are thus formed at the ohmic contact interface. It is well known that N vacancies are donors. As a result, the contact region would be highly doped which facilitates the direct tunneling [49]. The ohmic contact usually has a multi-layer structure. Al also has work function that is close to GaN's electron affinity and it has been shown that Ti/Al alloy can provide the lowest contact resistance to n-type GaN [50]. A metal/Au bi-layer is used to protect Ti and Al from possible oxidation which can increase the contact resistance. The metal commonly used to prevent the interdiffusion of Ti/Al and Au are Ni, Ti, Pd, Pt, Mo, Re, Ir and Nb [51].

1.2 Temperature measurements of GaN devices

Precise temperature measurement of semiconductor devices is very important because it can help us to understand the device self-heating and discover hot spot locations. Typically, there are three general categories of temperature measurement methods: electrical, contact probe, and optical measurements.

The junction forward voltage is simple, and is probably the most commonly used electrical parameter for measuring the temperature of a semiconductor device. The relationship between the current, voltage and the temperature of a junction is given by the well-known relation:

$$I = I_s \left[\exp\left(\frac{qV}{kT}\right) - 1 \right]$$

Junction temperature can thus be extracted from I-V-T plot. This method has two major disadvantages: first, it lacks spatial resolution; second, ideal I-V characteristic is required to achieve good precision.

Contact probe method utilizes scanning thermal tips, which are modified from Atomic force microscopy (AFM) tips with a temperature sensitive element such as a thermocouple. This method potentially offers high spatial resolution which allows mapping of spatial variations of thermal properties of a sample, such as temperature, thermal conductivity, and diffusivity with sub-micrometer resolution. However, because the tip is in contact with the substrate, thermal equilibrium of the device may be disturbed.

Infra-red (IR) radiation is industrial standard of temperature measurement method for packaged chips. Infrared light is emitted from the device when it is under operation because of black body radiation. By measuring the total emitted radiation from the device, the temperature can be determined. This method is an excellent method in temperature mapping of a packaged chip. However, the major disadvantage of this method is its resolution, which is limited by the wavelength of the infrared light. Typical resolution of this method is about $3 - 5$ μm.

Raman spectroscopy is a technique, which is based on Raman scattering, to explore the vibrational, rotational modes of molecules and crystals. In Raman spectrum measurement, a high intensity monochromatic laser is used to illuminate the sample. Depending on the scattering geometry, reflective or transitional Raman spectrum can be collected. Two sets of lines can be observed in Raman spectrum: Stokes lines, in which the final state is higher than the initial state; and anti-Stokes lines, in which the final state is lower than the initial state. The Energy level diagram of the Raman scattering is shown in figure 2.4.

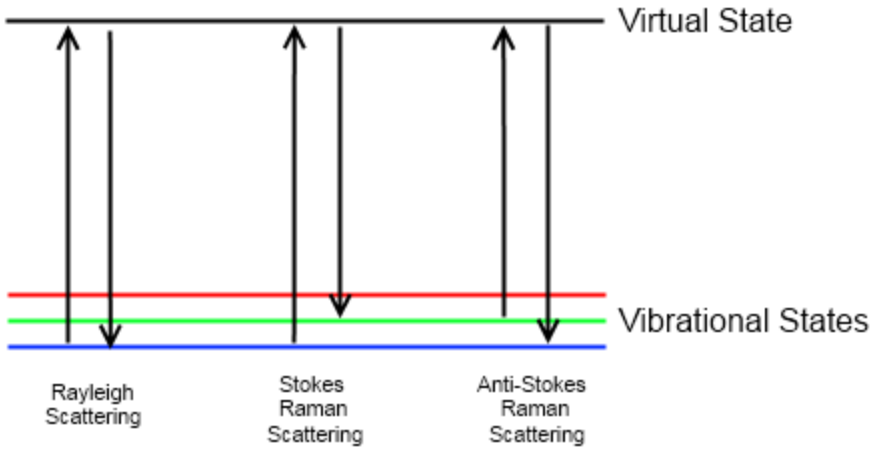

Figure 2.4 Energy level diagram of Raman Scattering

Raman spectroscopy measurement of device temperature is based on two mechanisms: first, the intensity ratio between the Stokes and the anti-Stokes line; second, shift of Raman peak and broadening of peak. The first method does not have good accuracy because of the large experimental error of Raman spectra intensity measurement. Micro-Raman spectroscopy method based on the measurement of the Raman peak shift upon temperature change can be used in determination of device temperature because of its high accuracy and high spatial resolution. For example, 1 μm spatial resolution and 10 °C temperature accuracy were achieved by micro-Raman spectroscopy for GaN-based Heterostructure field effect transistors (HFETs) [52,53]. Temperature determination of ultra-violet (UV) LED chips by Micro-Raman spectroscopy with good agreement with theory was reported [54,55]. The Raman spectroscopy is a non-contact, non-destructive and high resolution temperature measurement for semiconductor devices.

References:

[1] R. Singh, J. A. Cooper, Jr., M. R. Melloch, T. P. Chow, and J. W. Palmour, "SiC Power Schottky and PiN Diodes", IEEE Trans. Electron Devices **49**, 665 (2002).

[2] T. Kimoto, T. Urushidani, S. Kobayashi, and H. Matsunami, "High-Voltage (> 1 kV) Sic Schottky Barrier Diodes with Low On-Resistances", IEEE Electron Device Lett. **14**, 548 (1993).

[3] K. Shenai, R. S. Scott, and B. J. Baliga, "Optimum semiconductors for high-power electronics", IEEE Trans. Electron Devices **36**, 1811 (1989).

[4] D. D. Koleske, A. E. Wickenden, R. L. Henry, and M. E. Twigg, "Influence of MOVPE growth conditions on carbon and silicon concentrations in GaN", J. Cryst. Growth **242**, 55 (2002).

[5] E. G. Brazel, M. A. Chin, and V. Narayanamurti, "Direct observation of localized high current densities in GaN films", Appl. Phys. Lett. **74**, 2367 (1999).

[6] J. W. P. Hsu, M. J. Manfra, D. V. Lang, S. Richter, S. N. G. Chu, A. M. Sergent, R. N. Kleiman, L. N. Pfeiffer and R. J. Molnar, "Inhomogeneous spatial distribution of reverse bias leakage in GaN Schottky diodes", Appl. Phys. Lett. **78**, 1685 (2001).

[7] D. C. Look and R. J. Molnar, "Degenerate layer at GaN/sapphire interface: Influence on Hall-effect measurements", Appl. Phys. Lett. **70**, 3377 (1997).

[8] H. P. Maruska and J. J. Tietjen, "The Preparation and properties of Vapor - deposited single-crystal-line GaN", Appl. Phys. Lett. **15**, 327 (1969).

[9] W. M. Yim and R. J. Paff, "Thermal expansion of AlN, sapphire, and silicon", J. Appl. Phys. **45**, 1456 (1974)

[10] P. Waltereit, O. Brandt, A. Trampert, M. Ramsteiner, M. Reiche, M. Qi, and K. H. Ploog, "Influence of AlN nucleation layers on growth mode and strain relief of GaN grown on 6H–SiC(0001)", Appl. Phys. Lett. **74**, 3660 (1999).

[11] Y. Kato, S. Kitamura, K. Hiramatsu and N. Sawaki, "Selective growth of wurtzite GaN and $Al_xGa_{1-x}N$ on GaN/sapphire substrates by metalorganic vapor phase epitaxy", J. Cryst. Growth. **144**, 133 (1994).

[12] T. Suski, P. Perlin, H. Teisseyre, M. Leszczynski, I. Grzegory, J. Jun, M. Bockowski, S. Porowski and T. D. Moustakas, Appl. Phys. Lett. **67**, 2188 (1995).

[13] C. G. Van de Walle, C. Stampfl, and J. Neugebauer, "Theory of doping and defects in III–V nitrides", J. Cryst. Growth **189–190**, 505 (1998)

[14] J. Neugebauer and C. G. Van de Walle, "Role of hydrogen in doping of GaN", Appl. Phys. Lett. **68**, 1829 (1996).

[15] H. Tang, J. B. Webb, J. A. Bardwell, S. Raymond, and J. Salzman, "Properties of carbon-doped GaN",Appl. Phys. Lett. **78**, 757 (2001).

[16] P. Boguslawski, E. L. Briggs, and J. Bernholc, "Amphoteric properties of substitutional carbon impurity in GaN and AlN", Appl. Phys. Lett. **69**, 233 (1996).

[17] P. Visconti, K. M. Jones, M. A. Reshchikov, F. Yun, R. Cingolani, H. Morkoç, S. S. Park, and K. Y. Lee, "Characteristics of free-standing hydride-vapor-phase-epitaxy-grown GaN with very low defect concentration", Appl. Phys. Lett. **77**, 3743 (2000).

[18] A. Armstrong, A. R. Arehart, B. Moran, S. P. DenBaars, U. K. Mishra, J. S. Speck, and S. A. Ringel, Appl. Phys. Lett. **84**, 374 (2004).

[19] A. Hierro, D. Kwon, S. A. Ringel, M. Hansen, J. S. Speck, U. K. Mishra, and S. P. DenBaars, "Optically and thermally detected deep levels in n-type Schottky and p+-n GaN diodes", Appl. Phys. Lett. **76**, 3064 (2000).

[20] R. Zhang and T. F. Kuech, "Photoluminescence of carbon in situ doped GaN grown by halide vapor phase epitaxy", Appl. Phys. Lett. **72**, 1611 (1998).

[21] W. J. Moore, J. A. Freitas, Jr., G. C. B. Braga, R. J. Molnar, S. K. Lee, K. Y. Lee, and I. J. Song, "Identification of Si and O donors in hydride-vapor-phase epitaxial GaN", Appl. Phys. Lett. **79**, 2570 (2001).

[22] A. V. Fomin, A. E. Nikolaev, I. P. Nikitina, A. S. Zubrilov, M. G. Mynbaeva, N. I. Kuznetsov, A. P. Kovarsky, B. Ja. Ber, and D. V. Tsvetkov, "Properties of Si-Doped GaN Layers Grown by HVPE", Phys. Status Solidi A **188**, 433 (2001).

[23] E. V. Etzkorn and D. R. Clarke, "Cracking of GaN films", J. Appl. Phys. **89**, 1025 (2001)

[24] S. Pearton, *GaN and Related Materials II*, (Gordon and Breach, New York, 1999)

[25] S. Nakamura, Y. Harada, and M. Seno, "Novel metalorganic chemical vapor deposition system for GaN growth", Appl. Phys. Lett. **58**, 2021 (1991)

[26]C. Hemmingsson, P.P. Paskov, G. Pozina, M. Heuken, B. Schineller and B. Monemar, "Hydride vapour phase epitaxy growth and characterization of thick GaN using a vertical HVPE reactor", J. Cryst. Growth **300**, 32 (2007).

[27] K. Fujito, S. Kubo, H. Nagaoka, T. Mochizuki, H. Namita and S. Nagao, "Bulk GaN crystals grown by HVPE", J. Cryst. Growth **311**, 3011 (2009).

[28] T. Detchprohm, K. Hiramatsu, H. Amano, and I. Akasaki, "Hydride vapor phase epitaxial growth of a high quality GaN film using a ZnO buffer layer", Appl. Phys. Lett. **61**, 2688 (1992)

[29] K. Naniwae, S. Itoh, H. Amano, K. Itoh, K. Hiramatsu and I. Akasaki, "Growth of single crystal GaN substrate using hydride vapor phase epitaxy", J. Cryst. Growth **99**, 381 (1990).

[30] T. Paskova, E. Valcheva, J. Birch, S. Tungasmita, P.-O. Å. Persson, P. P. Paskov, S. Evtimova, M. Abrashev and B. Monemar, "Defect and stress relaxation in HVPE-GaN films using high temperature reactively sputtered AlN buffer", J. Cryst. Growth **230**, 381 (2001).

[31] A. Kasic, D. Gogova, H. Larsson, I. Ivanov, J. Birch, B. Monemar, M. Fehrer and V. Härle, "Highly homogeneous bulk-like 2″ GaN grown by HVPE on MOCVD–GaN template", J. Cryst. Growth **275**, e387 (2005).

[32] D. C. Reynolds, D. C. Look, B. Jogai, J. E. Hoelscher, R. E. Sherriff and R. J. Molnar, "Strain variation with sample thickness in GaN grown by hydride vapor phase epitaxy", J. Appl. Phys. **88**, 1460 (2000).

[33] Z. -Q. Fang, D. C. Look, J. Jasinski, M. Benamara, Z. Liliental-Weber and R. J. Molnar, "Evolution of deep centers in GaN grown by hydride vapor phase epitaxy", Appl. Phys. Lett. **78**, 332 (2001).

[34] T. Paskova, V. Darakchieva, P. P. Paskov, U. Södervall and B. Monemar, "Growth and separation related properties of HVPE-GaN free-standing films", J. Cryst. Growth **246**, 207 (2002).

[35] W. S. Wong, T. Sands, and N. W. Cheung, "Damage-free separation of GaN thin films from sapphire substrates", Appl. Phys. Lett. **72**, 599 (1998).

[36] L. Wang, M. I. Nathan, T.-H. Lim, M. A. Khan, and Q. Chen, "High barrier height GaN Schottky diodes: Pt/GaN and Pd/GaN", Appl. Phys. Lett. **68**, 1267 (1996).

[37] Z. Z. Bandić, P. M. Bridger, E. C. Piquette, T. C. McGill, R. P. Vaudo, V. M. Phanse, and J. M. Redwing, "High voltage (450 V) GaN Schottky rectifiers", Appl. Phys. Lett. **74**, 1266 (1999).

[38] Y. Zhou, M. Li, D. Wang, C. Ahyi, C.-C. Tin, J. Williams, M. Park, N. M. Williams, and A. Hanser, “Electrical characteristics of bulk GaN-based Schottky rectifiers with ultrafast reverse recovery”, Appl. Phys. Lett. **88**, 113509 (2006).

[39] H. Lu, R. Zhang, X. Xiu, Z. Xie, Y. Zheng, Z. Li, "Low leakage Schottky rectifiers fabricated on homoepitaxial GaN", Appl. Phys. Lett. **91**, 172113 (2007).

[40] “Electrical characteristics of low leakage Schottky rectifiers based on all hydride vapor phase epitaxy grown homoepitaxial layer and a bulk GaN wafer”

[41] J. R. LaRoche, F. Ren, K. Baik, S. J. Pearton, B. Shelton, and B. Peres, “Design of edge termination for GaN power Schottky diodes”, J. Electron. Mater. **34**, 370 (2005).

[42] T. G. Zhu, D. J. H. Lambert, B. S. Shelton, M. M. Wong, U. Chowdhury, and R. D. Dupuis, "High-voltage mesa-structure GaN Schottky rectifiers processed by dry and wet etching", Appl. Phys. Lett. **77**, 2918 (2000).

[43] B. S. Kang, F. Ren, Y. Irokawa, K. W. Baik, S. J. Pearton, C. C. Pan, G. T. Chen, J. I. Chyi, H. J. Ko, and H. Y. Lee, "Temperature dependent characteristics of bulk GaN Schottky rectifiers on free-standing GaN substrates", J. Vac. Sci. Technol. B **22**, 710 (2004).

[44] S. Lee, M. Ha, J. Lim, J. Her, K. Seo and M. Han, "Suppression of Leakage Current of Ni/Au Schottky Barrier Diode Fabricated on AlGaN/GaN Heterostructure by Oxidation", Jpn. J. Appl. Phys. **45**, 3398 (2006)

[45] A. P. Zhang, G. Dang, F. Ren, J. Han, A. Y. Polyakov, N. B. Smirnov, A. V. Govorkov, J. M. Redwing, X. A. Cao, and S. J. Pearton, "Al composition dependence of breakdown voltage in $Al_xGa_{1-x}N$ Schottky rectifiers", Appl. Phys. Lett. **76**, 1767 (2000).

[46] D. Alok and B. J. Baliga, "SiC device edge termination using finite area Argon implantation", IEEE Trans. Electron Devices **44**, 1013 (1997).

[47] Q. Z. Liu and S. S. Lau, “A review of the metal–GaN contact technology”, Solid-State Electron. **42**, 677 (1998).

[48] Z. -Q. Fang, D. C. Look, P. Visconti, D. -F. Wang, C. -Z. Lu, F. Yun, H. Morkoc, S. S. Park and K. Y. Lee, “Deep centers in a free-standing GaN layer”, Appl. Phys. Lett. **78**, 2178(2001).

[49] M. E. Lin, Z. Ma, F. Y. Huang, Z. F. Fan, L. H. Allen, and H. Morkoç, "Low resistance ohmic contacts on wide band-gap GaN", Appl. Phys. Lett. **64**, 1003 (1994).

[50] A. Motayed, R. Bathe, M. C. Wood, O. S. Diouf, R. D. Vispute, and S. N. Mohammad, "Electrical, thermal, and microstructural characteristics of Ti/Al/Ti/Au multilayer Ohmic contacts to n-type GaN", J. Appl. Phys. **93**, 1087 (2003).

[51] F. M. Mohammed, L. Wang, and I. Adesida, "The role of barrier layer on Ohmic performance of Ti/Al-based contact metallizations on AlGaN/GaN heterostructures", J. Appl. Phys. **100**, 023708 (2006).

[52] M. Kubal, S. Rajasingam, A. Sarua, M. J. Uren, T. Martin, B. T. Hughes, K. P. Hilton, and R. S. Balmer, “Measurement of temperature distribution in multifinger AlGaN/GaN heterostructure field-effect transistors using micro-Raman spectroscopy”, Appl. Phys. Lett. **82**, 124 (2003).

[53] M. Kuball, J. M. Hayes, M. J. Uren, T. Martin, J. C. H. Birbeck, R. S. Balmer, and B. T. Hughes, “Measurement of temperature in active high-power AlGaN/GaN HFETs using Raman spectroscopy”, IEEE Electron Device Lett. **23**, 7 (2002).

[54] V. Schwegler, S. S. Schad, C. Kirchner, M. Seyboth, M. Kamp, K. J. Ebeling, V. E. Kudryashov, A. N. Turkin, A. E. Yunovich, U. Stempfle, A. Link, W. Limmer, and R. Sauer,

"Ohmic Heating of InGaN LEDs during Operation: Determination of the Junction Temperature and Its Influence on Device Performance", Phys. Status Solidi A **176**, 783 (1999).

[55] A. Chitnis, J. Sun, V. Mandavilli, R. Pachipulusu, S. Wu, M. Gaevski, V. Adivarahan, J. P. Zhang, M. Asif Khan, A. Sarua, and M. Kuball, "Measurement of temperature distribution in multifinger AlGaN/GaN heterostructure field-effect transistors using micro-Raman spectroscopy", Appl. Phys. Lett. **81**, 3491 (2002).

Chapter Three

Device Fabrication and Characterization

3.1 Wafer dicing

The thickness of the freestanding wafer used in this fabrication is approximately 400 μm, and the dimension of wafer is about 10mm×10mm. The wafer needs to be diced into 4 5mm×5mm individual pieces in order to match the size of the photomask layout pattern.

The initial attempt was to separate the wafer is scratching vertical and horizontal lines using a diamond pencil and then breaking along the line. The attempt is unsuccessful due to two reasons: first, this technique showed a large cutting width and a rough cutting edge; second, separation along the scratching lines was difficult because of the anisotropy mechanical properties of wurtzite GaN wafer grown along c-axis.

Automated dicing machine (Assembly Technologies' Micro Automation 1500 wafer dicing saw) was then used. The machine utilizes a closed-circuit monitoring system with two split images to align the wafer before dicing. It is very important to choose the dicing blade to achieve small cutting width and smooth edge. Resin bond diamond blade is usually used to dice hard and brittle materials such as SiC, while sintered diamond blade is usually used to dice soft materials such as Si. It has been reported that the hardness of GaN is 10.8 GPa, which is comparable to Si at room temperature [1]. A Kulicke & Soffa sintered blade and a Dicing Blade

Technology resinoid blade were tested. The sintered blade at the same dicing condition showed a smaller cut width as well as a smoother cut edge.

Because the small size of the wafer, it is also important to choose right dicing parameters. The most important parameters are the spindle speed and the forward cutting speed. The typical parameters for large size (2", 3") silicon wafers are 25,000 revolutions per minute (RPM) and 100 mil/sec. However, dicing of GaN wafer using this condition created broken edges. The spindle speed and the forward cutting speed were then reduced to 20,000 RPM and 40 mil/sec separately, to suppress chipping.

3.2 Cleaning

The purpose of the cleaning process is to remove organic, ionic contaminants and native oxide. The GaN cleaning recipe is modified from the standard RCA cleaning. The cleaning process is carried out in a fume hood which is shown in figure 3.1. Each of the organic cleaning steps takes five minutes in an ultrasonic cleaner. The GaN sample is first immersed in acetone to degrease and then treated using Trichloroethylene (TCE) for further cleaning. A second acetone immersion removes the TCE residue. The sample is then immersed in methanol to dissolve acetone residue. The last methanol is used for complete removal of organic solvents. The sample is then well rinsed in deionized (DI) water and ready for ionic contaminants and native oxide removal. It has been reported that HCl/H_2O is an effective etchant of Ga_2O_3 [2]. The sample is then immersed in a heated (~100 °C) dilute HCl and DI H_2O solution at a 1:1 mix ratio. After treated in the solution for 10 minutes, the sample is rinsed again in DI water and blow-dried using N_2 gas.

Figure 3.1 Fume hood for sample cleaning

3.3 Photolithography

A key step of the fabrication processes is to transfer patterns from photo-masks to the substrates. Photolithography process consists of five steps: photoresist application, soft baking, mask alignment, exposure and development. The 5mm×5mm substrate is first attached to a mechanical support, usually a 3” silicon wafer, using silver paste. The image reversal photoresist AZ5214E, which is capable for both positive and negative applications, is then spin coated on the substrate at 4,000 RPM for 30 seconds. The high spin speed is to reduce the photoresist crowding at the corner of the substrate. The average thickness of the photoresist is approximately 1.5 μm. Figure 3.2 shows the Karl Suss MJB3 manual photo-mask aligner which is used in mask alignment and UV exposure.

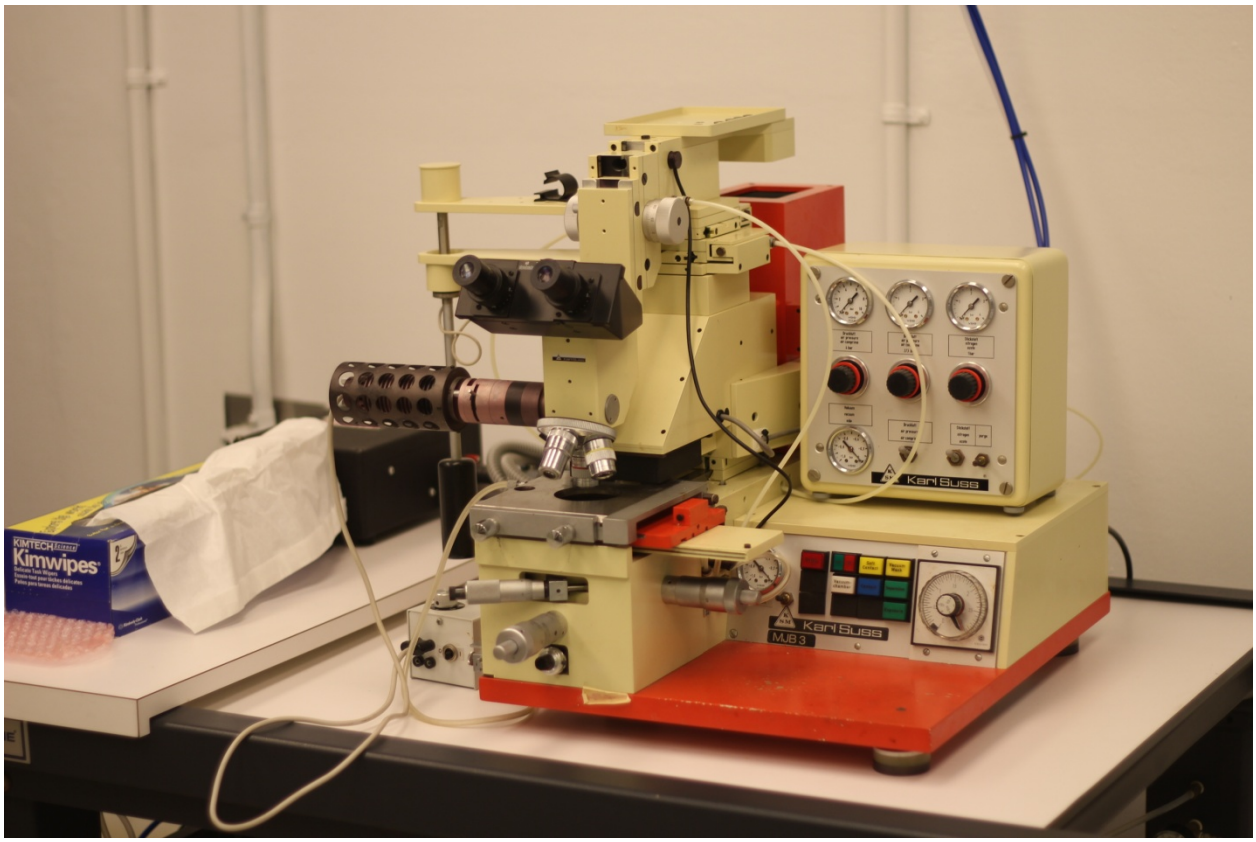

Figure 3.2 Karl Suss MJB3 photo-mask aligner

There are two typical categories of photo-masks: dark field masks, which have an opaque background and clear images; clear field masks, which have a clear background and opaque images. Both masks involve in the fabrication process. To transfer clear images on the substrate, a normal positive function of the photoresist is used. The photoresist first undergo a soft bake at 100 °C for 60 seconds, followed by a UV contact exposure through a dark field photo-mask for 30 seconds. The substrate is then developed in a 1:4 diluted AZ 400K developer for about 25 seconds. To transfer opaque images on the substrate, the negative capability is obtained through image reversal. The photoresist first undergo a soft bake at 100 °C for 60 seconds, followed by a UV contact exposure through a clear field photo-mask for 30 seconds, a thermal curing at 110 °C for 60 seconds, and then a UV flush exposure for 60 seconds. The development time for image reversal process is about 120 seconds.

3.4 Sputtering

DC magnetron sputtering system is used to deposit thin metal contacts onto the GaN substrate. During sputtering, ions of inert gas are accelerated in an electric field. The sputter atoms are then ejected from the target by the ion bombardment, and deposited onto the sample surface. Sputtering can provide better step coverage than electron-beam evaporation and has less radiation damage. The custom designed direct current (DC) magnetron sputtering system used in the fabrication process is shown in figure 3.3. The sputtering system has a vacuum chamber, a DC power supply and four sputtering guns, each of which is equipped with a chimney to guide the deposition and to prevent cross-contamination of the targets. The samples are mounted on the top rotational plate. The distance between the target and the sample is about 15 cm.

The vacuum chamber is first pumped down to a base pressure of 8×10^{-8} Torr to remove the atmospheric contaminants. Argon gas is then introduced to the chamber at a flow rate of 106.4 sccm. The pressure of the chamber is then stabilized at 20 mTorr for 5 minutes. A high voltage is applied between the anode and cathode to ignite plasma. A ring magnet is embedded underneath each of the target holders for two purposes. First, electrons and ions can be confined near the surface of the target to increase the plasma density, which can increase the sputtering rate. Second, overlap of atoms generated along the ring can increase the deposition throughput. Prior to deposition, a pre-sputtering process is used to remove trapped impurities at the surface of the targets. Depending on the metal, this process can vary from 30 seconds to 5 minutes. After pre-sputtering, the sample is placed right above the sputtering gun. A thin metal film is deposited on the surface of the sample.

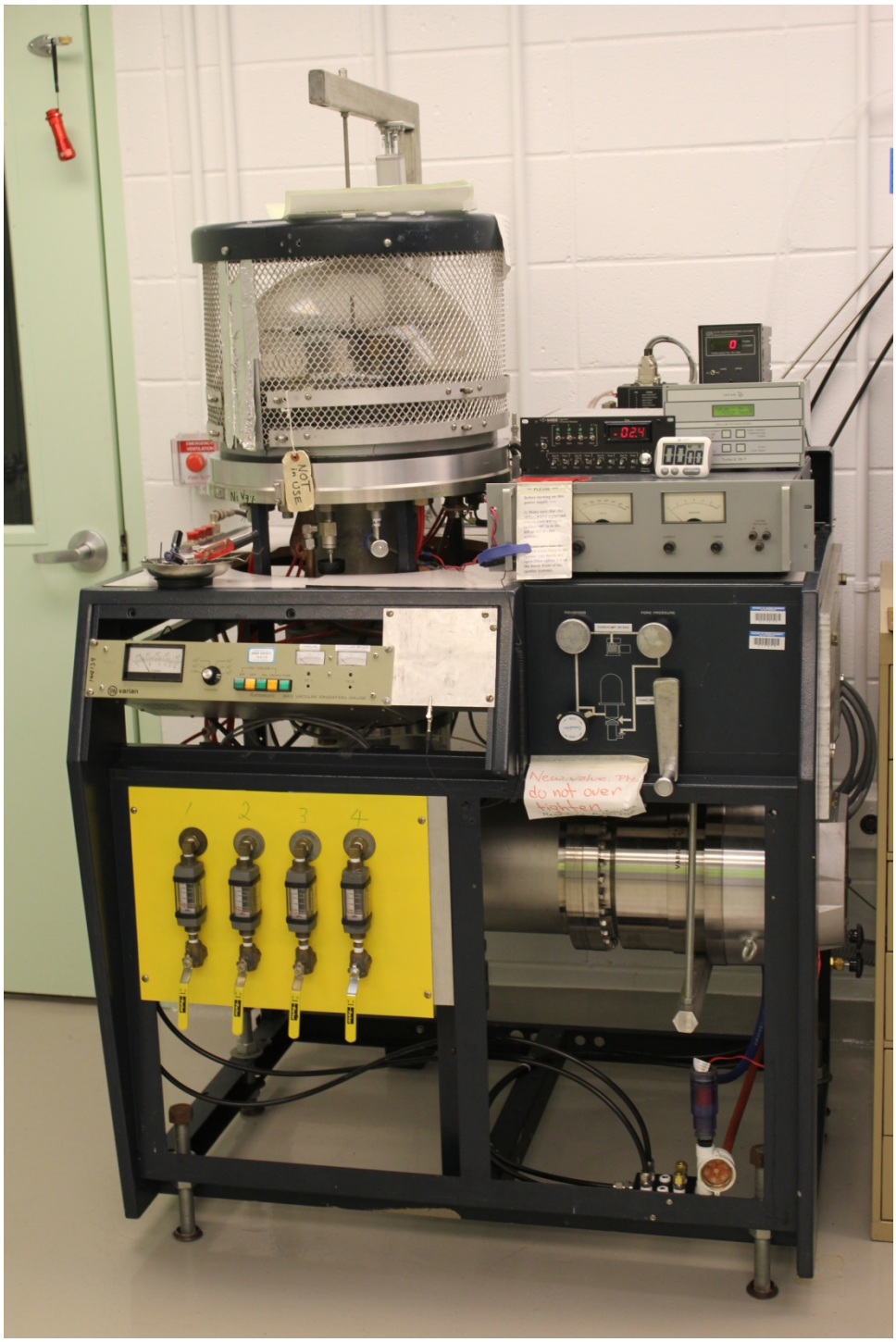

Figure 3.3 DC magnetron sputtering system

3.5 Rapid thermal annealing

Rapid thermal annealing (RTA) is used to form low resistance ohmic contact. By using high intensity lamps, or contact heating strips, RTA system can heat the sample to a high temperature within a short time. Multi layer metal films can thus alloy with the semiconductor material during the atom inter-diffusion process. The electrical properties of the metal-semiconductor interface are changed accordingly. Figure 3.4 shows the custom built RTA system in the fabrication, which consists of a vacuum chamber, a carbon strip heater and an infrared (IR) pyrometer.

The sample is first placed on the top of the carbon strip. In fabrication of vertical devices (i.e., the ohmic and Schottky contacts are on the different sides), the ohmic contact is kept contact with the carbon strip to facilitate heat transferring. In fabrication of lateral devices (i.e., the ohmic and Schottky contacts are on the same side), the ohmic contact is not in contact with the carbon strip in order to reduce carbon impurities. The IR pyrometer is focus on the carbon strip near the sample to monitor temperature. The reason is that pyrometer is calibrated using blackbody emission. Focusing IR pyrometer on the black carbon strip can provide better accuracy than focusing on the sample. After sample loading, the system is then pumped down to a base pressure of 2×10^{-7} Torr to remove possible contaminants. The system is then flushed with research grade N_2 gas. After the atmospheric pressure is reached and stabilized for 15 minutes in the vacuum chamber, the temperature of the carbon strip is elevated to a desired value within 10 seconds by introducing a large current. During the cooling process, the N_2 gas continues to flow into the chamber and brings the temperature back to the room temperature in approximately 10 minutes.

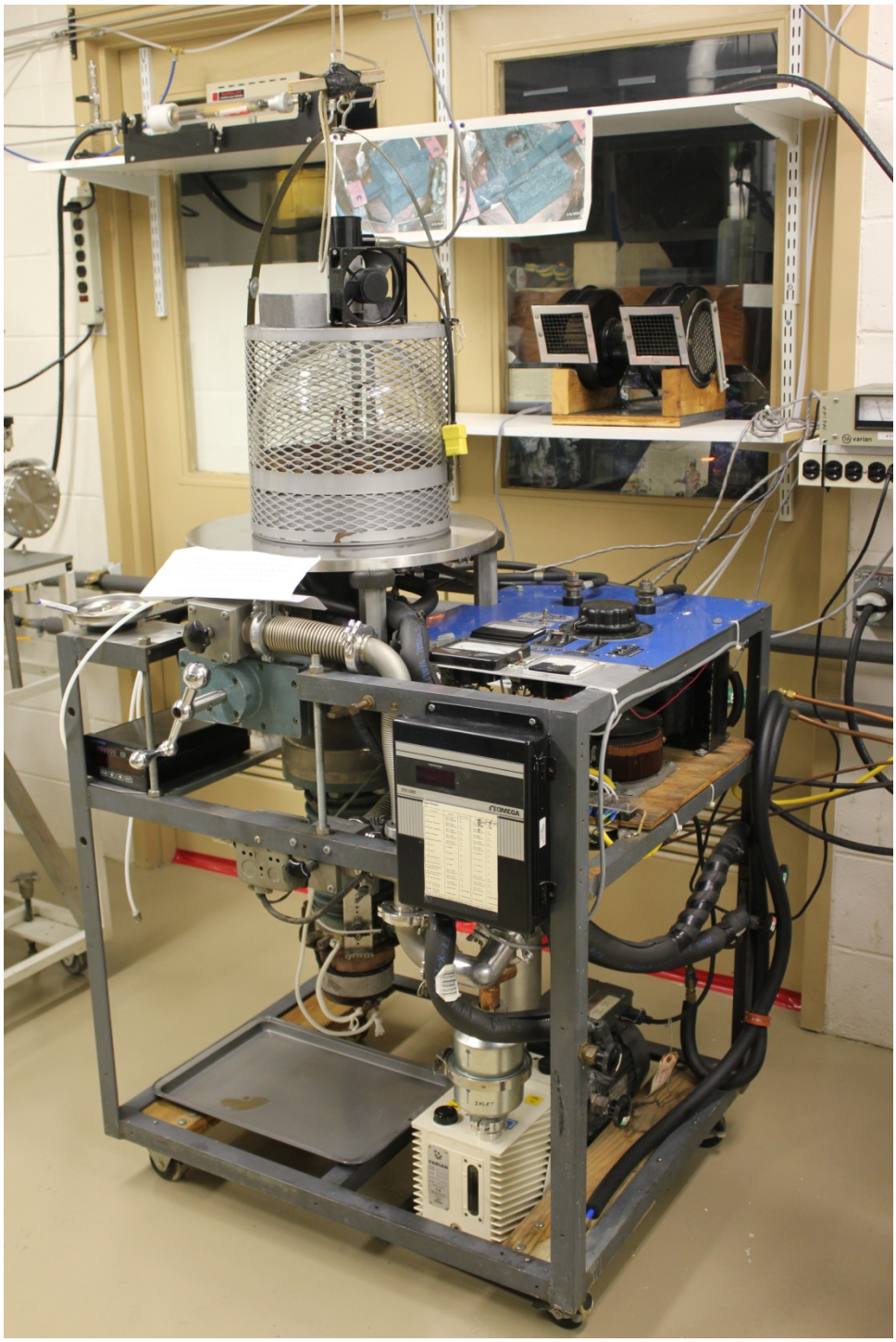

Figure 3.4 Rapid thermal annealing system

3.6 Reactive ion etching

Reactive ion etching (RIE) is widely used in GaN processing first because GaN is chemically stable and hard to process by wet etching techniques. The second reason is reactive ion etching can provide anisotropic etching profile. In an RIE process, the sample is usually placed on an isolated platter located in the center of a grounded vacuum chamber. Plasma of corrosive gases is then ignited by applying an RF electromagnetic field. An electric potential difference is then built between the plasma and the platter. The reactive ions are then accelerated along the electric field and collide with the surface of the sample. This process results in both physical and chemical etch. The custom made RIE system used in the fabrication process is shown in figure 3.5. The system is comprised of a cylindrical vacuum chamber, an isolated platter, an RF power supply with 13.65 MHz operating frequency (Advanced Energy's RFX-600) and an impedance matching unit (Advanced Energy's ATX-600).

The sample is prepared and loaded on the platter. Either photoresist or nickel thin film can be used as protective mask. The vacuum chamber is then pumped down to base pressure of 15 mTorr in 30 minutes. A reactive gas, which consists of 70% Ar and 30% Cl_2, is then introduced to the chamber at a flow rate of 12 sccm. The active constituent of the reactive gas is chlorine, while argon acts as carrying gas. After the pressure of the chamber stabilized at 56 mTorr for about 5 minutes, the RF power supply is turned on to initiate plasma. The forward etching power is set as 30 W. The impedance matching unit is then adjusted to minimize reflection power. A voltage difference from -150 V to -180 V is then gradually built between the chamber and the platter as the etching process goes on. Under the condition listed above, the etching rate of GaN substrate is determined as 2.5 μm/hour.

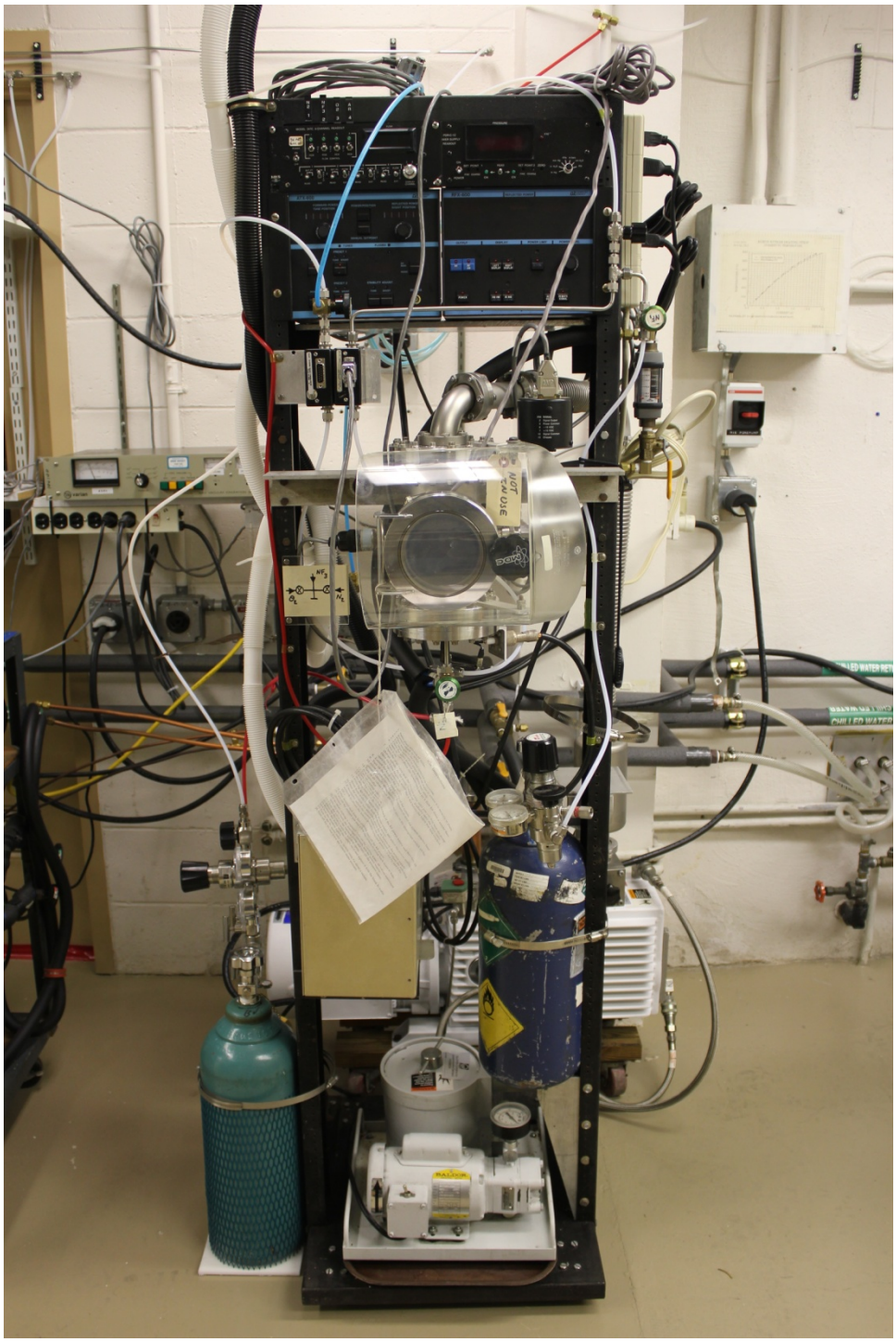

Figure 3.5 Reactive ion etching system

3.7 Lift-off

In a lift-off process, a pattern is defined by photolithography. A metallic film is then deposited onto the photoresist, which serve as a sacrificial layer. The photoresist under the metal film is dissolved with organic solvent (usually Acetone), leaving only the metallic film deposited on the substrate. The lift-off procedures are shown in figure 3.6.

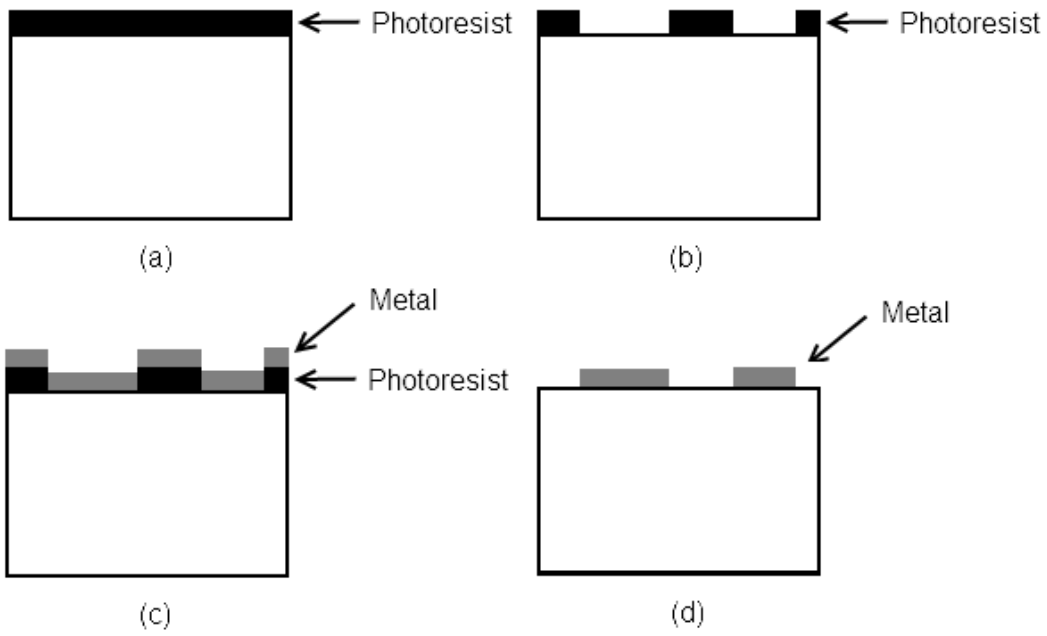

Figure 3.6 Lift off procedures: (a) Photoresist spin coating (b) Photolithography (c) Metal thin film sputtering (d) Photoresist removal by Acetone

3.8 High field and low field current-voltage measurement

Current-voltage measurement is a necessary tool to characterize the performance of the devices and to extract parameters such as Schottky barrier height, ideality factor and series resistance. The principle is simple: voltage is applied to the device, and the passing through current is measured. Both high field and low field I-V measurements are important because low field I-V system has a good accuracy to detect small current, while high field I-V system offers a wider measurement range.

Figure 3.7 shows the high field I-V measurement system which comprises of a Keithley 2410 Sourcemeter and a probe station. It can provide a voltage up to 1100 V and measure a current up to 1.05 A. The maximum source power is 22 W. The high voltage measurements of the devices are done in Fluorinert electric liquid to avoid spark formation.

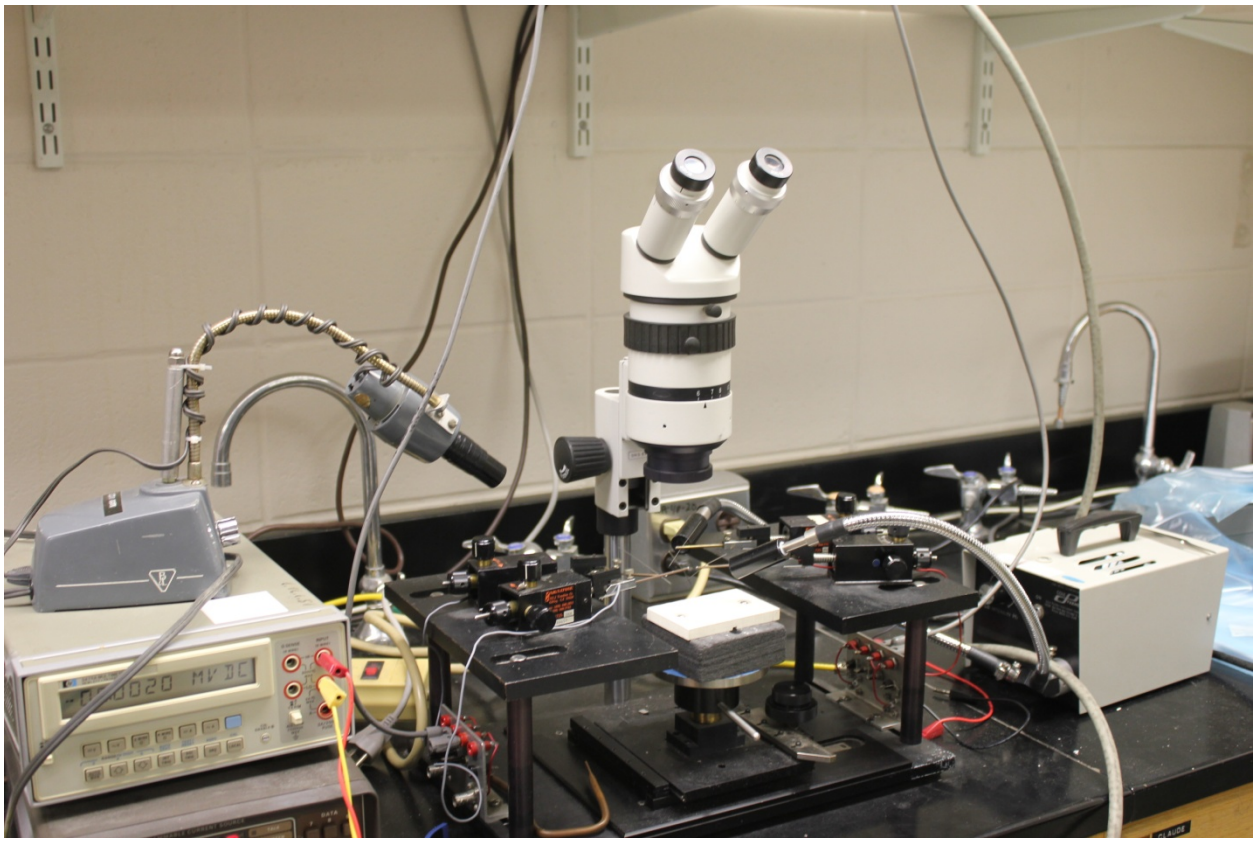

Figure 3.7 High field I-V measurement system

Figure 3.8 shows the low field I-V measurement system which comprises of a Keithley 6517 Electrometer, a 6487 Picoammeter, a metallic shield box, a UV light source, and a probe station with a ThermoCraft heater. Keithley 6517 Electrometer has a maximum current measurement capability of 10 mA and accuracy of 10 fA. Keithley 6487 Picoammeter can measure current ranging from 20 fA to 20 mA. The function of the shielding box is isolating the measurement system from the outside electromagnetic fields as well as keeping the probe station at a dark environment to reduce the light induced current. The heater, which can heat up to approximately 300 °C, enables temperature dependent I-V measurement. The deuterium/tungsten UV light source (DT 1000CE, Analytical Instruments, Inc.) is used for photocurrent measurement.

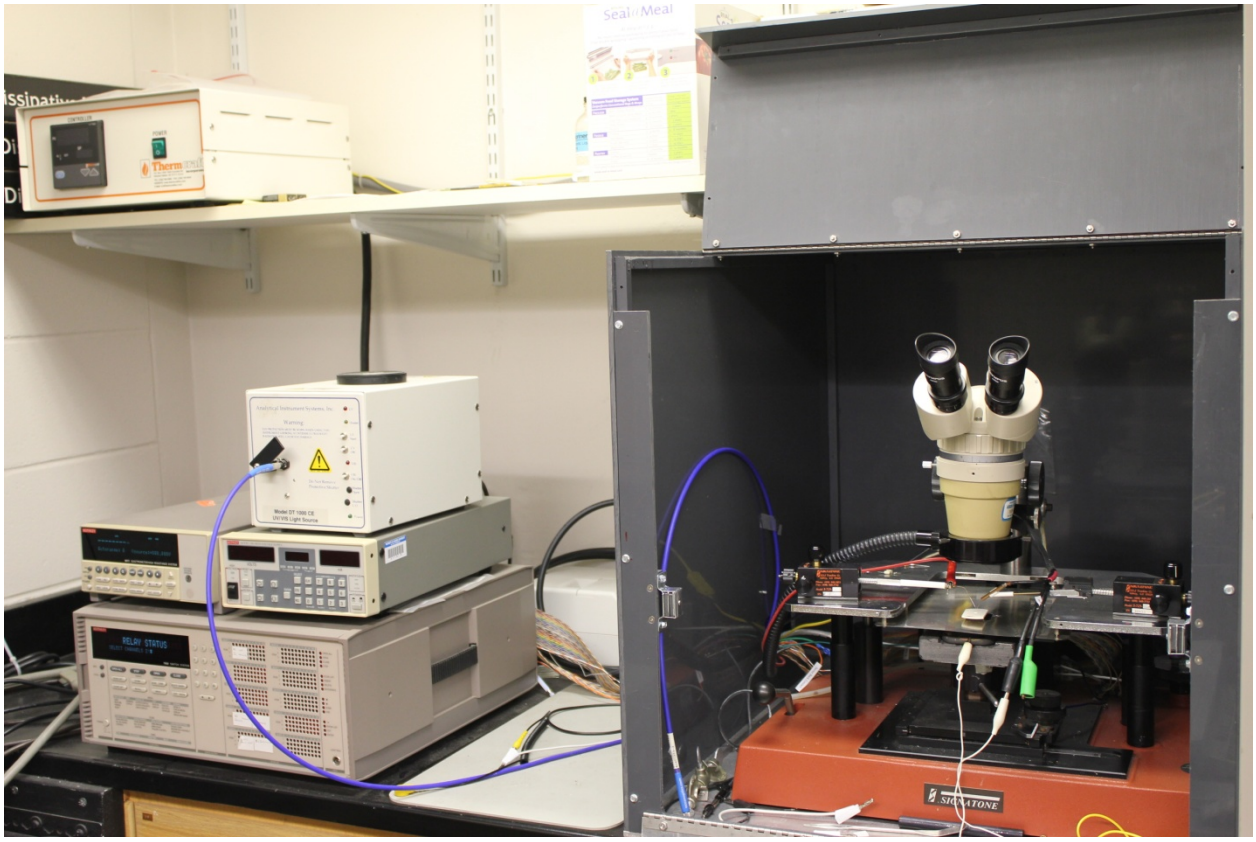

Figure 3.8 Low field I-V measurement system

3.9 Capacitance-voltage measurement

The Capacitance voltage measurement in generally used to determine the carrier concentration of the semiconductor material. The C-V technique is based on that the width of a space-charge region (SCR) depends on the applied reverse bias. A small AC voltage with high frequency is superimposed to determine the differential capacitance.

Figure 3.9 shows the C-V measurement system which comprises of a Keithley 595 Quasistatic CV meter, a Keithley 590 CV analyzer, a Keithley 230 voltage source and a shielded probe station. The system can provide both quasistatic and high frequency C-V characteristics. The amplitude of the AC signal is 10 mV and the frequency is 100 kHz. The C-V curve at high frequency measurement is more accurate because displacement current is dominant over the conductive leakage current in this case.

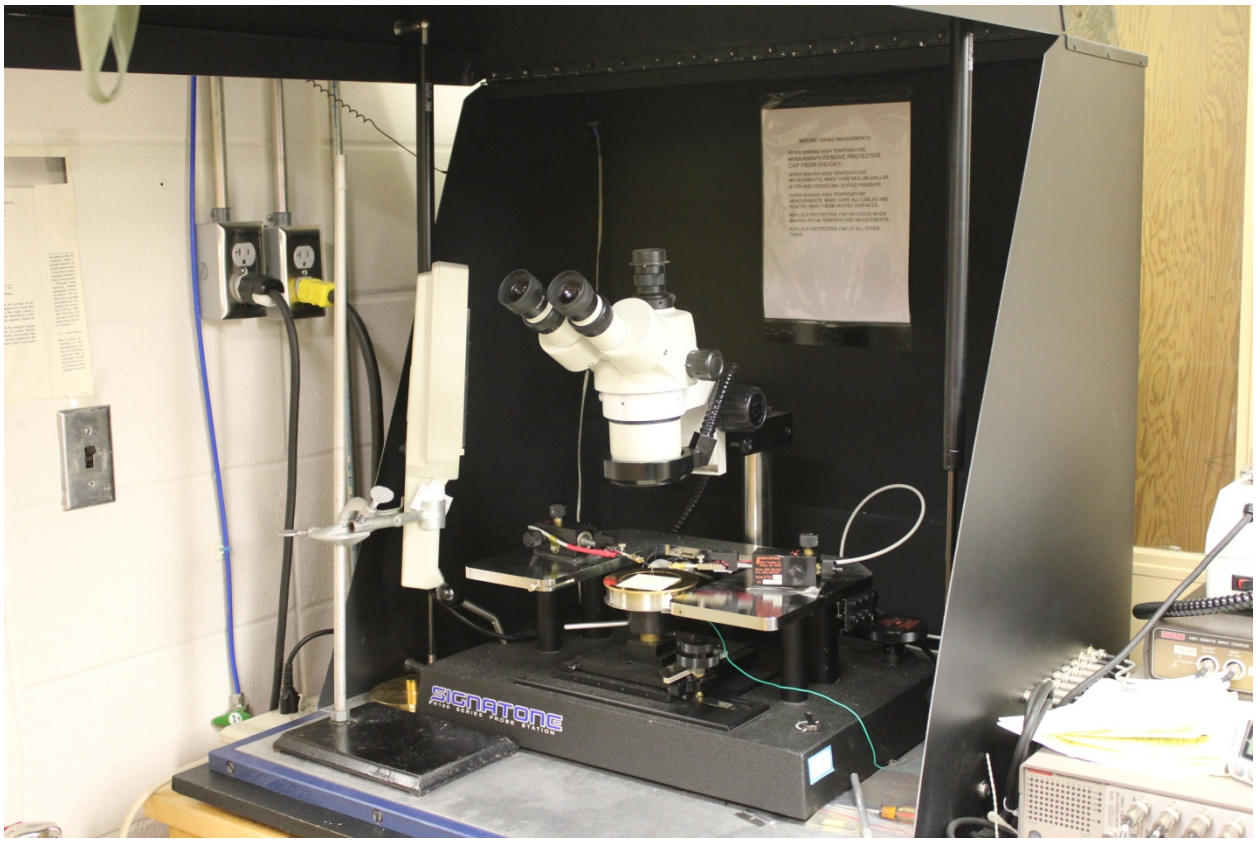

Figure 3.9 C-V measurement system

3.10 Raman spectroscopy and photoluminescence

Raman spectroscopy and photoluminescence (PL) are powerful optical characterization tools. Raman spectroscopy can be used to detect optical phonons, which are associated with basic material properties such as crystallographic structure and orientation. Photoluminescence is usually used to detect impurities and defects which can generate optically active deep energy levels. In Raman spectroscopy of semiconductor materials, photons from laser source interacts with optical phonons, resulting in down-shift (i.e., Stokes shift) or down-shift (i.e., Anti-Stokes Shift) of the frequency, which can be detected by Raman spectrometer. In a photoluminescence process, an incident laser beam excites electrons from a low energy level to a high energy level. The electrons then fall back to the original energy state and generate photons.

Figure 3.10 shows the Raman spectroscopy and photoluminescence system. The system has a Kimmon HeCd laser with two wavelengths: 441.563 nm (blue) and 325 nm (UV). The blue laser is used as an exciting source in Raman spectroscopy and the UV laser is used in the photoluminescence. The laser beam is guided through reflective mirrors and incident onto the sample. The laser spot has a diameter of ~5 μm when well focused. A Jobin Yvon spectrometer equipped with a thermal-electric cooled charge coupled device (CCD) is used to collect the Raman and PL signals. The Triax 550 spectrometer has a controllable slit entrance and two 3-inch holographic gratings of 2400 grooves/mm and 3600 grooves/mm. In Raman spectroscopy measurement, the slit size is set to 0.1 mm. The 2400 grooves/mm grating can offer a resolution of 1 cm^{-1} and the 3600 grooves/mm correspond to 0.2 cm^{-1} resolution. In PL measurement, grating of 2400 grooves/mm is usually used.

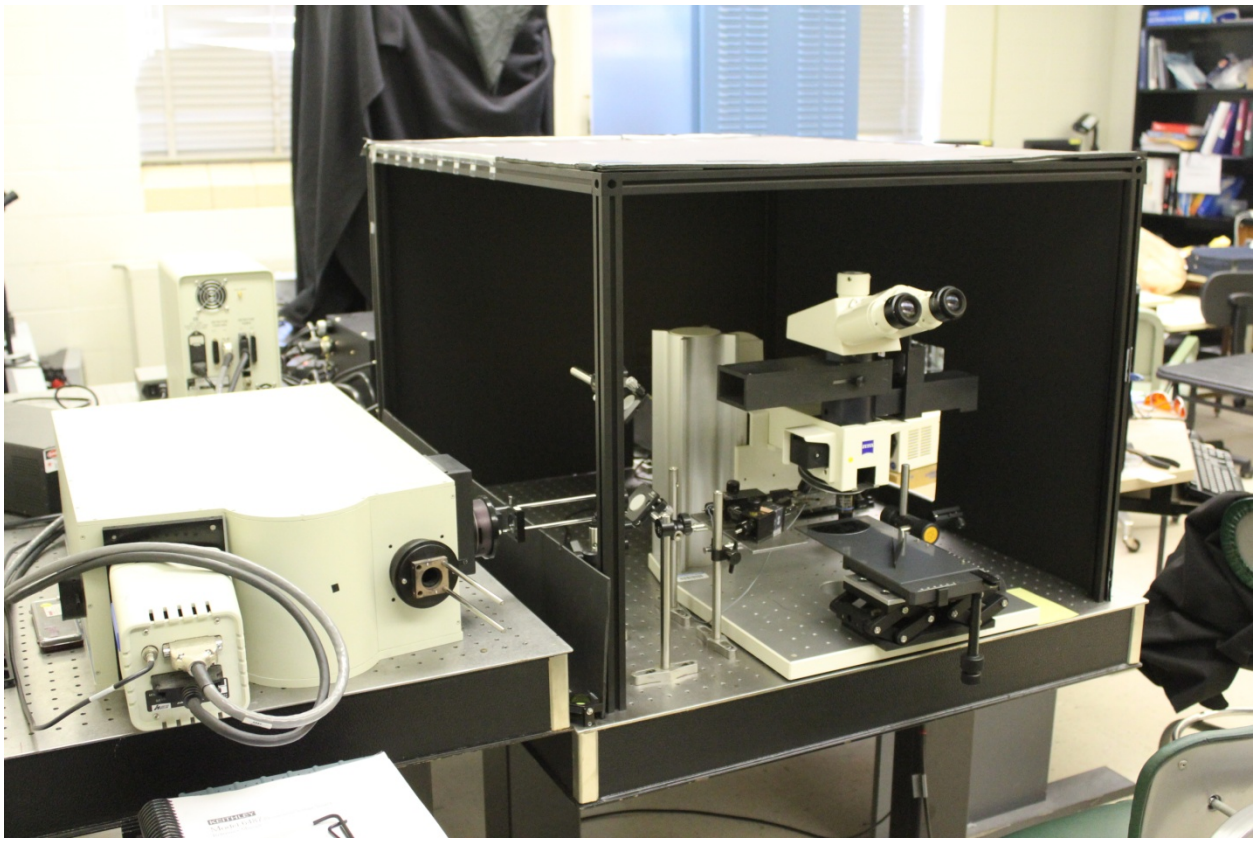

Figure 3.10 Raman spectroscopy and photoluminescence system

References

[1] I. Yonenaga, T. Hoshi, and A. Usui, “Hardness of Bulk Single-Crystal Gallium Nitride at High Temperatures”, Jpn. J. Appl. Phys. **39**, L200 (2000).

[2] S. W. King, J. P. Barnak, M. D. Bremser, K. M. Tracy, C. Ronning, R. F. Davis, and R. J. Nemanich, “Cleaning of AlN and GaN surfaces”, J. Appl. Phys. **84**, 5248 (1998).

Chapter Four

Ultra low leakage and high breakdown Schottky diodes fabricated on free-standing GaN substrate

4.1 Introduction

Because of its large band gap (3.4 eV), high breakdown field (3.0 MV/cm), high electron mobility (1250 $cm^2V^{-1}s^{-1}$), and high electron saturation velocity (2.5×10^7 cm/s), GaN is considered a promising substitute for current silicon solution in high power electronics. Due to their fast switching speed and low forward-voltage drop, GaN Schottky diodes have been studied extensively, and their breakdown voltage and reverse leakage current have both been improved remarkably. Schottky diodes with lateral device structure have been commonly fabricated on GaN grown on foreign substrate such as sapphire. Zhang *et al.* [1] reported lateral Schottky diode with 6350 V breakdown voltage. Bandić *et al.* [2] reported a leakage current density of 1×10^{-5} A/cm^2 at -100 V from lateral Schottky diodes with a field plate termination. In spite of the excellent reverse breakdown and leakage characteristics, the forward performances of the lateral devices are limited because of the poor thermal conductivity of the sapphire substrate. Vertical Schottky diodes became available in the past decade because both crystalline and surface qualities of bulk GaN substrate have been improved substantially. Zhou *et al.* [3] have achieved a reverse breakdown voltage of 630 V and Zhang *et al.* [4] have obtained a reverse breakdown voltage of 700 V. Lu *et al.* [5] have also reported vertical Schottky diodes fabricated on

homoepitaxial GaN substrate with leakage current less than 3×10^{-8} A on a 125×125 μm^2 contact, which is equivalent to a current density of 2×10^{-4} A/cm^2 at -100 V. Very recently, Saitoh *et al.* successfully fabricated GaN Schottky diode with world record figure of merit of 1.7GW/ cm^2 and reverse leakage of 8×10^{-4} A/cm^2 at reverse bias of 600V [6]. Suda *et al.* reported Schottky diode fabricated on HVPE grown GaN n- substrate near ideal I-V characteristics [7]. The Schottky diodes showed an ideality factor close to unity and reverse characteristics agreed well with thermionic field emission theory.

4.2 Experiment

Vertical Schottky diodes were fabricated on an n- GaN bulk substrate synthesized by hydride vapor phase epitaxy (HVPE) technique at Kyma Technologies. The substrate has a thickness of 447 μm, and the Ga face of the wafer was chemically and mechanically polished. The root mean square (rms) surface roughness of the Ga face over 380×380 μm^2 is about 0.93 nm, obtained by Veeco's optical profiler.

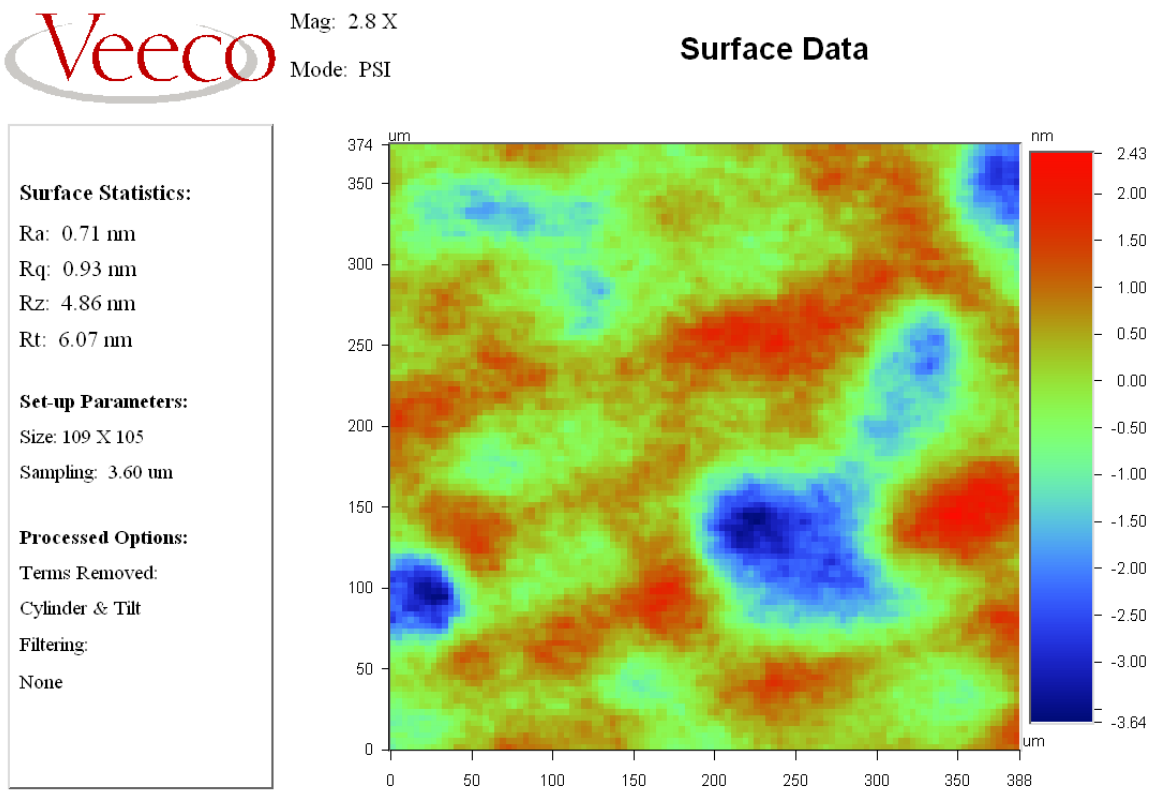

Figure 4.1 Optical profiler image of the Ga-face of the bulk GaN substrate

The X-ray diffraction measurement is carried out in Kyma Technologies. A full-width-at-half-maximum (FWHM) of the ω rocking curve from (0002) reflection is 598 arcsec, while the FWHM from the (10$\bar{1}$**Error! Bookmark not defined.**2) reflection is 351 arcsec. The ω rocking curves are shown in figure 4.2 (a) and (b).

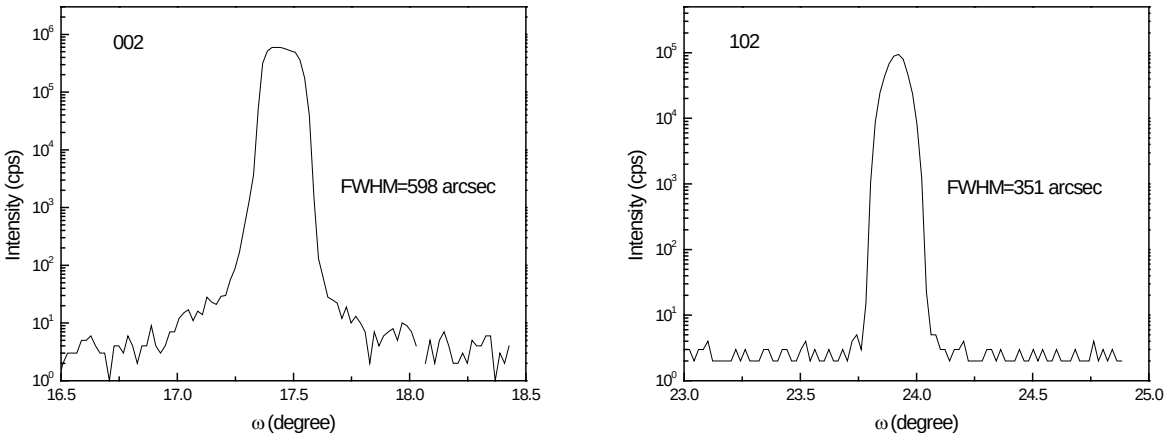

Figure 4.2 (a) ω rocking curve of (002) plane (b) ω rocking curve of (102) plane of the bulk GaN substrate

A near-band-edge emission peak at 368 nm (3.37 eV) with FWHM of 92 meV can be seen from photoluminescence (PL) spectrum collected at room temperature. Green luminescence (GL) was observed at 494 nm (2.51 eV). GL is caused by the transition from the conduction band or a shallow donor to a deep acceptor, which is probably associated with gallium vacancy-oxygen complex [8]. Reshchikov et al. also showed that the gallium vacancies are bound to structural defects such as threading dislocations [9]. The PL curve is shown in figure 4.3. The ratio of the intensity of the GL to that of the near-band-edge emission has a very low value of 0.031 and is associated with low edge and screw dislocations density [10].

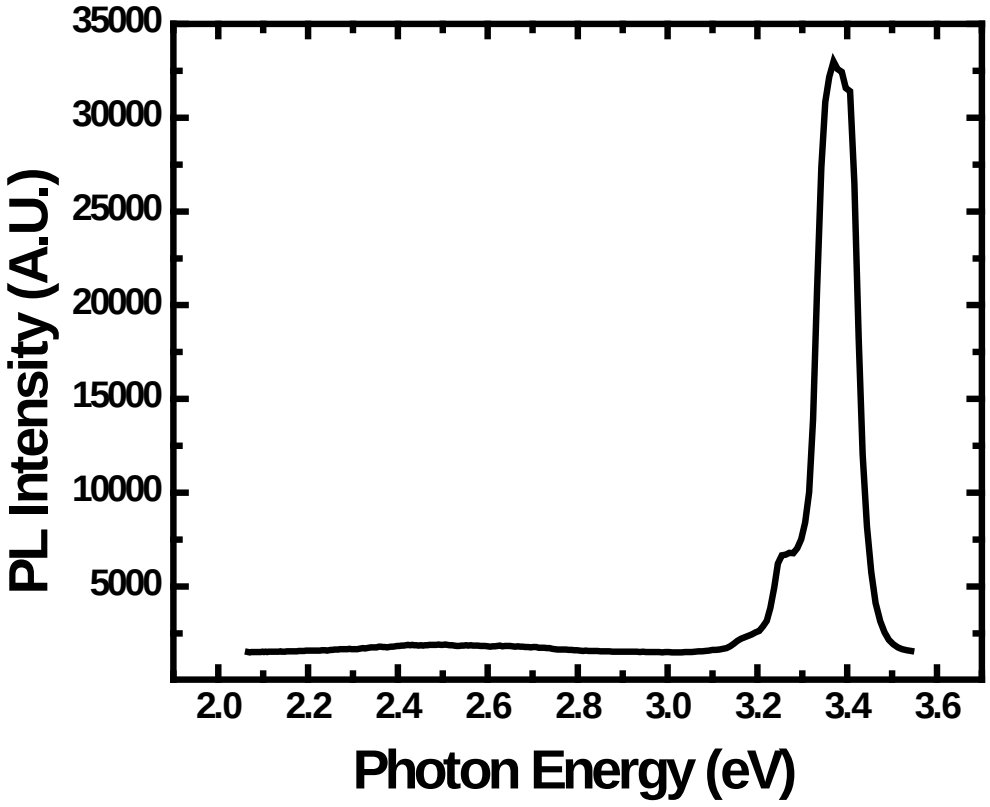

Figure 4.3 Photoluminescence spectrum of the bulk GaN substrate

It is well known that oxygen exhibits as shallow donor in GaN. Our study also showed that the concentration of oxygen impurities, which contributes to the unintentional n-type doping level of GaN, decreased over almost two orders of magnitude within the first 8 μm of thick GaN layers grown in polar direction [11]. A natural n-type doping level gradient was thus formed between the Ga-face and the N-face of the GaN substrate.

The GaN substrates were ultrasonically cleaned in the following organic solvents sequentially: acetone, trichloroethylene, acetone, methanol, and methanol (for 5 minutes in each chemical). Prior to the contact deposition, the surface of the substrate was cleaned with hydrochloric acid (HCl) solution. Ohmic contact of Ti (50 nm) /Al (100 nm) /Ni (50 nm) /Au (50

nm) was deposited on the N-face (backside) of the GaN wafer by DC magnetron sputtering in Ar ambient, followed by a rapid thermal annealing (RTA) in N_2 atmosphere at 750 °C for 30 seconds. Pt Schottky contact was deposited on the Ga-face after additional cleaning with solvents and HCl. The array of 100 nm thick circular Schottky contacts with 50 µm, 150 µm, and 300 µm in diameter was prepared. Figure 4.4 shows the Pt Schottky contacts deposited on the Ga-face of the bulk GaN substrate. Figure 4.5 shows the schematic diagram of the vertical GaN Schottky diodes. From the capacitance–voltage (C-V) measurement, a Schottky barrier height of 1.1 eV and an n-type unintentional doping concentration of $2.8\times10^{16}/cm^3$ were determined, which is shown in figure 4.6.

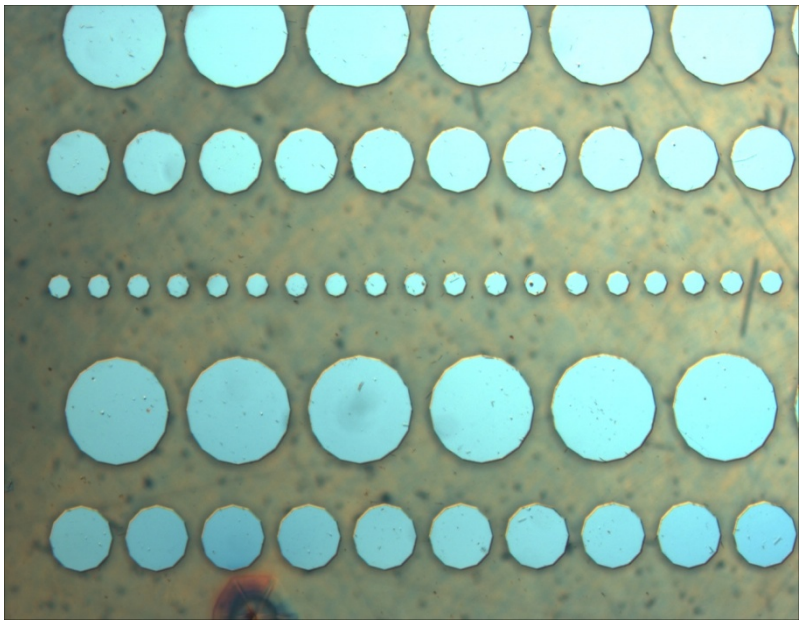

Figure 4.4 Pt Schottky contacts deposited on the Ga-face of the bulk GaN substrate

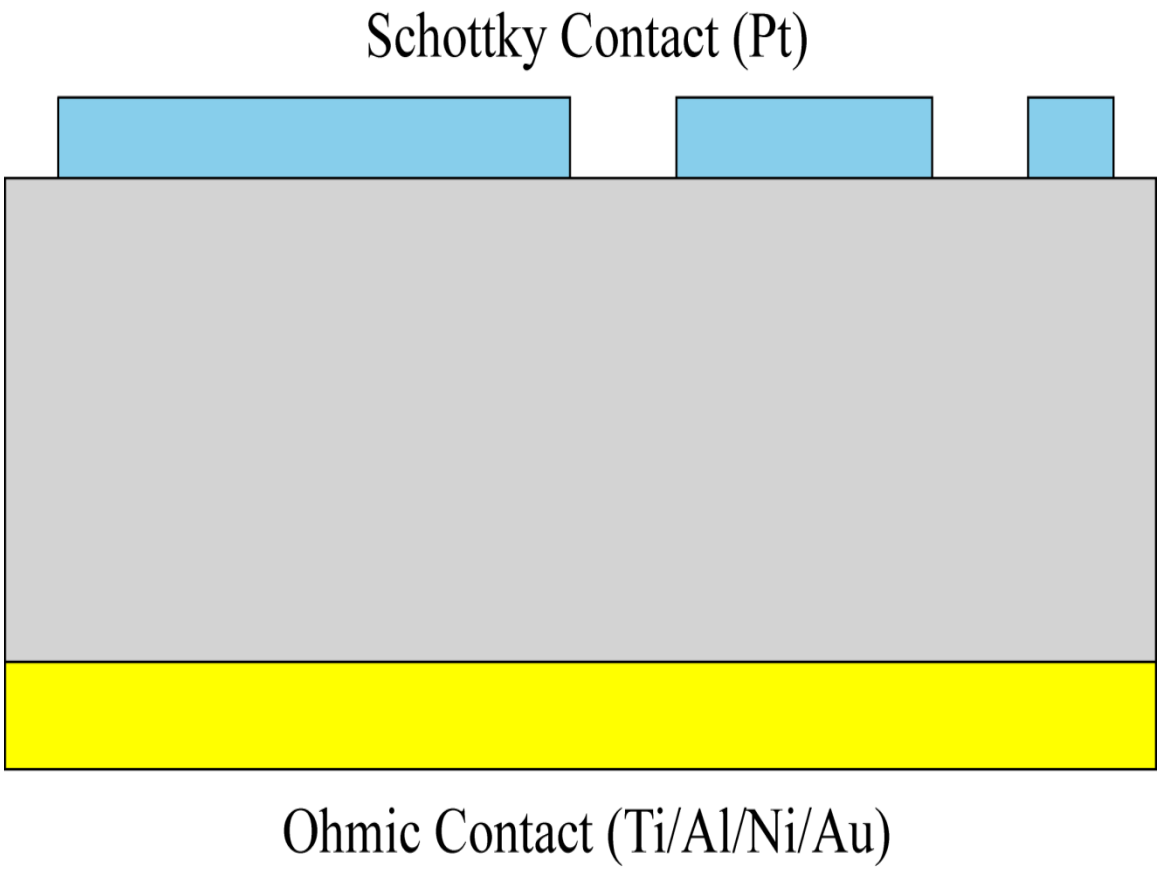

Figure 4.5 Schematic diagram of the vertical GaN Schottky diode

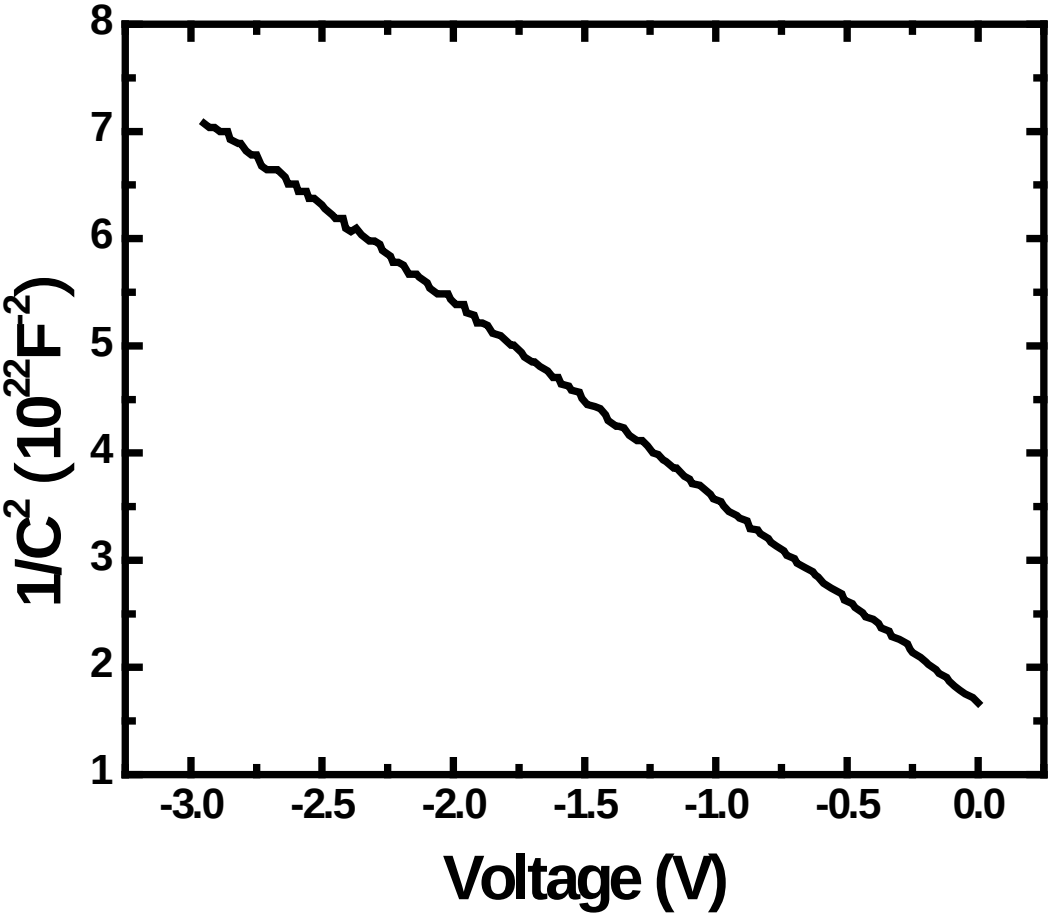

Figure 4.6 C-V curve of the vertical GaN Schottky diode

4.3 Results and discussion

Figure 4.7 shows the typical forward current-voltage (I-V) characteristics of the Schottky diodes. Figure 4.8 shows the reverse I-V measurement. The measurement was carried out in Fluorinert electronic liquid to avoid formation of a dielectric breakdown of air. The maximum breakdown voltages and the typical specific on-state resistances ($R_{on, sp}$) of the Schottky diodes with 50 µm, 150 µm and 300 µm diameter contacts were 600 V, 520 V, and 500V, and 1.3

$m\Omega cm^2$, 5.4 $m\Omega cm^2$ and 15.0 $m\Omega cm^2$, respectively. The Schottky diodes with a smaller contact exhibited lower specific on-state resistance because of the change in ratio between the Schottky contact resistance and the spreading resistance.

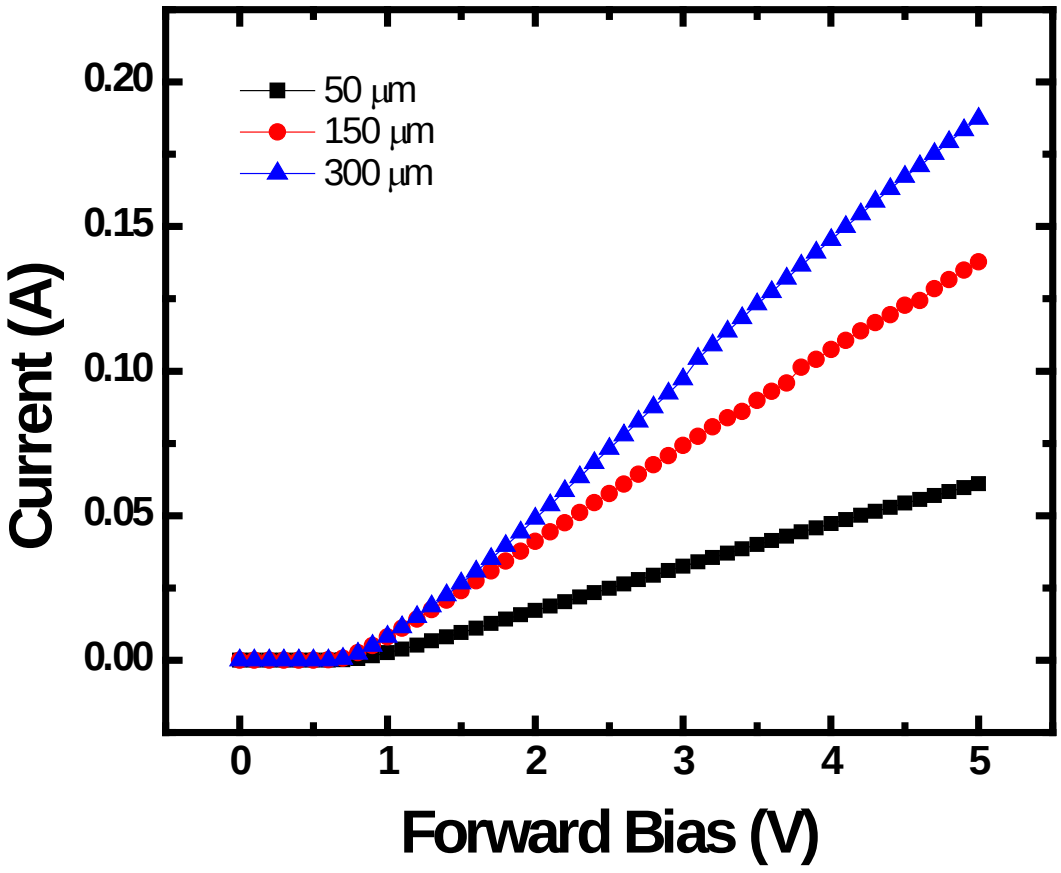

Figure 4.7 Forward I-V characteristics of the vertical GaN Schottky diodes

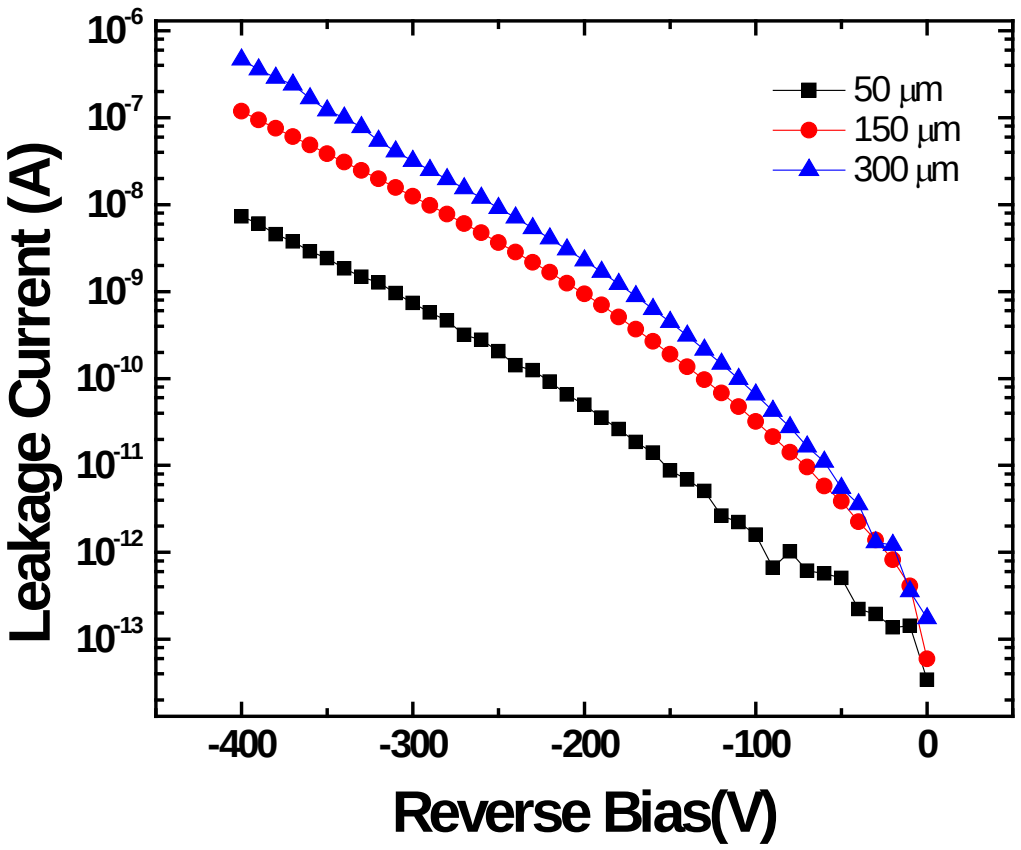

Figure 4.8 Reverse I-V characteristics of the vertical GaN Schottky diodes

The difference in breakdown voltage between the device with 50 μm diameter contact and 300 μm one is 100 V, which is lower than our previously reported value**Error! Bookmark not defined.** of 370 V. This possibly indicates the improvement of the crystal quality of the bulk GaN wafer via reduction in density of threading dislocation which may lead to premature breakdown especially at the Schottky contact periphery. The 50 μm diameter device exhibited a high figure-of-merit (V_B^2/R_{on}) of 275 MW/cm^2, and its turn-on voltage (defined as the forward bias when current density reaches 100 A/cm^2) was determined to be 0.95 V. A leakage current

density obtained from 50 μm diameter Schottky diode were 8.1×10^{-8} A/cm^2 and 3.7×10^{-4} A/cm^2 at -100 V and -400 V, respectively.

A temperature dependent I-V measurement was carried out to elucidate the current transportation mechanism. The Schottky diodes with a 300 μm diameter contact were used in this study because vertical current transport in the device with larger contact can be modeled better than the one with smaller contact by using a one-dimensional current transportation theory. The current was collected by a Keithley 6487 low compliance picoammeter from -150 V to 0.7 V and by a Keithley 2410 high compliance SourceMeter in the 0.8 V - 3 V range. Figure 4.9 shows the I-V curve of the Schottky diodes measured at various temperatures ranging from 300 K to 450 K.

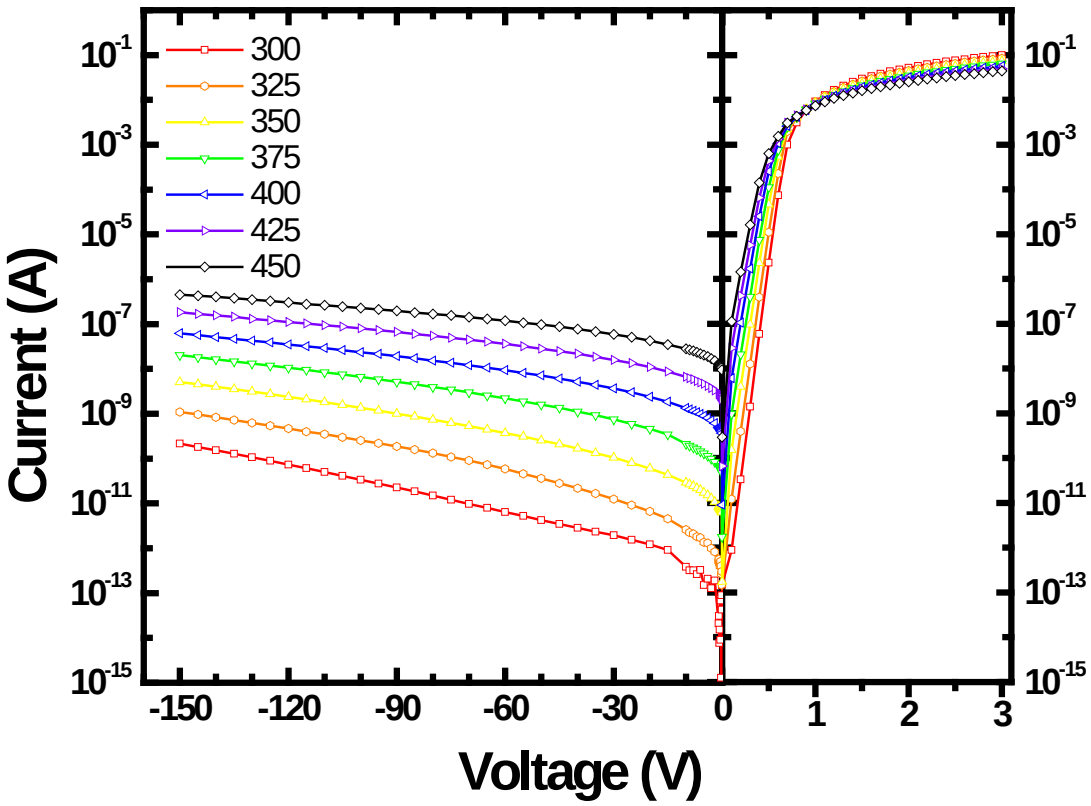

Figure 4.9 Temperature dependent I-V characteristics of the vertical GaN Schottky diodes

The current transportation mechanism across the metal-semiconductor contact is determined by the characteristic energy E_{00}, which is defined as follows [12]:

$$E_{00} \equiv \frac{q\hbar}{2}\sqrt{\frac{N}{m^{*}\varepsilon_s}} \tag{4.1}$$

where N is the doping concentration, and m^* is the electron effective mass. Considering $m^* = 0.22\ m_e$, $\varepsilon_s = 9.5$, $N = 2.8\times10^{16}/cm^3$, the value of E_{00} is determined to be 2.15 meV. Since kT (~25 meV @ room temperature)$\gg E_{00}$, the thermionic emission (TE) dominates over field emission (FE) process. The I-V relationship of the Schottky barrier diodes in the TE regime is given by [12]:

$$I_{TE} = I_0\left\{\exp\left[\frac{q(V - IR_s)}{nkT}\right] - 1\right\} \tag{4.2}$$

where n is the ideality factor, R_s is the series resistance, and I_0 is the saturation current with the following expression [12]:

$$I_0 = AA^{*}T^2\exp\left[-\frac{q\Phi_B}{kT}\right] \tag{4.3}$$

where A is the contact area, A^* is the effective Richardson's constant, and Φ_B is the Schottky barrier height. The series resistance R_s is obtained from the method proposed by Cibils *et al*. [13] The ideality factor n and saturation current I_0 are then extracted by fitting the I-V curve to equation 4.2. Figure 4.10 shows the plot of R_s *vs*.T and n *vs*.T. We can observe a larger series resistance R_s at high temperature and a less dependent temperature ideality factor n.

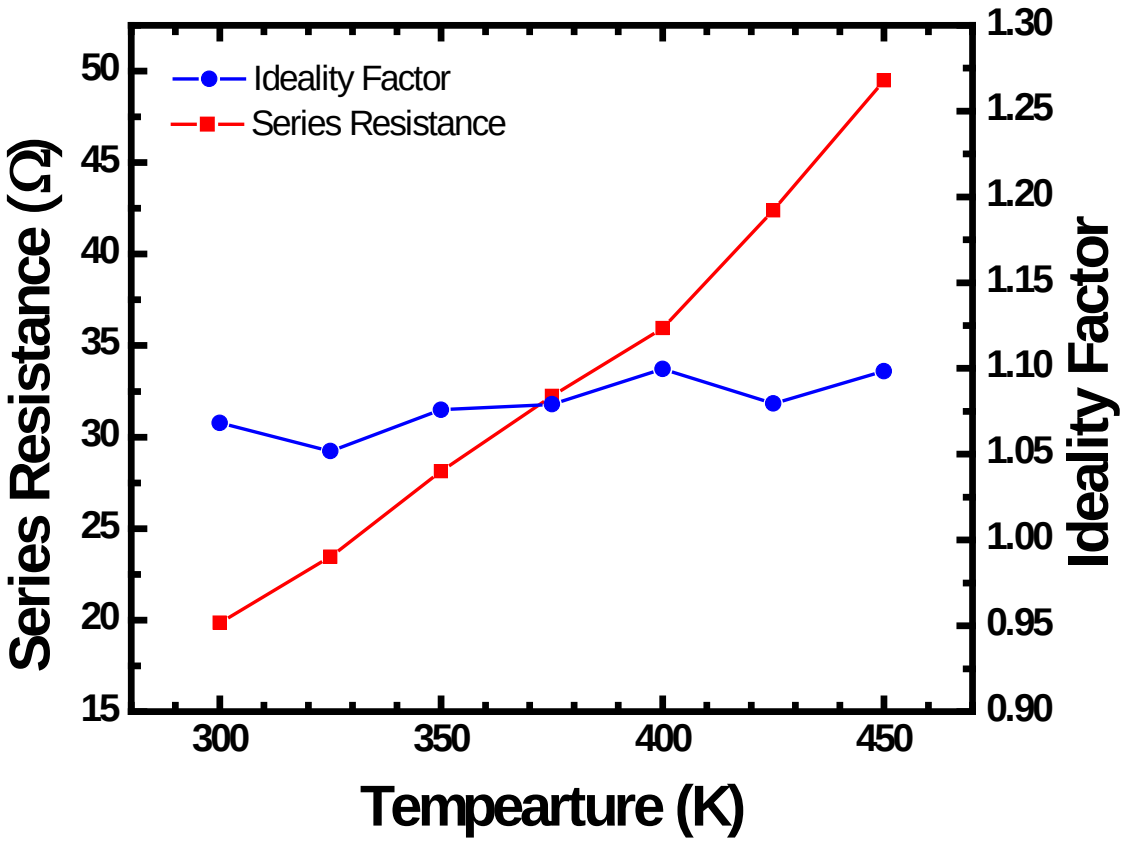

Figure 4.10 Temperature dependent ideality factor and series resistance of the vertical GaN Schottky diode

Further current transportation characteristics were studied using Arrhenius plot. By rearranging equation (3) we are able to get:

$$\ln(\mathrm{J}/\mathrm{T}^2) = \ln(\mathrm{A}^*) - \frac{\mathrm{q}\Phi_\mathrm{B}}{\mathrm{kT}} \qquad (4.4)$$

Figure 4.11 shows the Arrhenius plot of the ideal saturation current and leakage currents. The effective Richardson's constant A^* and Schottky barrier height for Pt contact can be determined from the linear curve fit of $\ln(J/T^2)$ vs. $1/T$. The value extracted from the saturation current

was 6.18 $Acm^{-2}K^{-2}$, which was in good accordance with the value of 6.61 $Acm^{-2}K^{-2}$ reported by Guo *et al.* [14]. The measured value was lower than the calculated theoretical value of 26.4 $Acm^{-2}K^{-2}$. Hacke *et al.* [15] suggested that the low A^* was due to the interfacial barrier through which the electron must tunnel, and Guo *et al.* [14] suggested it was caused by the decrease of the effective contact area. Reverse bias I-V-T data was also fitted according to equation (4) to provide activation energy. A dramatic decrease in activation energy from 0.97eV to 0.54eV was found when reverse bias increases from 1V to 150V. This may due to three reasons. First of all, the Schottky barrier was lowered due to image force at higher reverse bias. Second, Schottky barrier was also narrowed, making TFE transportation mechanism more important at high reverse bias. Third, there are also defect-assisted tunneling and other leakage mechanisms that have ohmic nature which has been reported by Yu *et al.* [16] Miller *et al.* [17] and Hashizume *et al.* [18] previously, contributing increase in leakage current at high reverse bias.

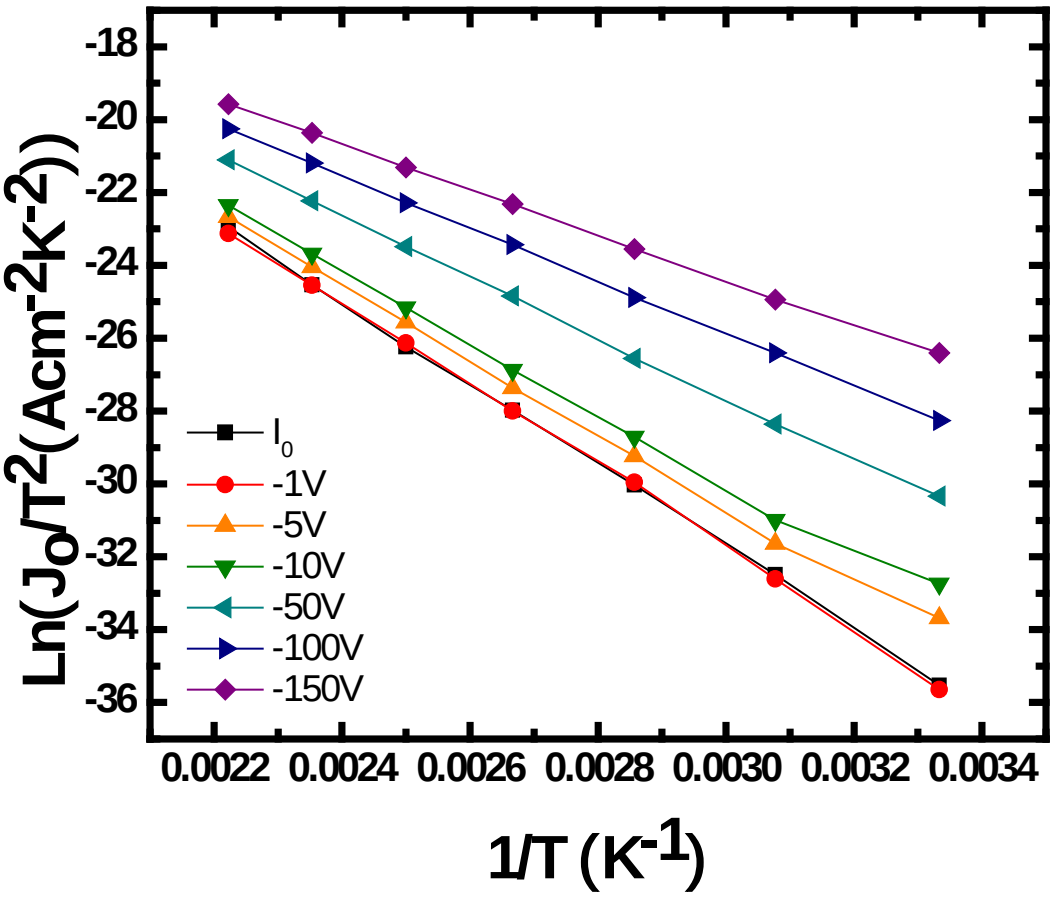

Figure 4.11 Arrhenius plots of the 300 μm diameter Schottky diodes of the ideal saturation current and leakage current at various reverse biases

4.4 Summary and Conclusions

In summary, vertical Schottky diodes with Pt Schottky contact and Ti/Al/Ni/Au full backside ohmic contact were fabricated on bulk n- GaN substrate. The bulk substrate showed natural n-type doping level gradient between the Ga-face and the N-face. The Schottky diodes showed a minimum turn-on voltage of 0.95 V, a specific on-state resistance of 1.3 $m\Omega cm^2$, and a breakdown voltage of 600 V. The devices also exhibited a high breakdown voltage and

extremely low leakage current densities of 8.1×10^{-8} A/cm^2 and 3.7×10^{-4} A/cm^2 at -100 V and -400 V, respectively. This low leakage characteristic is possibly due to the high quality n- GaN substrate and high quality metal-GaN interface. Temperature-dependent I-V measurements were also carried out, and the TE current transportation mechanism was confirmed in forward regimes, while the current transportation under reverse bias was dependent on the reverse bias and thus more complicated. Further work is required to elucidate the reverse transportation mechanism.

References

[1] A. P. Zhang, J. W. Johnson, F. Ren, J. Han, A. Y. Polyakov, N. B. Smirnov, A. V. Govorkov, J. M. Redwing, K. P. Lee, and S. J. Pearton, "Lateral $Al_xGa_{1-x}N$ power rectifiers with 9.7 kV reverse breakdown voltage", Appl. Phys. Lett. **78**, 823 (2001).

[2] Z. Z. Bandić, P. M. Bridger, E. C. Piquette, T. C. McGill, R. P. Vaudo, V. M. Phanse, and J. M. Redwing, "High voltage (450 V) GaN Schottky rectifiers", Appl. Phys. Lett. **74**, 1266 (1999).

[3] Y. Zhou, D. Wang, C. Ahyi, C. Che, J. Williams, M. Park, N. Mark Williams, and A. Hanser, "High breakdown voltage Schottky rectifier fabricated on bulk n-GaN substrate", Solid-State Electron. **50**, 1744 (2006).

[4] A. P. Zhang, J. W. Johnson, B. Luo, F. Ren, S. J. Pearton, S. S. Park, Y. J. Park, and J.-I. Chyi, "Vertical and lateral GaN rectifiers on free-standing GaN substrates", Appl. Phys. Lett. **79**, 1555 (2001).

[5] H. Lu, R. Zhang, X. Xiu, Z. Xie, Y. Zheng and Z. Li, "Low leakage Schottky rectifiers fabricated on homoepitaxial GaN", Appl. Phys. Lett. **91**, 172113 (2007).

[6] Y. Saitoh, K. Sumiyoshi, M. Okada, T. Horii, T. Miyazaki, H. Shiomi, M. Ueno, K. Katayama, K. Kiyama, and T. Nakamura, "Extremely Low On-Resistance and High Breakdown Voltage Observed in Vertical GaN Schottky Barrier Diodes with High-Mobility Drift Layers on Low-Dislocation-Density GaN Substrates", Appl. Phys. Express **3**, 081001 (2010).

[7] J. Suda, K. Yamaji, Y. Hayashi, T. Kimoto, K. Shimoyama, H. Namita, and S. Nagao, "Nearly Ideal Current–Voltage Characteristics of Schottky Barrier Diodes Formed on Hydride-Vapor-Phase-Epitaxy-Grown GaN Free-Standing Substrates", Appl. Phys. Express **3**, 101003 (2010).

[8] M. A. Reshchikov, H. Morkoç, S. S. Park, and K. Y. Lee, "Two charge states of dominant acceptor in unintentionally doped GaN: Evidence from photoluminescence study", Appl. Phys. Lett. **81**, 4970 (2002).

[9] M. A. Reshchikov, H. Morkoç, S. S. Park, and K. Y. Lee, "Yellow and green luminescence in a freestanding GaN template", Appl. Phys. Lett. **78**, 3041 (2001).

[10] J. Y. Shi, L. P. Yu, Y. Z. Wang, G. Y. Zhang, and H. Zhang, "Influence of different types of threading dislocations on the carrier mobility and photoluminescence in epitaxial GaN", Appl. Phys. Lett. **80**, 2293 (2002).

[11] T. Paskova, A. Hanser, E. Preble, K. Evans, R. Kröger, F. Tuomisto, R. Kersting, R. Alcorn, S. Ashley, C. Pagel, E. Valcheva, P. P. Paskov and B. Monemar, "Defect and emission distributions in bulk GaN grown in polar and nonpolar directions: a comparative analysis", Proc. SPIE **6894**, 68940D (2008).

[12] S. M. Sze, *Physics of Semiconductor Devices* (Wiley, New York, 1981).

[13] R. M. Cibils and R. H. Buitrago, "Forward I-V plot for nonideal Schottky diodes with high series resistance", J. Appl. Phys. **58**, 1075 (1985).

[14] J. D. Guo, M. S. Feng, R. J. Guo, F. M. Pan, and C. Y. Chang, "Study of Schottky barriers on n-type GaN grown by low-pressure metalorganic chemical vapor deposition", Appl. Phys. Lett. **67**, 2657 (1995).

[15] P. Hacke, T. Detchprohm, K. Hiramatsu, and N. Sawaki, "Schottky barrier on n-type GaN grown by hydride vapor phase epitaxy", Appl. Phys. Lett. **63**, 2676 (1993).

[16] L. S. Yu, Q. Z. Liu, Q. J. Qiao, S. S. Lau, and J. Redwing, "The role of the tunneling component in the current–voltage characteristics of metal-GaN Schottky diodes", J. Appl. Phys. **84**, 2099 (1998).

[17] E. J. Miller, X. Z. Dang, and E. T. Yu, “Gate leakage current mechanisms in AlGaN/GaN heterostructure field-effect transistors”, J. Appl. Phys. **88**, 5951 (2000).

[18] T. Hashizume, J. Kotani, and H. Hasegawa, “Leakage mechanism in GaN and AlGaN Schottky interfaces”, Appl. Phys. Lett. **84**, 4884 (2004).

Chapter Five

High breakdown Schottky diodes fabricated on homoepitaxial GaN substrate

5.1 Introduction

GaN has drawn great attention in the development of future high power and high speed power electronics (e.g. power inverters) because of its large band gap and high breakdown field. The basic building block of the power electronics is half-bridge circuit which has two modules connected in series, each of which is composed of a three-terminal switch and a two terminal rectifier [1]. Currently, the modules used in the industrial power inverters utilize Si based power metal oxide semiconductor field-effect transistor (MOSFETs) or Insulated-gate bipolar transistors (IGBTs) as the three terminal switches and Si / SiC based p-i-n or Schottky diodes as the two terminal rectifiers [2]. GaN based Schottky diode is considered as a strong challenger of the current Si / SiC based rectifier because of its material nature. However, lots of efforts are required before GaN based Schottky diodes can replace its Si / SiC counterparts. The major difficulty of GaN is lack of high quality substrate with low defect and impurity levels. The emerging technology of HVPE synthesized bulk GaN substrate can offer great advantages such as low dislocation and low impurity densities. Zhang *et al.* reported GaN Schottky diodes with a maximum breakdown voltage of 450 V, a specific on-state resistance of 20.5 $m\Omega \cdot cm^2$ and a figure-of-merit of 10 $MW \cdot cm^{-2}$ [3]. Ip *et al.* reached a maximum breakdown voltage of ~600 V and a specific on-state resistance as low as 2.6 $m\Omega \cdot cm^2$ [4]. Zhou *et al.* reported GaN Schottky diodes with a breakdown voltage of 630 V and a specific on-state resistance of 2.2 $m\Omega \cdot cm^2$, leading to a figure-of-merit of 180 $MW \cdot cm^{-2}$ [5]. Lu *et al.* achieved a very low turn-on voltage

of 0.9 V and a low specific on-state resistance of 2.56 mΩ·cm^2 [6]. The quality of GaN and the performance of GaN based Schottky diodes are both improving steadily. However, the breakdown voltage is still far from the theoretical limit.

5.2 Experiment

The GaN substrate used in this study composes of two layers. The n+ bulk GaN substrate was synthesized by HVPE at Kyma Technologies. The n- GaN epilayer was grown at North Carolina State University and Sandia National Laboratories, separately. The epilayer was grown using MOCVD. Table 5.1 shows the specifications of the GaN substrates used in this study.

Sample No.	Epi/Substrate	Structure of the epilayer
N1	NCSU/Kyma	n- GaN 5μm
N2	NCSU/Kyma	n- GaN 7 μm
N3	NCSU/Kyma	n- GaN 10 μm
N4	NCSU/Kyma	n- GaN 10 μm
S1	Sandia/Kyma	n- GaN 5 μm (~2×10^{16} cm^{-3}) on n+ GaN 0.5 μm (2×10^{18} cm^{-3})
S2	Sandia/Kyma	n- GaN 5 μm (~2×10^{16} cm^{-3}) on n+ GaN 0.5 μm (2×10^{18} cm^{-3})
S3	Sandia/Kyma	n- GaN 3.5 μm (~4×10^{16} cm^{-3}) on n+ GaN 0.5 μm (2×10^{18} cm^{-3})
S4	Sandia/Kyma	n- GaN 3.5 μm (~4×10^{16} cm^{-3}) on n+ GaN 0.5 μm (2×10^{18} cm^{-3})

Table 5.1 specifications of the GaN substrate

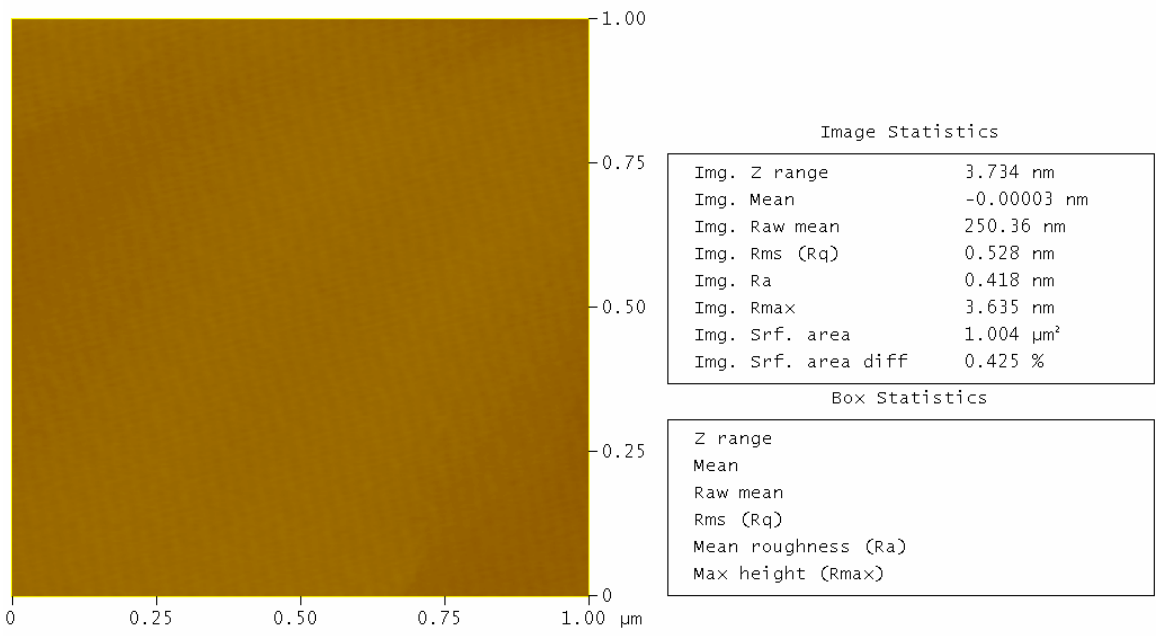

Figure 5.1 AFM image of the GaN substrate (N2)

Figure 5.1 shows a typical AFM image of the substrate (sample N2). The RMS roughness of the substrate is 0.528 nm over 1 μm^2. Prior to device fabrication, the wafer was cleaned in a series of organic solvents (acetone, trichloroethylene, acetone, methanol, and methanol) using an ultrasonic bath for 5 minutes each and then in a heated HCl solution for 10 mintues. Backside ohmic contact Ti (50nm)/Al (100nm)/Ni (50nm)/Au (50nm) was deposited sequentially on the N-face, followed by a rapid thermal annealing (RTA) process in N_2 ambience at 750°C for 30 seconds. Pt Schottky contacts were then deposited on the Ga-face using magnetron sputtering. The Schottky contacts have diameters of 50 µm, 150 µm and 300 um and a thickness of 100 nm. A typical view of Schottky contacts deposited on the GaN substrate is shown in figure 5.2.

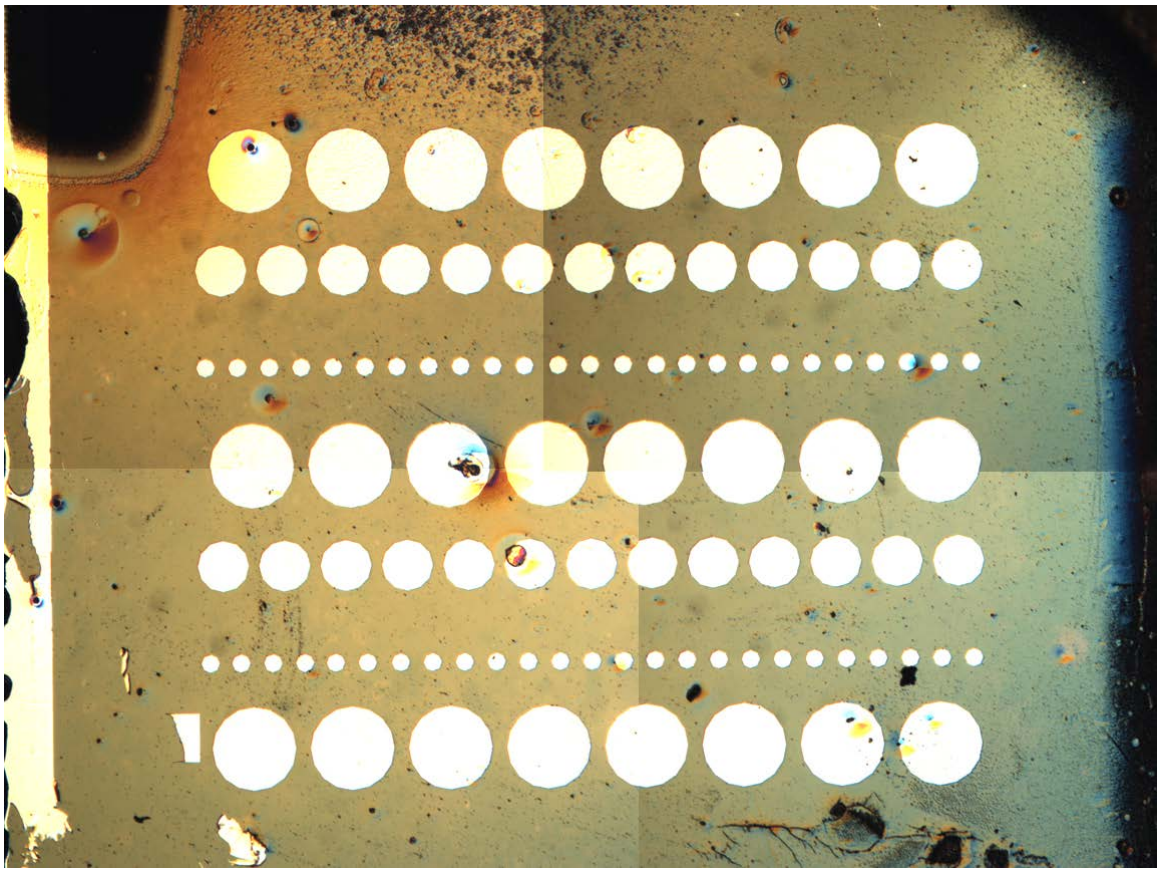

Figure 5.2 Pt Schottky contacts deposited on the GaN substrate (N1)

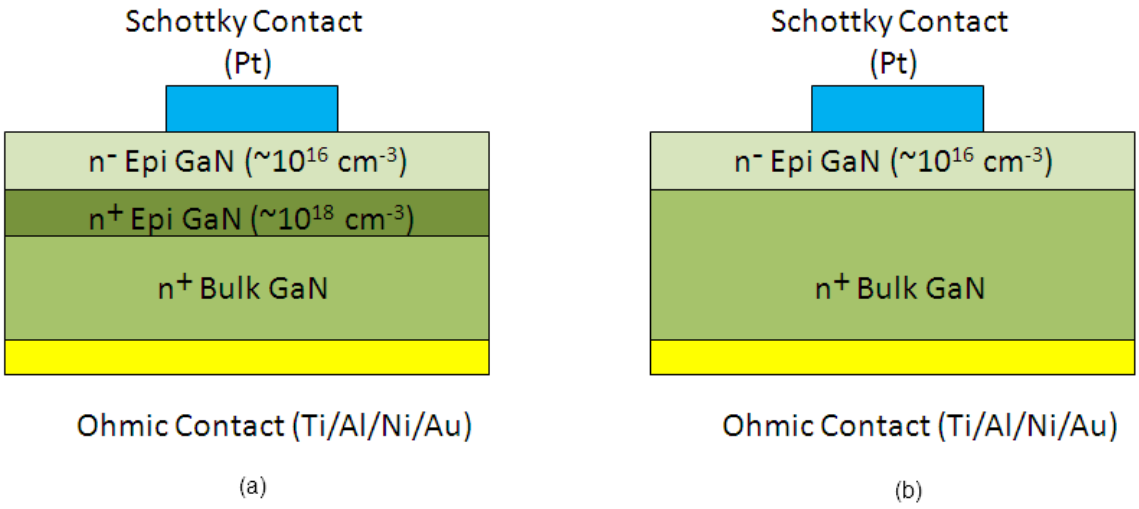

Figure 5.3 Schematic views of the Schottky diodes fabricated on the GaN substrates

(a) S1-S4 (b) N1-N4

The N batch GaN sample have n- epi layer grown directly on the n+ substrate, while the S batch GaN wafer have a MOCVD grown n- on n+ double layer. Schematic views of the Schottky diodes are shown in figure 5.3 (a) and (b).

5.3 Results and discussion

Forward I-V measurements of the Schottky diodes were first carried out using a Keithley 6517 Electrometer/High Resistance Meter. Breakdown voltages of the Schottky diodes were then measured using a Keithley 2410 high compliance SourceMeter in Fluorinert electronic liquid in order to avoid spark formation. The maximum breakdown voltage of the N batch is 980 V (N1 substrate, 50μm in diameter device). Forward and reverse I-V characteristics of the largest breakdown voltage (980V) device are shown in figure 5.4 (a) and (b). The specific on-state resistance of the device is 71 $m\Omega cm^2$.

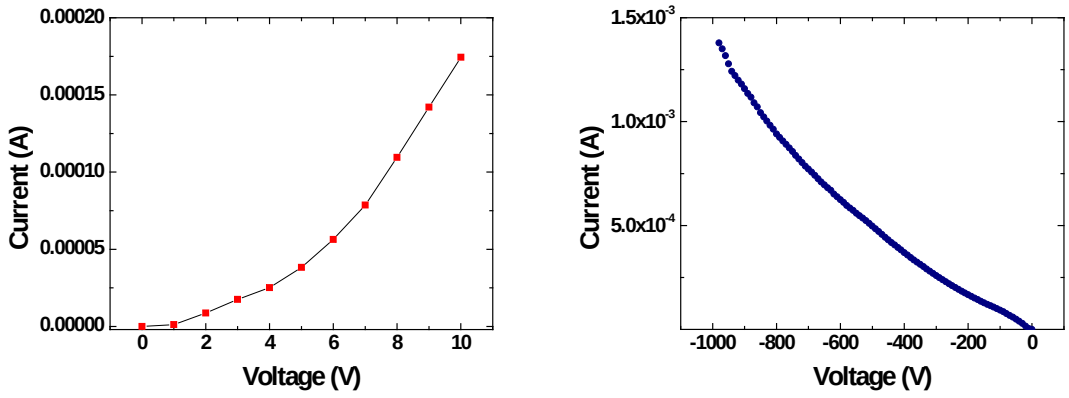

(a) (b)

Figure 5.4 Forward (a) and reverse (b) characteristics of the GaN Schottky diode with 980 V breakdown voltage

Figure 5.5 shows the statistics of forward current at 10 V and reverse breakdown voltage of the N batch GaN Schottky diodes. The round red dots represent small size devices (50 μm in diameter), the rectangular green dots represent medium size devices (150 μm in diameter) and the triangular blue dots represent large size devices (300 μm in diameter).

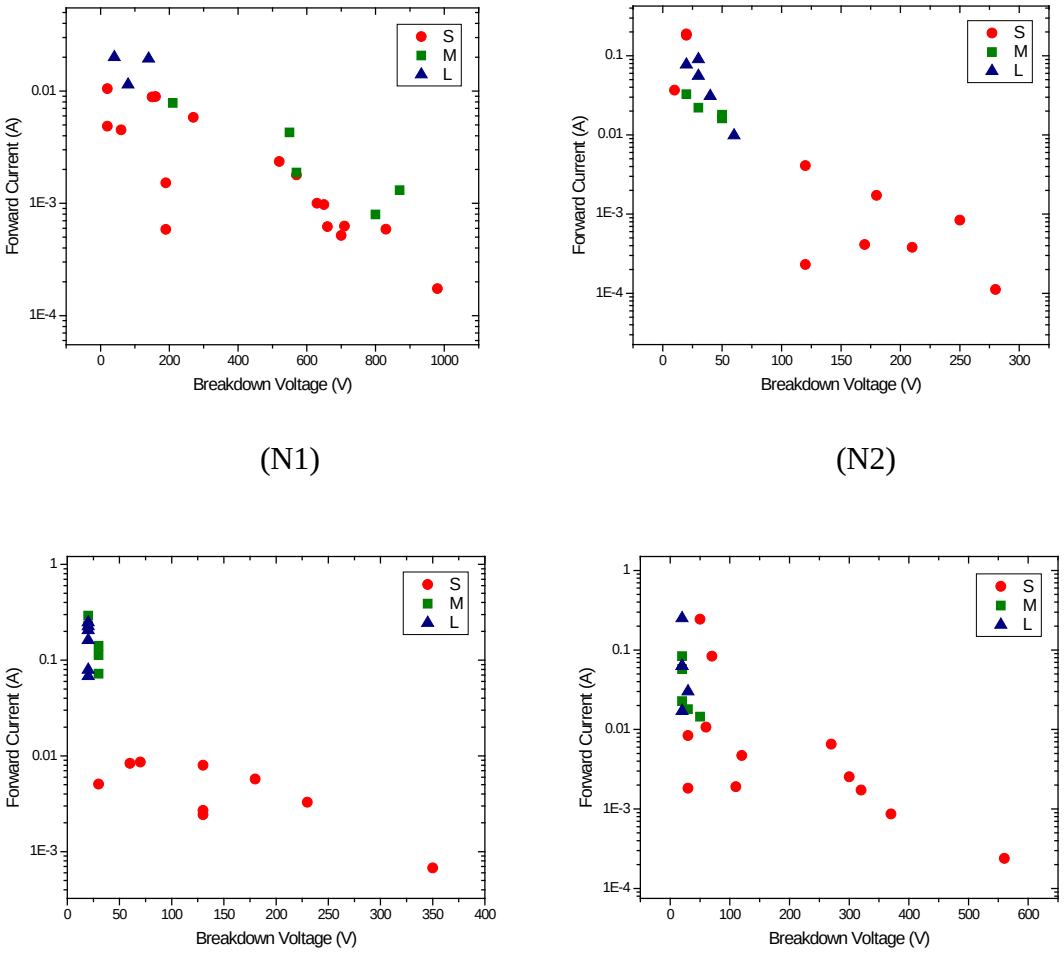

(N1) (N2)

(N3) (N4)

Figure 5.5 Forward current at 10 V vs. reverse breakdown voltage of the N batch GaN Schottky diodes

As we can see from the plots, devices fabricated on N1 substrate, which have a 5-μm-thick n- epilayer, show the best breakdown characteristics. Devices fabricated on substrate N2, N3 and N4, although with a large thickness, have breakdown voltages no more than 600 V. As the thickness of the epilayer increases, the breakdown voltages of medium size and large size device dramatically decrease to less than 100 V. These phenomena are probably due to the defects caused by the MOCVD growth of very thick GaN layer. It can also be seen that small size devices have much better chance to reach high breakdown voltage, which indicates the larger size contact have higher probability to have defect-assisted breakdown, especially at the contact periphery. Figure 5.6 shows the device after breakdown. As we can see from the figure, the breakdown happened at the periphery of the devices.

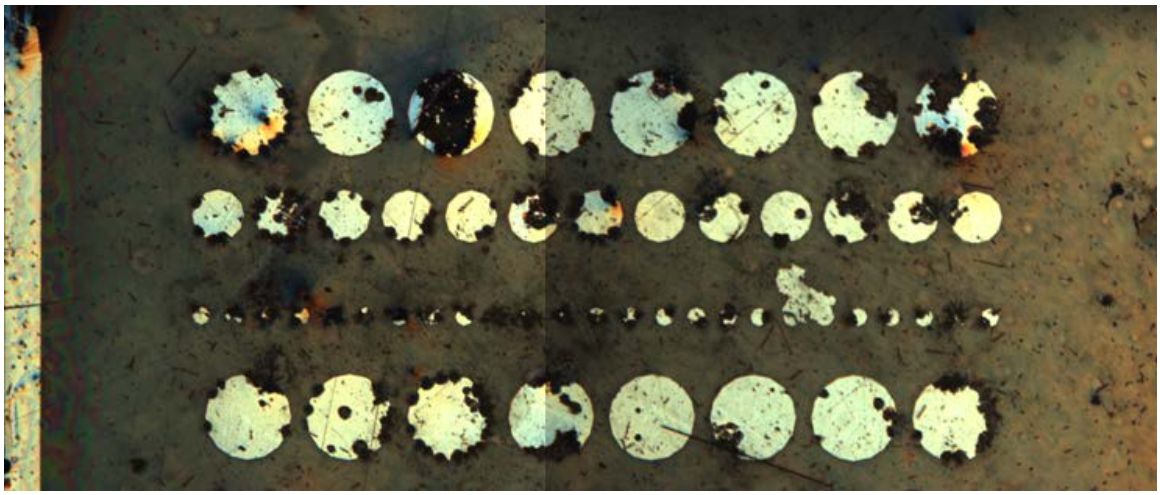

Figure 5.6 GaN Schottky diodes after breakdown

The maximum breakdown voltage of S batch GaN Schottky diodes is about 320 V (S1 substrate, 150μm in diameter device), which is much less than the N batch devices. Figure 5.7 (a) and (b) shows the forward and reverse I-V characteristics of the largest breakdown voltage device.

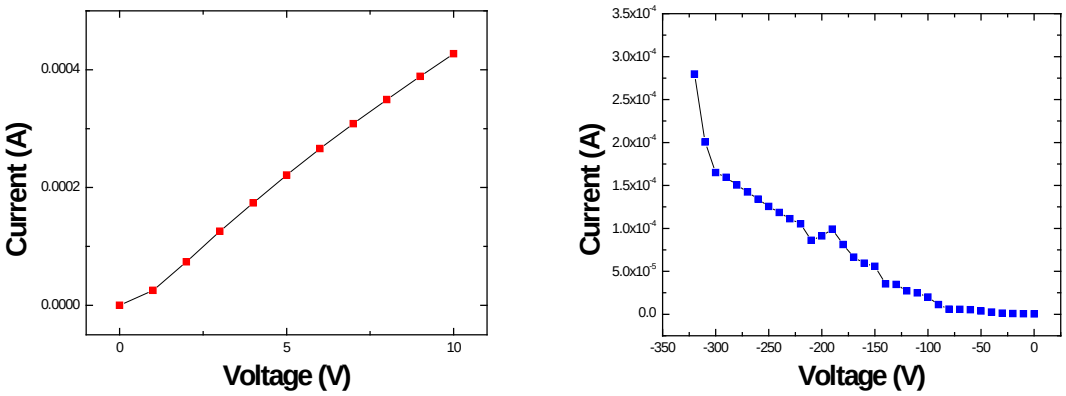

(a) (b)

Figure 5.7 Forward (a) and reverse (b) characteristics of the GaN Schottky diode with 320 V breakdown voltage

Figure 5.8 shows the statistics of forward current at 10 V and reverse breakdown voltage of the S batch Schottky diodes. As we can see from the plots, those devices shows less breakdown voltage compared with the N batch device. This is probably due to the less thickness of MOCVD grown GaN layer. The uniformity of the devices is better than the N batch device. Medium and large size devices can reach breakdown voltage of more than 200 V in the S batch device, while in devices fabricated on N2, N3 and N4 the value is usually below 100 V. It can also be seen that devices fabricated on S2 and S4 substrate showed very good forward characteristics. The minimum specific on-state resistance of the devices is only 0.82 $m\Omega cm^2$.

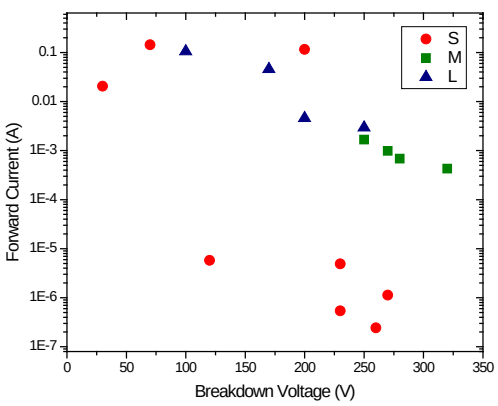

(S1)

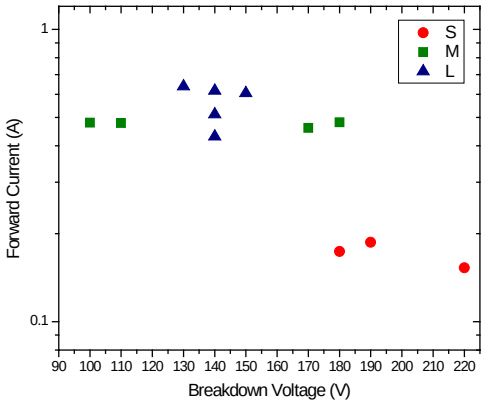

(S2)

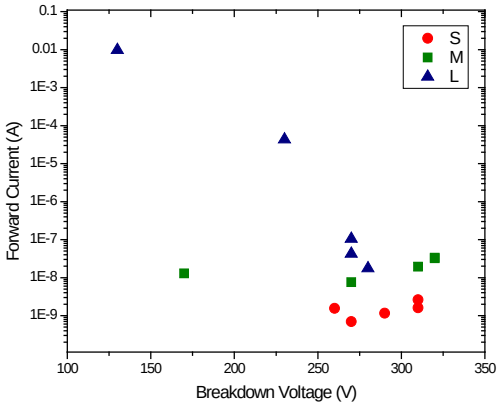

(S3)

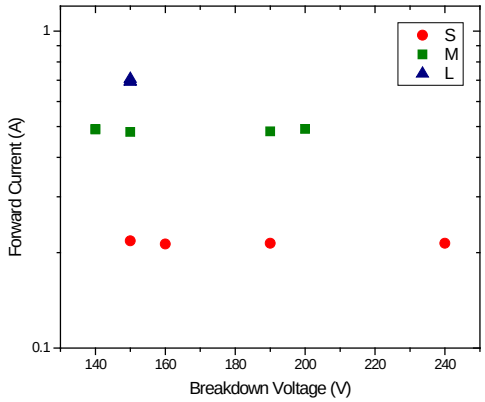

(S4)

Figure 5.8 Forward current at 10 V vs. reverse breakdown voltage of the S batch GaN Schottky diodes

5.4 Summary and Conclusions

Vertical GaN Schottky rectifiers were fabricated using a standalone n^- bulk GaN substrate and n^+ bulk GaN substrates with MOCVD grown n^- GaN epilayer. The N batch Schottky diodes fabricated on MOCVD grown epi/bulk substrate showed a very high breakdown voltage of 980

V. The S batch Schottky diodes also exhibited a very low on-state specific resistance of 0.82 $m\Omega cm^2$. Further study need to be carried out to achieve both high breakdown and low on-state specific resistance on the same device.

References

[1] A. Elasser and T. P. Chow, “Silicon carbide benefits and advantages for power electronics circuits and systems”,Proc. IEEE **90**, 969 (2002).

[2] H.-R Chang, E. Hanna, and A. V. Radun, " Development and demonstration of silicon carbide (SiC) motor drive inverter modules" IEEE Power Electronics Specialists Conference (PESC), **1**, 211 (2003)

[3] J. W. Johnson, J. R. LaRoch, F. Ren, B. P. Gila, M. E. Overberg, C. R. Abernathy, J. -I. Chyi, C. C. Chuo, T. E. Nee, C. M. Lee, K. P. Lee, S. S. Park, Y. J. Park and S. J. Pearton, “Schottky rectifiers fabricated on free-standing GaN substrates”, Solid-State Electron. **45**, 405 (2001).

[4] K. Ip, K. H. Baik, B. Luo, F. Ren, S. J. Pearton, S. S. Park, Y. J. Park and A. P. Zhang, “High current bulk GaN Schottky rectifiers”, Solid-State Electron. **46**, 2169 (2002).

[5] Y. Zhou, D. Wang, C. Ahyi, C. Che, J. Williams, M. Park, N. Mark Williams, and A. Hanser, “High breakdown voltage Schottky rectifier fabricated on bulk n-GaN substrate”, Solid-State Electron. **50**, 1744 (2006).

[6] H. Lu, D. Cao, X. Xiu, Z. Xie, R. Zhang, Y. Zheng and Z. Li, “Schottky rectifiers fabricated on bulk GaN substrate analyzed by electron-beam induced current technique”, Solid-State Electron. **52**, 817 (2008).

Chapter Six

In-Situ Temperature Measurement of GaN-based Ultraviolet Light Emitting Diodes by Micro-Raman Spectroscopy

6.1 Introduction

Due to their high power-conversion efficiency, long lifetime, and low operating cost, light-emitting diodes (LEDs) have been widely used in solid-state lighting applications. It is expected that white LEDs will gradually replace traditional lighting such as incandescent and fluorescent bulbs [1]. However, to achieve this goal, LED chips need to be designed so as to minimize heat generation and improve heat sinking, since their lifetime and luminous efficacy decrease as the junction temperature increases [2]. Figure 6.1 shows the relationship between the forward voltage applied on a GaN LED chip and the normalized output electroluminescence (EL) intensity. It is clearly shown that the EL intensity of LED drops dramatically after maximum value is reached when a continuously increasing forward voltage is applied. This phenomenon is due to power dissipated at the junction by non-radiative recombination and Joule heating which results in an elevation of the junction temperature. Therefore, it is very important to accurately determine the junction temperature of the LED during its operation.

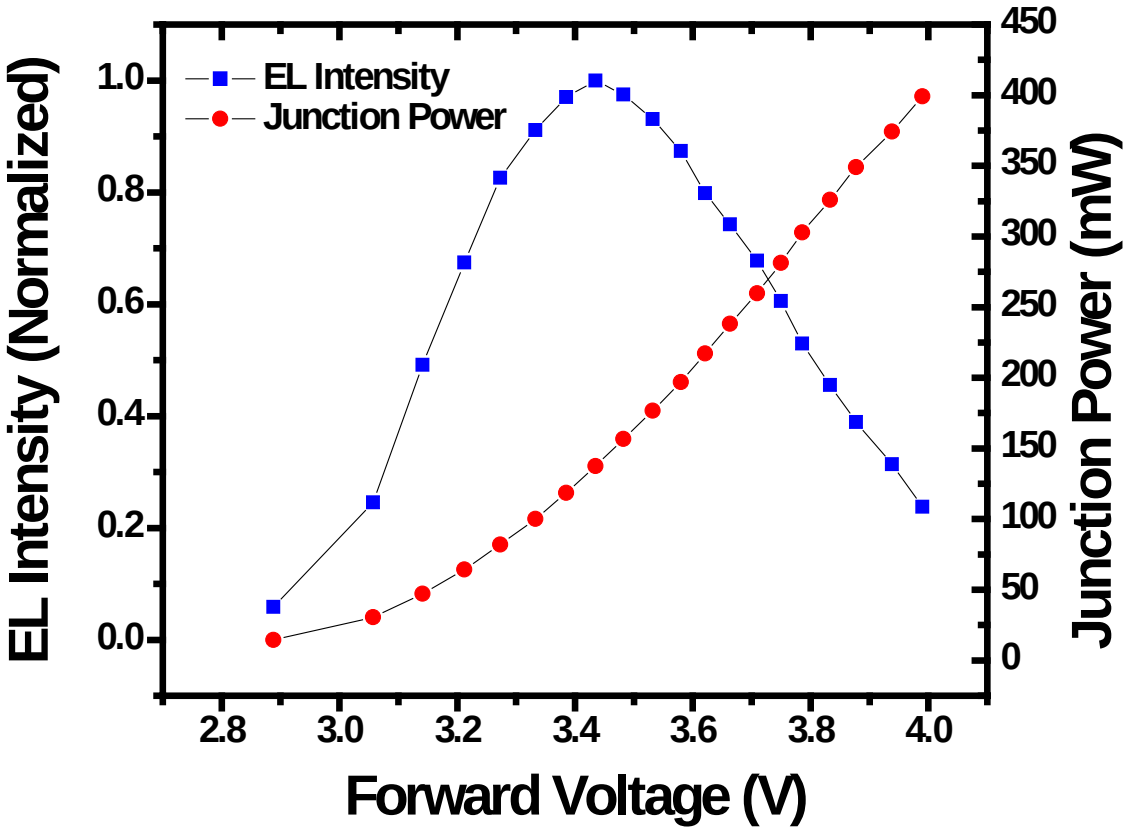

Figure 6.1 Normalized EL intensity of GaN LED chip as applied forward voltage increases

Temperature measurement methods of semiconductor devices fall into three categories: physical contact, electrical, and optical [3]. The electrical measurement method of LED temperature is based on the temperature dependent forward voltage, derived from the Shockley diode equation and Varshni relation [4]. This method, although provides the average junction temperature with good accuracy, lacks spatial resolution information. The existing optical methods determine the junction temperature from the slope of the high-energy portion of the electroluminescence (EL) peak [5,6] and/or the shift of the EL peak [4]. However, even these

methods offer no spatial resolution and are applicable to only a single emission peak in the EL spectrum. The micro-Raman spectroscopy method, based on the measurement of the Raman peak shift upon temperature change, can be used to determine device temperature because of its high accuracy and high spatial resolution. For example, 1 μm spatial resolution and 10 K temperature accuracy were achieved by micro-Raman spectroscopy for GaN-based HFETs [7,8,9]. The advantage of micro-Raman spectroscopy over EL-based methods is that it is also applicable to LEDs which exhibit multiple EL peaks. Temperature determination of ultraviolet (UV) LED chips by micro-Raman spectroscopy with good agreement with theory was reported previously. Schwegler et al. determined the temperature of InGaN multiple-quantum-well (MQW) LEDs during operation using micro-Raman and another two methods [10]. Chitnis et al. studied the self-heating effects in deep-UV LEDs grown on sapphire by micro-Raman [11]. However, the details of the temperature measurements were not discussed. In addition, the shift of Raman peak position due to the stress in the epilayer was not considered. Therefore, herein we report on the details of the determination of the junction temperature of UV LEDs based on the Raman spectra corrected for stress-induced peak shift.

6.2 Experiment

Unpackaged UV LED chips (model NS360C-2SAA; Nitride Semiconductors Co., Ltd.) were used in this study. The lateral dimensions of the device are 0.3 mm × 0.3 mm, and the total thickness is 75 μm. The device has two arms to facilitate current spreading. n-Type GaN was grown on a sapphire substrate, followed by deposition of an n-type AlGaN layer, a quantum well of InGaN and AlGaN, a p-type AlGaN layer, and a p-type GaN layer. A transparent Ni/Au was then deposited to provide p-type contact. The device structure of the chips is shown in figure 6.2.

EL and micro-Raman spectra were collected by a Jobin-Yvon's spectroscopy system. A Kimmon Electric's He-Cd laser with 442 nm line was used as an excitation source. Raman spectra were collected in backscattering geometry. The laser was illuminated on the transparent p-electrode. The diameter of the laser spot was approximately 5 μm. The backscattered Raman signal was then collected by the microscope objective lens and delivered to the spectrometer. The multichannel collection mode was used, and the integration time was 3 s. The system was calibrated using the Raman peak of single-crystal silicon. A grating with a 3600 mm^{-1} groove density was used, providing spectral resolution of 0.2 cm^{-1}. It is convenient to analyze the $E_2^{(2)}$ mode, because it has the most intense peak among all modes allowed by the Raman selection rule.

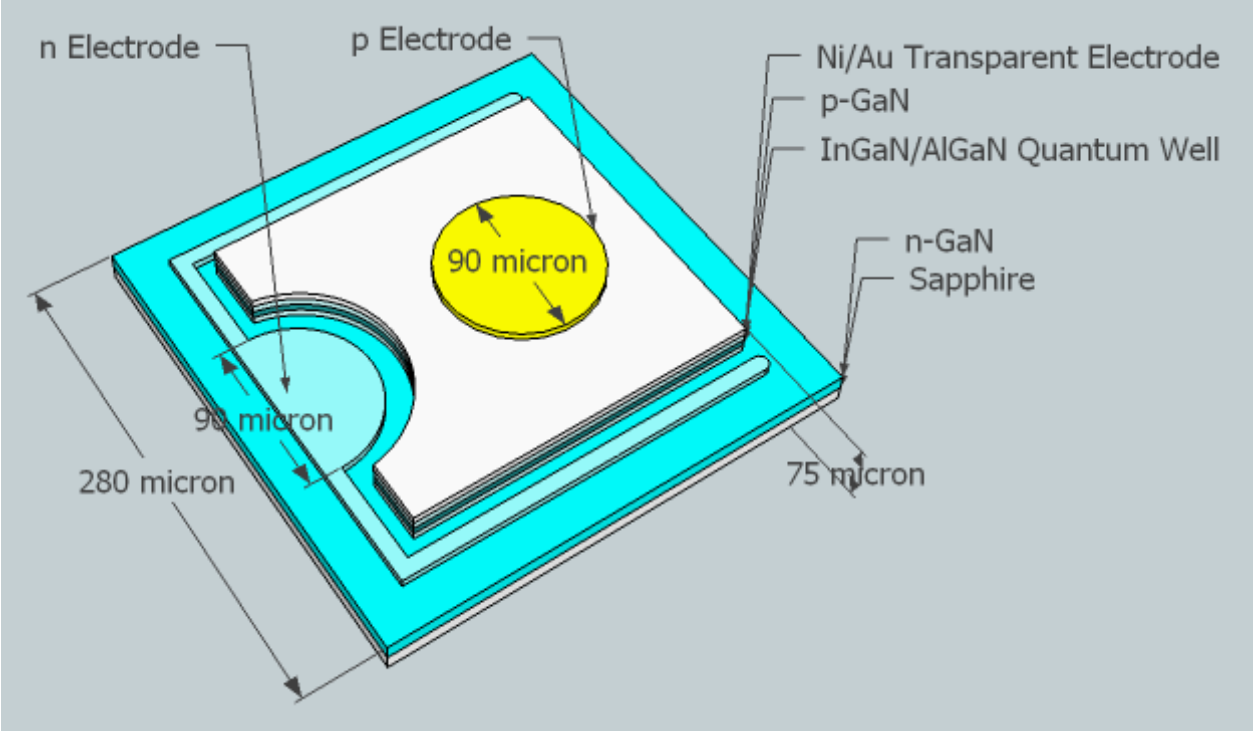

Figure 6.2 Structure of the UV LED chips

6.3 Results and discussion

Since there is variation in the reported peak positions for the $E_2^{(2)}$ mode, we collected the Raman spectrum from a stress-free bulk GaN wafer as a reference [12,13,14,15,16,17,18,19,20]. Figure 6.3 shows the Raman spectrum collected from the GaN LED chip. It was found that the Raman peak position collected from our LED chip was ~1.8 cm^{-1} higher than that obtained from the bulk wafer. We believe that the upshift of the peak observed from the chip is due to compressive stress in the GaN layer deposited on sapphire. The linear relation between the shift in a Raman peak and biaxial stress has been reported by Kisielowski et al. [21] as:

$$\sigma_a = -\frac{\Delta\omega}{k_a} \qquad (6.1)$$

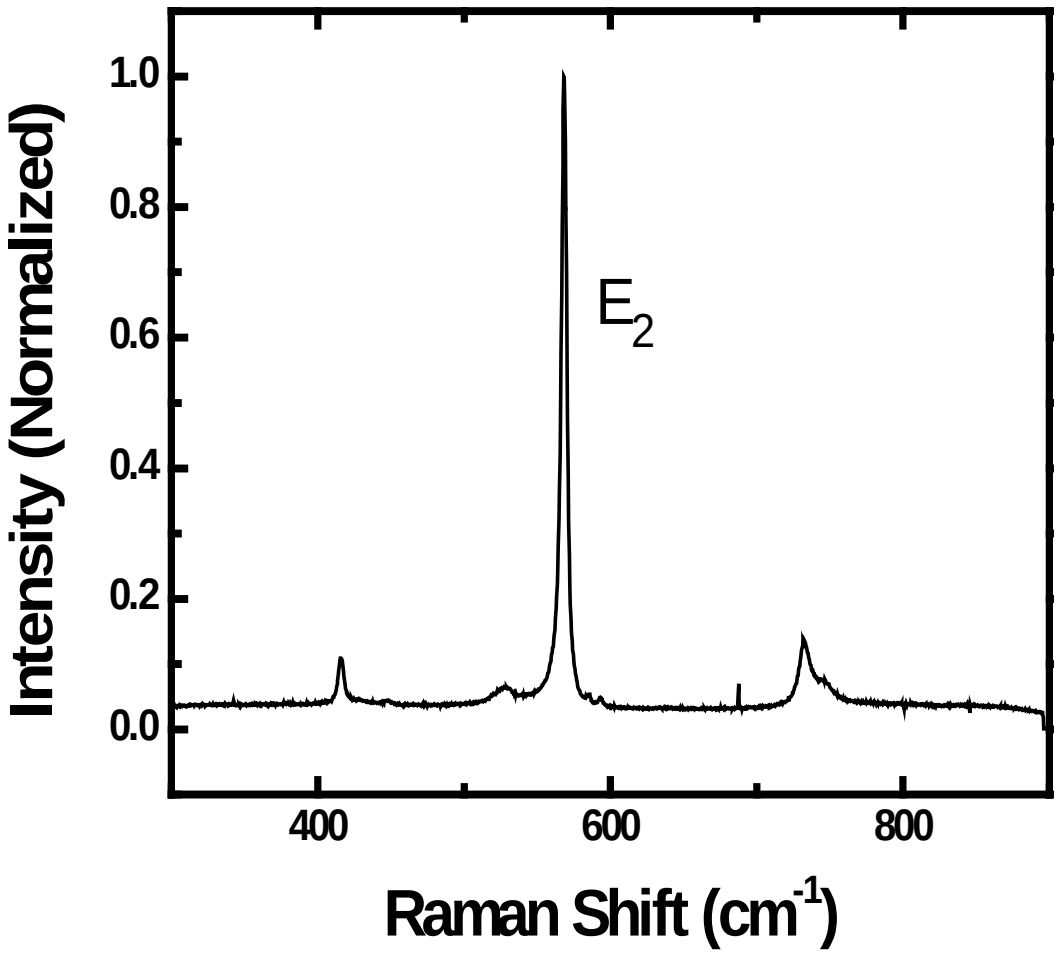

Figure 6.3 Raman spectrum of the GaN LED chip at room temperature

Initially, the temperature dependency of the spectral position and the full-width at half-maximum (FWHM) of the Raman peak were investigated via passive heating of the chip. Figure 6.4 shows the schematic diagram of the reference Raman measurement of the LED chip under passive heating. The LED chips were attached onto a ceramic plate and then heated by a hot stage (Fisher Scientific) from room temperature to 600 K in increments of 10 K. The temperature

of the plate was measured by a K-type (chromel–alumel) thermocouple (Omega). The temperature was stabilized for 10 min before each Raman spectrum was collected.

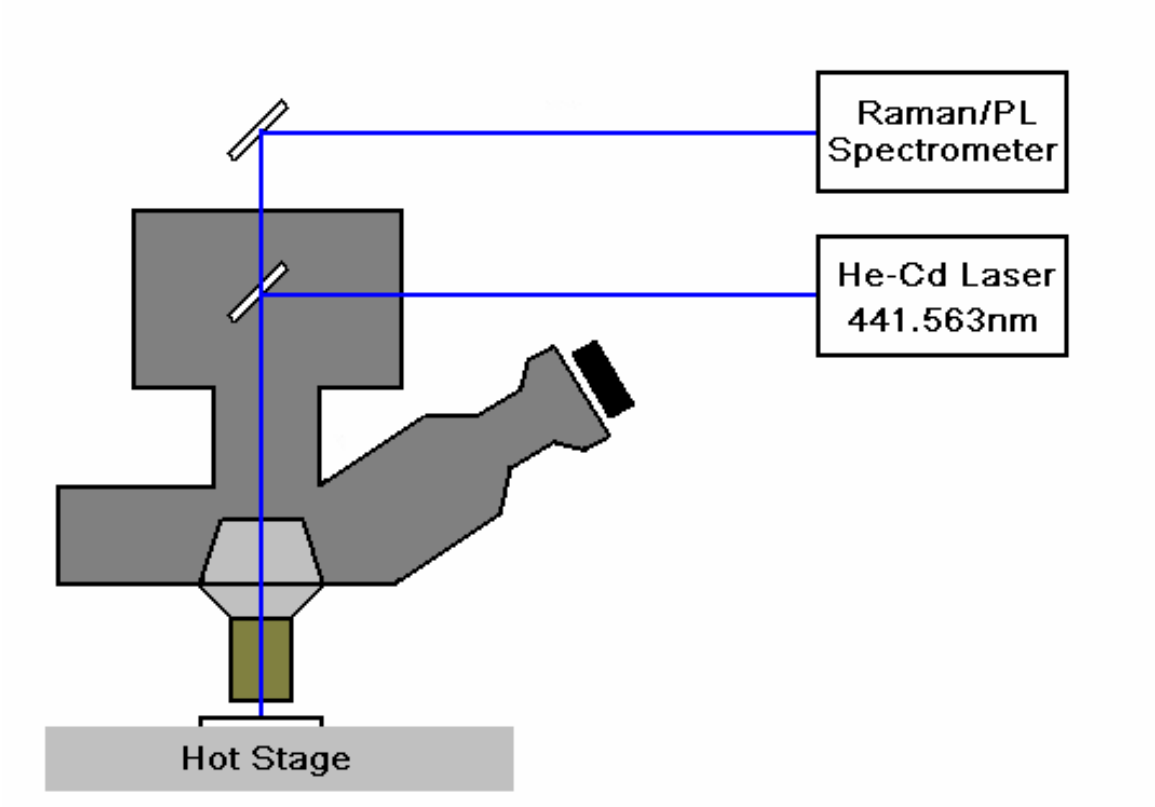

Figure 6.4 Schematic diagram of reference Raman measurement of the LED chip under passive heating

The position and the FWHM of the Raman peak were obtained by curve fitting with a Lorentzian function. Previously, the temperature dependence of a Raman peak was reported by Cui et al. [22] and Liu et al. [23] as

$$\omega = \omega_0 - \frac{\alpha}{e^{\beta\hbar c\omega_0/k_B T} - 1} \tag{6.2}$$

where α and β are fitting parameters and ω_0 is the Raman peak position at 0 K. The temperature

dependent change in FWHM is stated as follows [23]:

$$\Gamma(T) = \Gamma_0[1 + \frac{2}{e^{\beta\hbar c\omega_0/2k_BT} - 1}] \quad (6.3)$$

where Γ_0 is the FWHM at 0 K. As can be seen in figure 6.5, a downshift and broadening of the Raman peak were observed. Note that we have considered the Raman peak shift due to compressive strain, and the corrected Raman peak was used. Parameters of equation 2 were found by fitting equation 6.2 to the Raman spectrum; the fitting results were as follows; ω_0 = 569.0 ± 0.3 cm^{-1}, α = 78.6 ± 17.3 cm^{-1}, and β = 10.8 ± 1.0. Since the uncertainty of equation 2 is much less than that of equation 6.3, Equation 6.2 was used to determine the temperature of the LED during operation.

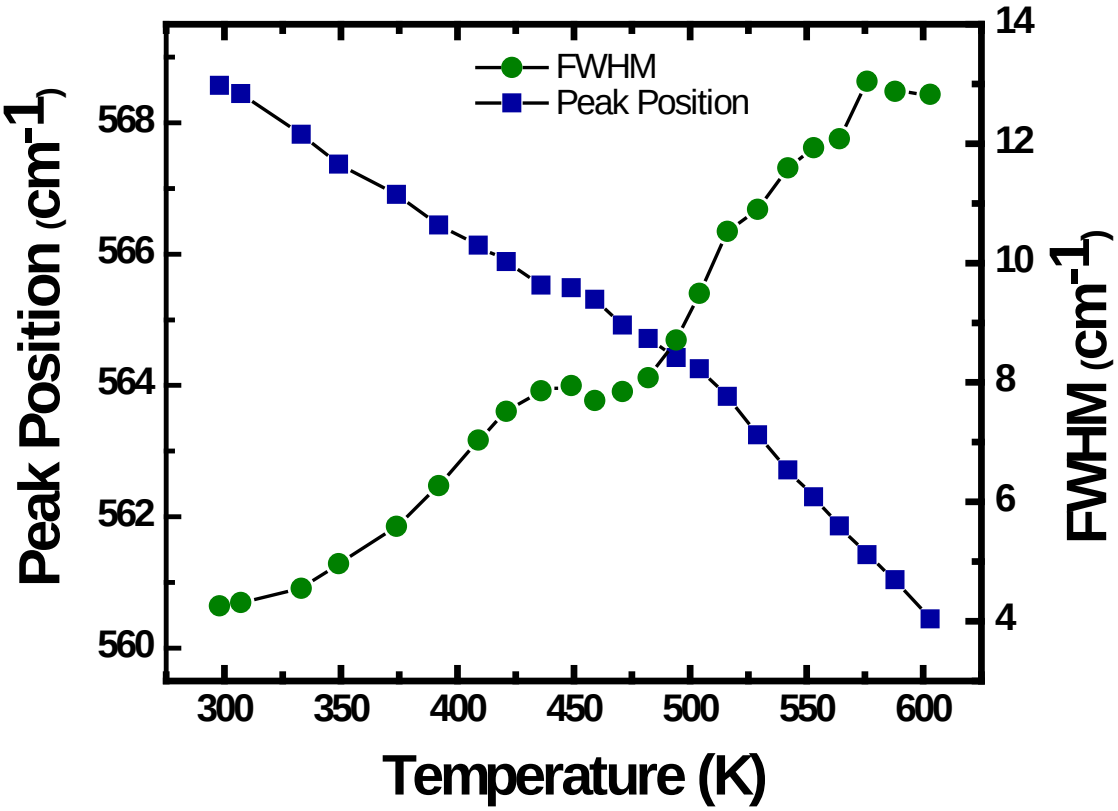

Figure 6.5 Temperature dependent spectral position and FWHM of the Raman $E_2^{(2)}$ mode

After the calibration measurement, the electrodes of the LED chips were wire-bonded to screen-printed gold contact pads on the ceramic plate. A Tektronix CPS 250 power supply is used to apply voltage on the LED chips. Raman spectra are collected when the LED chip is under operation. The laser is focused on different locations of the transparent p electrode which is shown in figure 6.6.

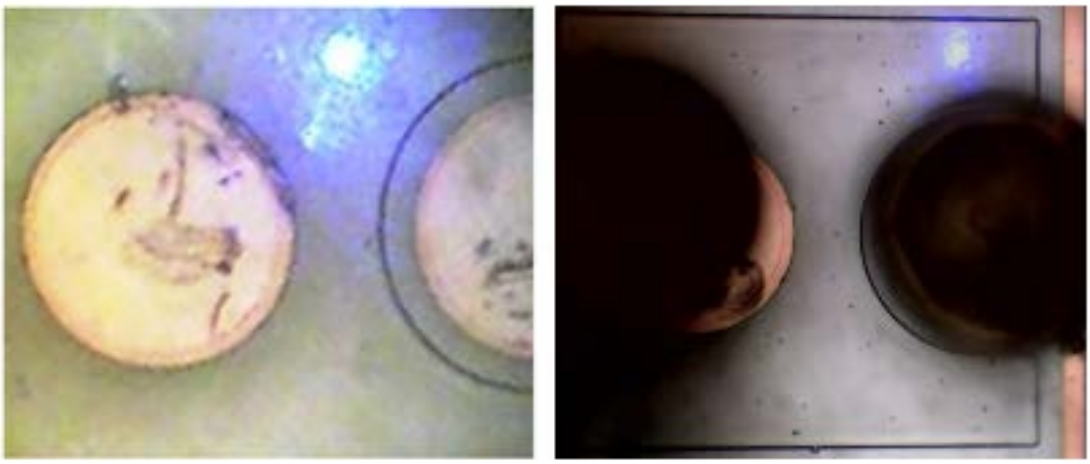

Figure 6.6 Focused laser on LED chip before and after wire bonding

Because of the power loss from manual wire-bonding and low optical extraction rate due to the lack of encapsulation, no EL spectra were observed for current flows from 0 mA to 40 mA. The UV light emitted by the LED chips was detected at a forward current of 50 mA, and the maximum EL intensity was reached at 110 mA. EL spectra of the LED chips for forward currents from 50 mA to 110 mA were then collected. The schematic diagram of the Raman measurement of LED under operation is shown in figure 6.7.

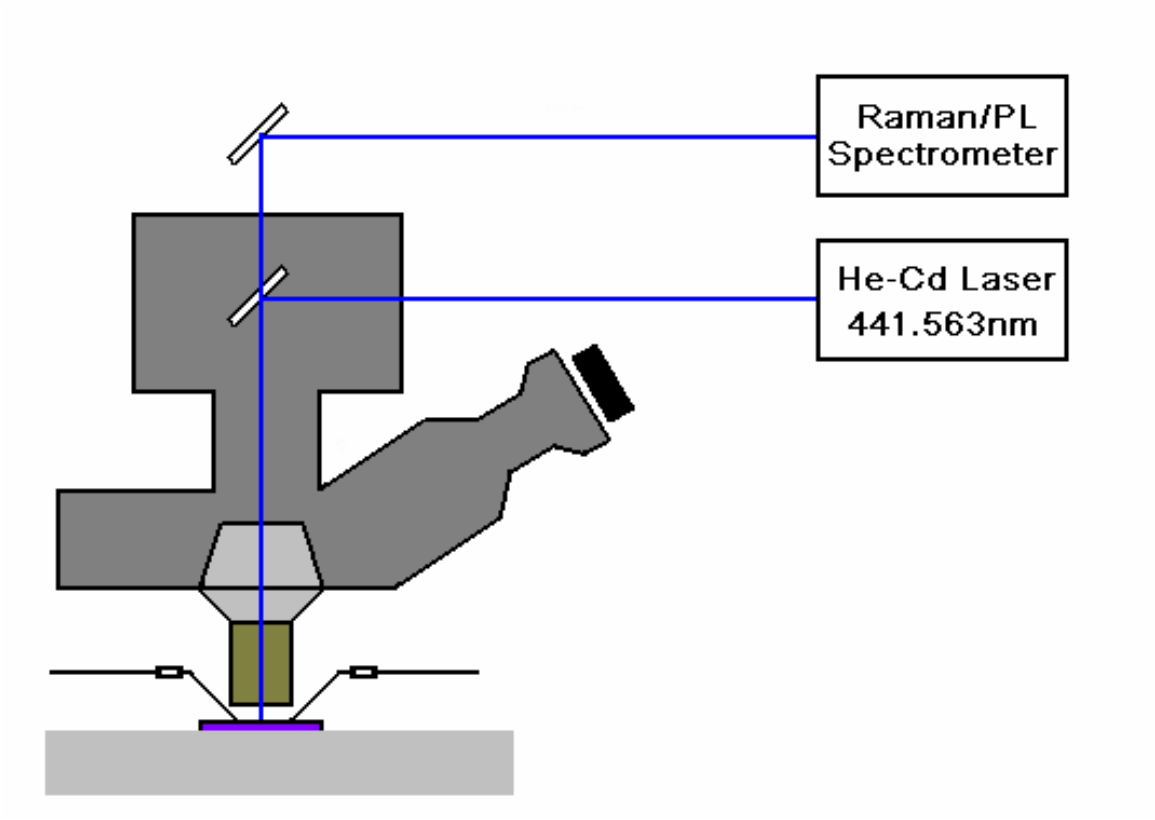

Figure 6.7 Schematic diagram of Raman measurement of the LED chip under operation

As can be seen from figure 6.8, the wavelengths of the emission peak shifted from 370 nm to 375 nm as the forward current increased. Note also that the EL spectra of LED chips exhibit multiple emission peaks. The Raman spectra from the devices were collected in situ as the forward current level was changed. Since the wavelength of the He-Cd laser is 442 nm, it does not overlap with the UV LED EL spectrum. However, as the forward current increases, the intensity of the emission peak increases and the emission peak of the LED chips were red-shifted. As a result, spectral background subtraction was performed prior to the curve-fitting analysis. Figure 6.8 shows the $E_2^{(2)}$ Raman peaks of the LED chips at different current levels.

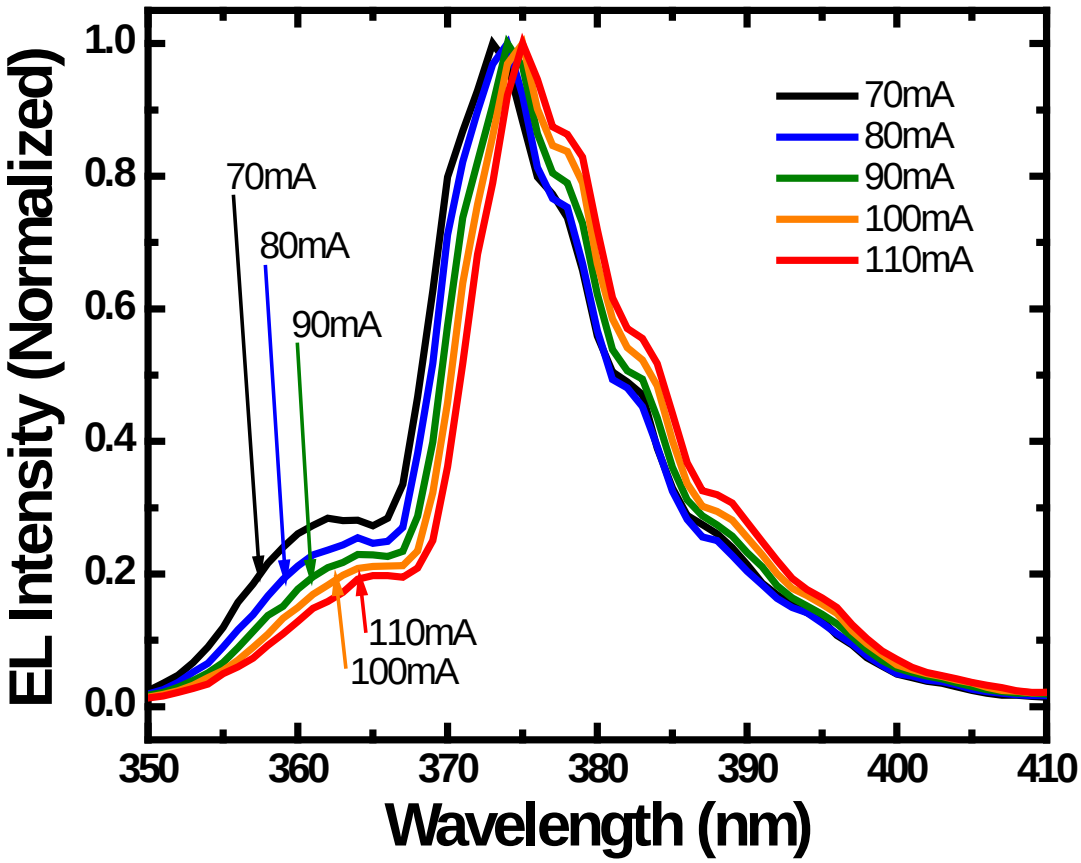

Figure 6.8 UV LED electroluminescence spectra

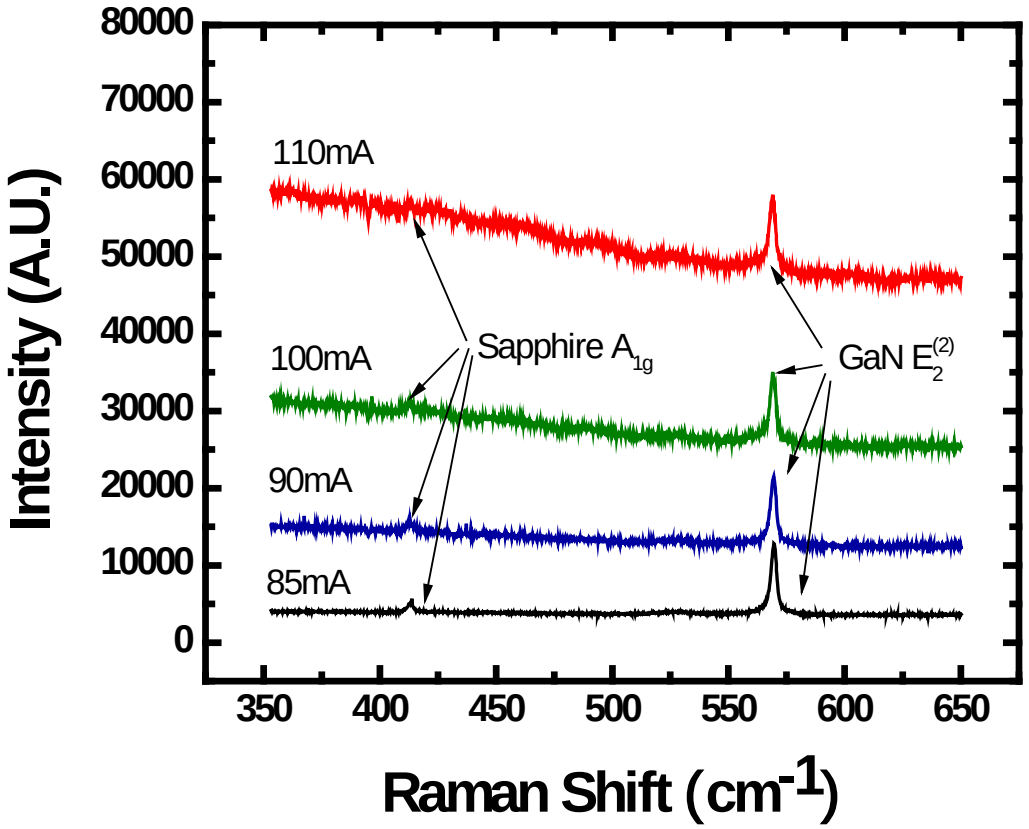

Figure 6.9 $E_2^{(2)}$ Raman peaks of the LED chips at different current levels

The change in the Raman peak position and FWHM of the Raman peak as a function of forward current are shown in figure 6.10. As the forward current increased, the junction temperature of the devices increased, and a broadening and downshift of the peak was observed. By solving for T from equation 6.2, we can derive an expression for the junction temperature as a function of Raman peak position as follows:

$$T = \frac{\beta \hbar c \omega_0}{k_B \ln(\frac{\alpha}{\omega_0 - \omega} + 1)} \tag{6.4}$$

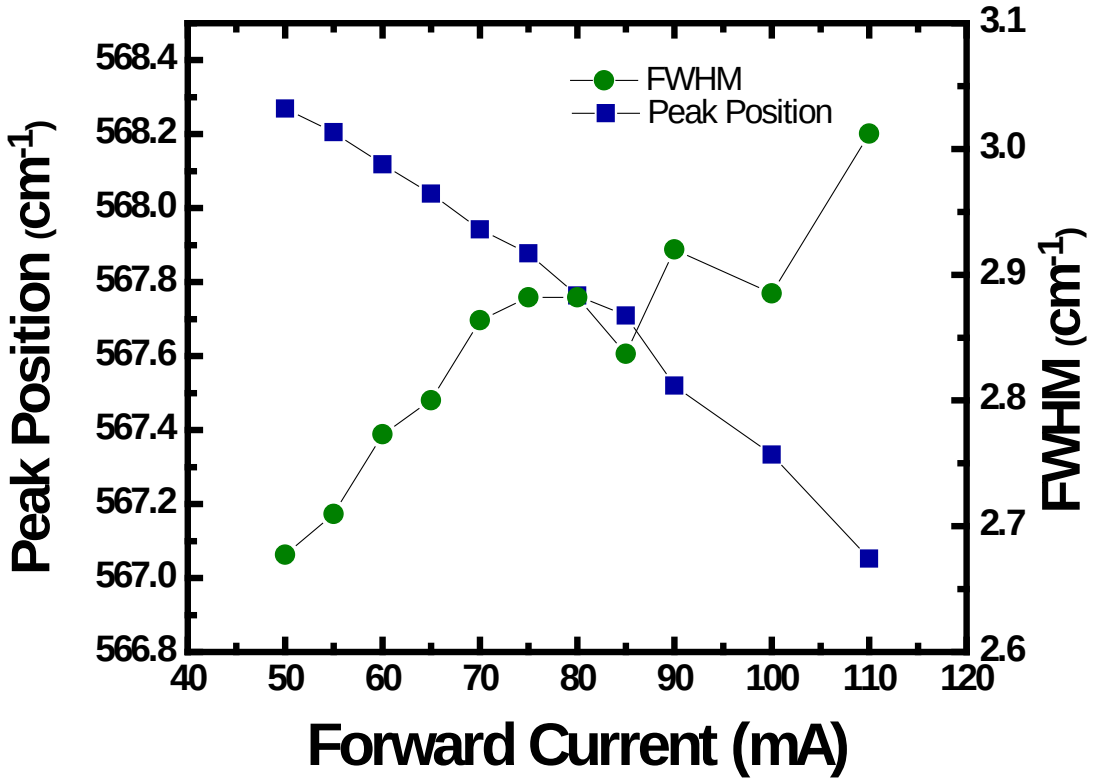

Figure 6.10 Shift of Raman Peak and FWHM as forward current increases

By using the parameters obtained from the passive heating measurement, junction temperatures at each current level can be determined. Figure 6.11 shows the relationship between the junction temperature and the forward current in the light emitting current range. As the forward current increases, the junction temperature also increases. The temperature of the device increased from 27 °C (at 50 mA) to 107 °C (at 110 mA). We have also calculated the thermal resistance of the LED chips mounted on the ceramic plate. The thermal resistance increased from

59.8 K/W (at 50 mA) to 188.6 K/W (at 100 mA).

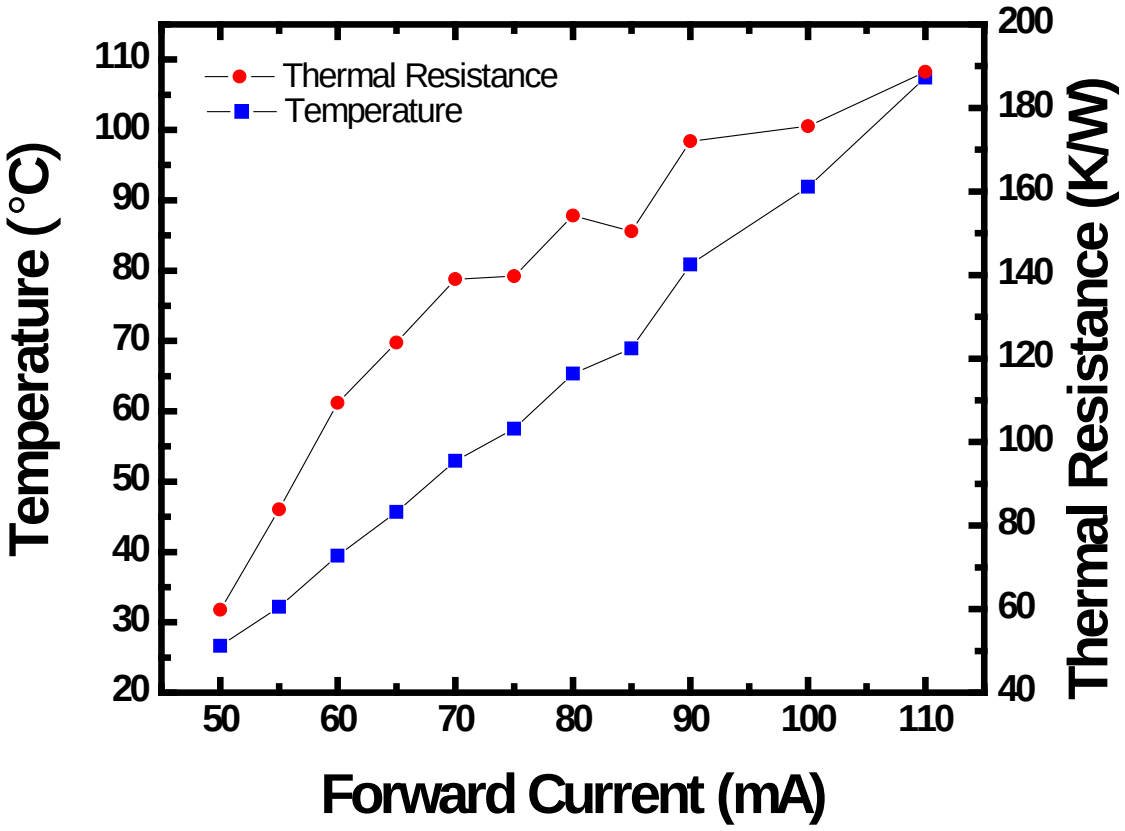

Figure 6.11 Junction temperature and thermal resistance of LED under forward bias determined by Micro-Raman spectroscopy

6.4 Summary and Conclusions

In conclusion, a method using in situ Raman spectroscopy has been developed to determine the junction temperatures of LEDs under operation. The method was applied to measure the junction temperature of UV LED chips. As the forward current increased from 50

mA to 110 mA, the junction temperature increased from 27 °C to 107 °C. We have demonstrated the viability of using micro-Raman spectroscopy for determining the junction temperature of UV LEDs accurately and with better spatial resolution than with traditional electrical and optical methods.

References:

[1] J. Y. Tsao, “Solid-state lighting: lamps, chips, and materials for tomorrow”, IEEE Circuits Devices Mag. **20**, 28 (2004).

[2] E. Fred Schubert, *Light-Emitting Diodes*, 2nd ed. (Cambridge University Press, Cambridge, 2006).

[3] D. L. Blackburn, Proceedings of the 20th IEEE Semiconductor Thermal Measurement and Management Symposium (2004), p. 70.

[4] Y. Xi, J.-Q. Xi, Th. Gessmann, J. M. Shah, J. K. Kim, E. F. Schubert, A. J. Fischer, M. H. Crawford, K. H. A. Bogart, and A. A. Allerman, “Junction and carrier temperature measurements in deep-ultraviolet light-emitting diodes using three different methods”, Appl. Phys. Lett. **86**, 031907 (2005).

[5] S. Chhajed, Y. Xi, Y.-L. Li and Th. Gessmann, “Influence of junction temperature on chromaticity and color-rendering properties of trichromatic white-light sources based on light-emitting diodes”, J. Appl. Phys. **97**, 054506 (2005).

[6] Z. Vaitonis, P. Vitta, and A. Žukauskas, “Measurement of the junction temperature in high-power light-emitting diodes from the high-energy wing of the electroluminescence band”, J. Appl. Phys. **103**, 093110 (2008).

[7] M. Kubal, S. Rajasingam, A. Sarua, M. J. Uren, T. Martin, B. T. Hughes, K. P. Hilton, and R. S. Balmer, “Measurement of temperature distribution in multifinger AlGaN/GaN heterostructure field-effect transistors using micro-Raman spectroscopy”, Appl. Phys. Lett. **82**, 124 (2003).

[8] M. Kuball, J. M. Hayes, M. J. Uren, T. Martin, J. C. H. Birbeck, R. S. Balmer, and B. T. Hughes, “Measurement of temperature in active high-power AlGaN/GaN HFETs using Raman spectroscopy”, IEEE Electron Device Lett. **23**, 7 (2002).

[9] Y. Ohno, M. Akita, S. Kishimoto, K. Maezawa, and T. Mizutani, “Temperature Distribution Measurement in AlGaN/GaN High-Electron-Mobility Transistors by Micro-Raman Scattering Spectroscopy”, Jpn J. Appl. Phys. **41**, L452 (2002).

[10] V. Schwegler, S. S. Schad, C. Kirchner, M. Seyboth, M. Kamp, K. J. Ebeling, V. E. Kudryashov, A. N. Turkin, A. E. Yunovich, U. Stempfle, A. Link, W. Limmer, and R. Sauer, “Ohmic Heating of InGaN LEDs during Operation: Determination of the Junction Temperature and Its Influence on Device Performance”, Phys. Status Solidi (a) **176**, 783 (1999).

[11] A. Chitnis, J. Sun, V. Mandavilli, R. Pachipulusu, S. Wu, M. Gaevski, V. Adivarahan, J. P. Zhang, M. Asif Khan, A. Sarua, and M. Kuball, “Self-heating effects at high pump currents in deep ultraviolet light-emitting diodes at 324 nm”, Appl. Phys. Lett. **81**, 3491 (2002).

[12] J. Nakahara, T. Kuroda, H. Amano, I, Akasaki, S. Minomura, and I. Grzegory, “Raman spectra of thin film of GaN”, Ninth Symposium Record of Alloy Semiconductor Physics and Electronics (1990), p. 391.

[13] D.D. Manchon Jr., A.S. Baker Jr., P.J. Dean, and R.B. Zetterstrom, “Optical studies of the phonons and electrons in gallium nitride”, Solid State Commun. **8**, 1227 (1970).

[14] T. Kozawa, T. Kachi, H. Kano, Y. Taga, M. Hashimoto, N. Koide, and K. Manabe, “Raman scattering from LO phonon-plasmon coupled modes in gallium nitride”, J. Appl. Phys. **75**, 1098 (1994).

[15] P. Perlin, C. J.-Carillon, J. P. Itie, A. S. Miguel, I. Grzegory, and A. Polian, “Raman scattering and x-ray-absorption spectroscopy in gallium nitride under high pressure”, Phys. Rev.

B **45**, 83 (1992).

[16] A. Tabata, R. Enderlein, J. R. Leite, S. W. da Silva, J. C. Galzerani, D. Schikora, M. Kloidt, and K. Lischka, “Comparative Raman studies of cubic and hexagonal GaN epitaxial layers”, J. Appl. Phys. **79**, 4137 (1996).

[17] G. Burns, F. Dacol, J. C. Marinace, and B. A. Scott, “Raman scattering in thin-film waveguides”, Appl. Phys. Lett. **22**, 356 (1973).

[18] T. Azuhata, T. Sota, K. Suzuki, and S. Nakamura, “Polarized Raman spectra in GaN”, J. Phys.: Condens. Matter **7**, L129 (1995).

[19] L. Bergman, D. Alexon, P.L. Murphy, R. J. Nemanich, M. Dutta, M. A. Strocio, C. Balkas, H. Shin, and R. F. Davis, “Raman analysis of phonon lifetimes in AlN and GaN of wurtzite structure”, Phys. Rev. B **59**, 12977 (1999).

[20] V. Yu Davydov, Yu. E. Kitaev, I. N. Goncharuk, A. N. Smirnov, J. Graul, O. Semchinova, D. Uffmann, M. B. Smirnov, A. P. Mirgorodsky, and R. A. Evarestov, “Phonon dispersion and Raman scattering in hexagonal GaN and AlN”, Phys. Rev. B **58**, 12899 (1998).

[21] C. Kisielowski, J. Krüger, S. Ruvimov, T. Suski, J. W. Ager III, E. Jones, Z. Liliental-Weber, M. Rubin, E. R. Weber, M. D. Bremster, and R. F. Davis, Phys. Rev. B **54**, 17745 (1996).

[22] J. B. Cui, K. Amtmann, J. Ristein, and L. Ley, “Noncontact temperature measurements of diamond by Raman scattering spectroscopy”, J. Appl Phys **83**, 7929 (1998).

[23] M. S. Liu, L. A. Bursill, S. Prawer, K. W. Nugent, Y. Z. Tong and G. Y. Zhang, “Temperature dependence of Raman scattering in single crystal GaN films”, Appl. Phys. Lett. **74**, 3125 (1999).